MSc Thesis

Analysis of propeller slipstream effects on the directional stability using a potential flow model

Nicolaas Johannes van Wonderen

Delft University of Technology

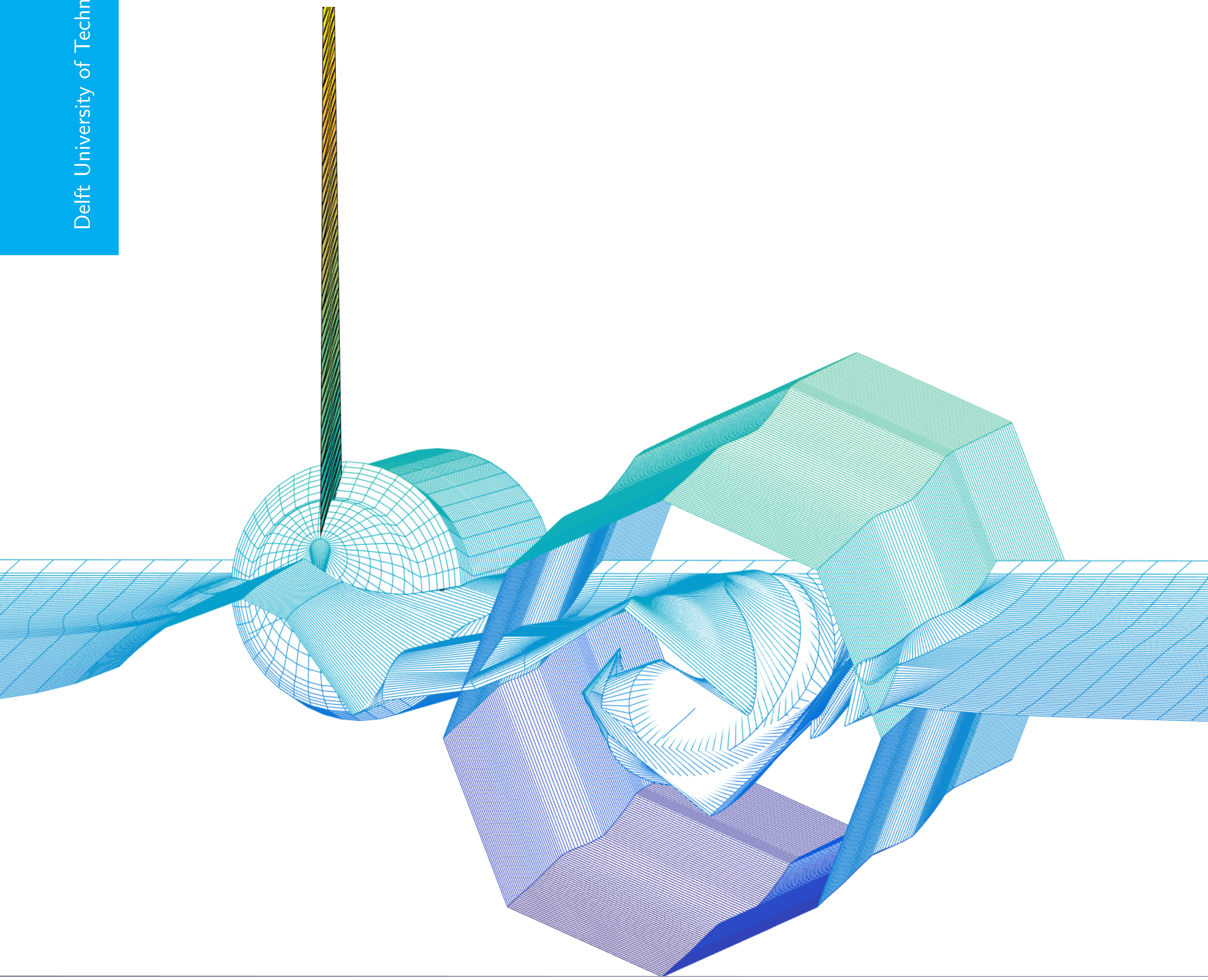

TU Delft Delft University of Technology

Challenge the future

MSc Thesis

Analysis of propeller slipstream effects on the directional stability using a potential flow model

by

N.J. van Wonderen 4170466

Date: January 15^{th}, 2017
Supervisor: Dr.ir. Roelof Vos

TU Delft
Delft University of Technology

ABSTRACT

Recent rise in aircraft operating costs and increased awareness of environmental importance have raised the interest of finding solutions to operate aircraft with less emissions and lower cost. Part of this solutions can be found in the aircraft design. Innovations made within the design of aircraft can have drastic effects on the fuel consumption.

Regarding the aircraft design, the design of an aircraft is strongly linked with the propulsion system. The aircraft design is adapted in combination with the propulsion system to achieve the maximum efficiency, by optimising the aerodynamic, structural and propulsive performance. To reduce emissions, the interest of propeller aircraft has increased because of its higher propulsive efficiency. It is expected that in the near future advanced turbo-props will be developed with higher propulsive efficiency than turbofans while operated at the same Mach numbers. Therefore, there is a renewed interest in turbo-props and prop-fans. The propeller slipstream of these engines has an effect on the longitudinal, lateral and directional stability, control, and trim of the aircraft. This research focuses on the effects of the propeller slipstream on the directional stability of the aircraft.

Current conceptual design of the vertical tail is mainly based on semi-empirical relations, of which the Data Compendium (US Air Force) DATCOM method is used the most frequently. This method is based on windtunnel measurements of aircraft models, mostly fighter aircraft, with different geometries compared to current turbo-prop aircraft. The effectiveness of the installed vertical tail is strongly affected by the aircraft configuration because of the interference effects of the wing, fuselage and horizontal tail. Additionally it was found that only a few semi-empirical relations are available in open literature to account for the effect of the propeller slipstream on the directional stability. Although in literature it was found that the propeller slipstream has a significant influence on the directional stability, especially in One Engine Inoperative (OEI) conditions. Therefore there is the need for an analysis tool which is able to predict the directional stability derivatives of the aircraft under the influence of a propeller slipstream within a short computational time such that it can be used in the conceptual design phase.

The objective of this research is to analyse and identify the effects of the propeller slipstream on the aircraft directional stability derivatives for different aircraft and empennage configurations by expanding and using a potential flow model, to improve the vertical tail design in the conceptual design phase. A potential flow model previously developed within the Flight Performance and Propulsion group has been retrieved, validated and expanded to be able to simulate different aircraft and empennage configurations under various conditions. The expansion to the model has been made especially concerning the modelling of different geometries and configurations. This has been achieved by expanding the wing, fuselage and empennage model.

Because the propeller slipstream effects on the vertical tail are largely dependent on the lift distribution over the wing-fuselage combination under influence of the propeller slipstream, first an extensive verification and validation has been performed on the spanwise lift coefficient. Validation of the model, has shown that the model can predict the spanwise lift coefficient of the wing-fuselage-propeller combination with sufficient accuracy for the conceptual design phase. Here it was found that the accuracy of the model decreases when the angle of attack increases, the lift coefficient cre-

ated by the wing behind the down-going blade was found to be over-estimated.

The aircraft model used for the research has been based on typical turboprop dimensions and parameters. This has been done to focus the analysis of the model on turbo-prop aircraft in comparison to the semi-empirical methods. From the sensitivity analysis the minimum amount of panels is determined where convergence of the results is achieved. Since the computational time increases significantly with the amount of panels in flow direction, the amount is kept to a minimum of 75 panels. The computational time for the model without the propeller installed is ≈25 seconds and with one propeller installed ≈50 seconds.

First an extensive parametric analysis and validation have been made without the propeller slipstream present. The parametric analysis consists of first analysing the isolated vertical tail and adding the fuselage, wing and horizontal tail to analyse the interference effects on the vertical tail. This first step in analysing the directional stability using the potential flow model is very important: first because it shows the potential flow model is able to predict the directional stability derivatives for different aircraft configurations and secondly because it's a baseline which later the influence of propeller slipstream effects can be compared with. From this analysis it was found that the model shows good comparison for the isolated vertical tail and to the correction curves for the different interference effects with the results obtained by Della Vecchia using a RANS solver. It was found that for all three interference effects, the fuselage, the wing, and the horizontal tail have a significant influence on the vertical tail effectiveness. For the analysis of the two example aircraft, Fokker 50 and an ATR 42, the difference of the prediction of the side force coefficient of the vertical tail under a sideslip angle between the DATCOM method and the model were found to be significant (up to 11%) and smaller but still significant with the Vertical Tail Design Stability and Control (VeDSC) method (7-8%).

After the extensive analysis and validation of the results without the propeller slipstream, in the second part of the results the influence of the propeller slipstream on the directional stability is analysed using the potential flow model. The same parametric approach has been used as for the condition no propeller was installed, making it possible to study the effects of the propeller slipstream. Depending on the aircraft configuration and conditions significant effects were found on the interference effects, especially for the propeller and wing location. When evaluating the complete aircraft configuration the side force created by the vertical tail under a sideslip angle ($C_{Y_{\beta_v}}$) increases with 5 to 7 % under the influence of the propeller slipstream. When evaluating the yawing moment coefficient of the two example aircraft, the Fokker 50 and the ATR 42, at zero degree angle of sideslip the influence of the rotation direction of the propeller is very clear. The inboard up rotating propeller generates a yawing moment which is 26 to 28% larger compared to the outboard up rotating propeller generating the same thrust.

Concluding, the potential flow model shows promising results to operate in a conceptual design tool to improve the conceptual vertical tail design. Contrary to the current design process where semi-empirical relations are used and the propeller slipstream is neglected, the model allows for calculation of the forces and moments of the various parts of the aircraft under influence of the propeller slipstream. The potential flow model however is limited to calculate the forces and moments for small angles since viscous effects are not taken into account, limiting the functionality of the model. Additionally is recommended to perform an extensive validation of the results under influence of the propeller slipstream before implementing the model into a conceptual design tool.

ACKNOWLEDGEMENTS

This master thesis has been written to obtain my MSc of Delft University of Technology from the faculty of Aerospace Engineering. With this research I hope to improve future vertical tail design of propeller aircraft, to improve the overall efficiency of the aircraft. The flow around the aircraft, influenced by the aircraft geometry and additionally made more complex by the propeller slipstream, forms a complex system which needs to be predicted in a fast and accurate way. This challenge was the drive throughout my work.

I would like to thank my supervisor, Dr.ir. Roelof Vos and Ir. Nando van Arnhem for their valuable advise and guidance during this project. Last I want to thank my family and especially my parents for their unconditional support during the last 5 years.

Contents

List of Figures

Nomenclature

Acronyms

AOA	Angle of Attack
CFD	Computational Fluid Dynamics
CS	Certicfication Specification
DATCOM	United States Air Force Data Compendium
EASA	European Aviation Safety Agency
FAA	Federal Aviation Administration
HTC	High Thrust Condition
IU	Inboard Up
LTC	Low Thurst Condtion
MSc	Master of Science
MTOW	Maximum Take-Off Weight
NACA	National Advisory Committee for Aeronautics
NASA	National Aeronautics and Space Administration
NS	Navier-Stokes
OEI	One Engine Inoperative
OU	Outboard up
RANS	Reynolds Averaged Navier-Stokes
TU Delft	Technical University Delft
VLM	Vortice Lattice Method
VSAERO	Vortex Separation AEROdynamis
VeDSC	Vertical tail Design Stability and Control

Symbols

Latin

$\widehat{A}$	Influence matrix	$[-]$
a	Axial velocity factor of the propeller slipstream	$[-]$
a'	Angular velocity factor of the propeller slipstream	$[-]$
A_h	Aspect ratio horizontal tail	$[-]$
AR	Aspect Ratio	$[-]$
AR_h	Aspect ratio horizontal tail	$[-]$
AR_V	Aspect ratio vertical tail	$[-]$
b	Wingspan	$[m]$
b_v	Reference tail height	$[m]$
c	Reference chord length	$[m]$
C_D	Drag coefficient (3D)	$[-]$
C_P	Pressure coefficient	$[-]$
c_l	Section lift coefficient	$[-]$
C_{L_α}	Lift coefficient with angle of attack	$[-]$
C_n	Yawing moment coefficient	$[-]$

C_Y	Side force coefficient	$[-]$
C_{Y_β}	Side force coefficient under sideslip angle	$[-]$
$C_{Y_{\beta_v}}$	Side force coefficient under sideslip angle by vertical tail	$[-]$
C_{Y_V}	Side force coefficient of the vertical tail	$[-]$
D	Diameter	$[m]$
D	Drag force	$[N]$
D	Propeller Diameter	$[m]$
f_D	Fuselage Diameter	$[m]$
F_p	Propeller force	$[N]$
F_T	Force created by vertical tail	$[N]$
h_w	Wing height	$[m]$
i_w	Incidence angle wing	$[°]$
J	Advance ratio	$[-]$
k	Correction factor	$[-]$
l	Reference length	$[m]$
L	Length	$[m]$
L	Lift force	$[N]$
l_f	Fuselage Length	$[m]$
M	Mach number	$[-]$
N	Yawing moment	$[Nm]$
p	Pressure	$[Pa]$
p_s	Static pressure	$[Pa]$
p_t	Total pressure	$[Pa]$
q	Dynamic pressure	$[Pa]$
r	Superellips radius	$[-]$
R	Rotor radius	$[m]$
R	Contraction	$[-]$
Re	Reynolds number	$[-]$
S	Surface area	$[m^2]$
S_{ref}	Reference area	$[m^2]$
S_V	Surface area vertical tail	$[m^2]$
t	Time	$[s]$
T	Temperature	$[K]$
T	Thrust	$[N]$
T_c	Thrust Coefficient	$[-]$
u	Velocity in x-direction	$[m/s]$
U_∞	Free stream velocity in x-direction	$[m/s]$
v	Velocity in y-direction	$[m/s]$
V_∞	Free stream velocity	$[m/s]$
V_a	Axial velocity	$[m/s]$
V_{mc_a}	Minimum control speed in flight	$[m/s]$
V_s	Stall speed	$[m/s]$
V_t	Tangential velocity	$[m/s]$
W	Width	$[m]$
x	x-coordinate	$[-]$
X	x-coordinate	$[-]$
x_0	Reference x-coordinate	$[-]$
y	y-coordinate	$[-]$
y_0	Reference y-coordinate	$[-]$

Z	Height	$[m]$
Z_0	Reference z-coordinate	$[-]$
z_h	Vertical position of horizontal tail	$[m]$

GREEK

α	Angle of attack	$[°]$
α_0	Zero lift angle of attack	$[°]$
β	Sideslip angle	$[°]$
δ_r	Rudder deflection	$[°]$
δ_v	Velocity thickness	$[m]$
η	Normalised reference coordinate	$[-]$
Γ	Circulation	$[m^2/s]$
Λ	Sweep angle	$[°]$
λ	Taper ratio	$[-]$
θ	Dynamic viscosity	$[Pa \cdot s]$
Ω	Angular velocity of the propeller	$[rad/s]$
ω	Vorticity	$[1/s]$
ϕ	Flow angle with respect to the propeller plane	$[rad]$
ρ	Fluid density	$[kg/m^3]$
σ	Sidewash angle	$[°]$
θ_{geo}	Geometric blade angle	$[°]$
θ_{sw}	Swirl angle	$[°]$
ξ	Normalised reference coordinate	$[-]$
ζ	Normalised reference coordinate	$[-]$

1 INTRODUCTION

1.1. MOTIVATION AND PROBLEM STATEMENT

Recent rise in aircraft operating costs and increased awareness of environmental importance have raised the interest of finding solutions to operate aircraft with less emissions and lower cost. Part of these solutions can be found in the aircraft design. Innovations made within the design of aircraft can have drastic effects on the fuel consumption.

Regarding the aircraft design, the design of an aircraft is strongly linked with the propulsion system it is provided with. The aircraft design is adapted in combination with the propulsion system to achieve the maximum efficiency, by optimising the aerodynamic, structural and propulsive performance.

To reduce emissions, the interest of propeller aircraft has increased because of its higher propulsive efficiency. It is expected that in the near future advanced turbo-props will be developed with higher propulsive efficiency than turbofans while operated at the same Mach numbers [1]. Therefore, there is a renewed interest in turbo-props and prop-fans [2]. The propeller slipstream of these engines has an effect on the longitudinal, lateral and directional stability, control, and trim of the aircraft.

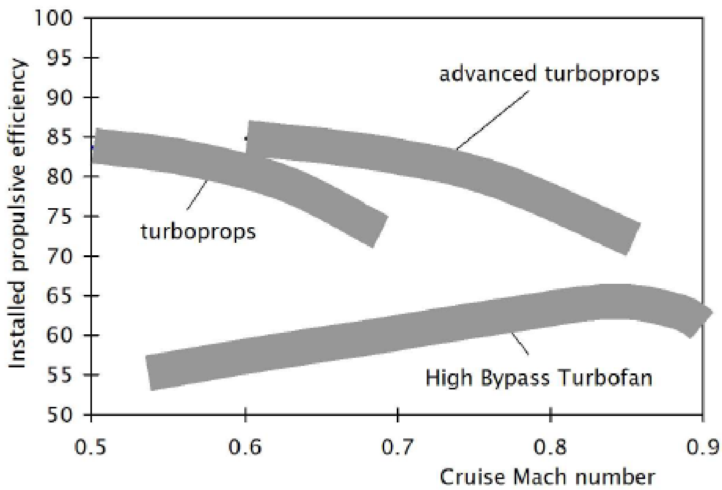

Figure 1.1: Aircraft engine efficiency comparison for different kind of engine types as a function of Mach number [3]

Most conceptual design techniques for vertical tail design are still based on semi-empirical relations, where the United States Air Force Data Compendium (DATCOM) is used the most frequently [4]. These semi-empirical relations are derived from windtunnel measurements by the National Advisory Committee of Aeronautics (NACA), who performed windtunnel measurement from the 30's to the 50's [5]. These measurements were performed on aircraft configurations and geometries different from current turbo-prop aircraft geometries, making these methods outdated and giving a preliminary design estimation which does not necessarily match the turbo-prop aircraft. Lots of geometries were tested, i.e. rectangular, elliptical and swept wings, symmetrical and unsymmetrical airfoils, slender bodies with rounded or sharp edges, tails of different aspect ratio and size [6][7][8][9][10]. Performed tests dealt with geometries quite different from the actual transport aircraft, being more similar to World War II fighter aircraft [11][12]. In fact most of the work of the NACA was pushed by war and the aim of the early tests was to gain a certain knowledge on the physics of the problem of directional stability and control.

The traditional use of these semi-empirical relations in the preliminary design of multi-engine propeller aircraft has resulted in considerable safety factors and possible over-dimensioning of the vertical tail, due to limited understanding of the effects driving the design.[13] This over-dimensioning leads to an increase of drag and weight of the aircraft, which decreases its efficiency and increases operating costs. Improving the vertical tail design can, however, only be done while keeping safety of the aircraft in mind. For this reason, more knowledge is required of the effects of the propeller slipstream on the vertical tail and how the tail sizing process can be improved by including these effects.

The vertical tail design is driven amongst others by the critical condition of one engine inoperative in take-off conditions, where the high power setting has a significant influence on directional stability and control. This has already been addressed by Raymer[14]: "Wing mounting of engines introduces engine-out controllability problems that force an increase in the size of the rudder and vertical tail." and Torenbeek[15]: "The yawing and rolling moments induced by engine failure present control problems and downgrade the flight performance, in particular when the engine fails in the takeoff." For this reason the focus will be especially on the directional stability derivatives in the One Engine Inoperative (OEI) condition.

The function of the vertical tail is to provide directional stability to the aircraft. This is done by generating a restoring moment when a perturbation of a stable condition occurs. The vertical tail is a lifting surface, like a wing, generating lift under a sideslip angle. The lift generated, a side force with respect to the aircraft, is dependent on the shape of the vertical tail itself. Additionally the vertical tail is strongly dependent on the aircraft configuration since the interference effects of other aircraft components (wing, fuselage and horizontal tail) have a strong influence on the effectiveness of the vertical tail and the flow it experiences [5][14].

When analysing the currently most used turbo-prop aircraft, it can be noticed they consist of different wing and empennage configurations. While most turbo-prop aircraft use a high wing configuration, because of the ground-clearance of the propeller [14], also low wing turbo-prop aircraft are being manufactured. The empennage configurations differ also widely: most high wing aircraft use a T-tail configuration, to clear the horizontal tail out of the propeller-wing wake but also turbo-prop aircraft have been made with a conventional tail (Fokker 50). Finally the vertical tail itself has different aspect, taper ratios and can consist of a dorsal fin. Examples of four widely used turbo-propeller aircraft are given in Figure 1.2. From the figure it can be seen that the aircraft vary in configuration and especially the empennage configuration. Because the propeller is mounted in front of the wing, in close vicinity of the fuselage the propeller slipstream affects the interference effects, changing the spanwise pressure distribution and the sidewash at the vertical tail.

(a) (b) (c) (d)

Figure 1.2: Four common used turbo-prop aircraft in civil aviation: (a) ATR 72, (b) Fokker 50, (c) Fairchild Swearingen Metroliner, (d) Bombardier Dash 8

Extreme flight conditions often set severe design requirements for tail surfaces. Examples for this are minimum control speed with One Engine Inoperative (OEI) or maximum cross-wind aircraft capability: stability and control must be ensured even for very large angles of sideslip, up to 25 degree. These requirements are stated by the Federal Aviation Authorities (FAA) and by the European Aviation Safety Agency (EASA). These requirements are crucial for all twin-engine commuter aircraft because all the ground performance are strictly related to the minimum control speed (V_{M_C}) which mainly depends from the engine failure speed (V_{E_F}), clearly related to vertical tail design. As a matter of fact CS-25 of the aircraft regulations relates the certification speeds to the V_{M_C}.. Finally a performance improvement also means the commercial success of an aircraft, given the capability to be more competitive in several scenarios respect to competitors.

One of the major problems found during the literature study was that most models concentrated on the correct modelling of the propeller forces and moments, assuming an undisturbed propeller slipstream behind the propeller, [16] [17] [18]. Other models that include the wing, neglect the slipstream deformation and swirl recovery due to the wing or the rotation of the slipstream completely [19], [20]. Others have incorporated the propeller slipstream with the wing and include the rotational effects [21], using a lifting line approach to estimate the propeller/wing interaction. It is interesting to have a simple method to estimate the lift over the wing however the position of the slipstream and the shape and strength at the empennage are not known.

Possible of the shelf solutions e.g. Tornado, a Vortex Lattice Method for linear aerodynamic wing design applications in conceptual aircraft design or in aeronautical education, don't allow for the modelling of the propeller and focus on the wing and fuselage lift distribution. The same was found for VSAERO, the tool now used extensively within the aerospace department. VSAERO couples integral methods of potential and boundary layer flows for low runtimes. Again because of the lack of the possibility to model the propeller-wing interaction and because the program has a non-modular structure, it was no option to use within this research project.

The main problem regarding this research and the reasons why semi-empirical methods are still widely used in the preliminary design phase is the following: the combination of the fuselage wing and propeller create a very complex flow structure which is difficult to predict accurately with a numerical model [3]. The fuselage and propeller influence the lift distribution over the wing and at the same time the wing influences the flow with respect to the propeller and fuselage. Secondly, a complex vortex field is created behind the wing, consisting of the vortex field created by the wing, propeller and fuselage. Thirdly there is the requirement that the computational time has to be low for a conceptual design tool. The analysis of the directional stability derivatives is only a small piece of information in the complex process of designing a complete aircraft. Therefore the analysis should be quick and have to provide sufficient accuracy within a short time limit, leaving higher order CFD analysis out of the options.

These three requirements are therefore creating a contradiction: on one hand a complex flow structure has to be modelled, requiring extensive computational power and on the other hand this has to be done within a limited computational time. This contradiction also created a challenge during this research, being able to link a complex aerodynamic analysis to the conceptual vertical tail design of a propeller aircraft.

In the recent past renewed research has been performed within the Flight Performance and Propulsion group at Delft University of Technology. The modelling is be based on a potential model developed by A. van Nispen which is later expanded by M. Schroijen [22] [23]. The model allows to calculate the propeller slipstream effects on the lift and drag distribution over the wing and fuselage. Additionally the tool can predict the vortex field created by the wing, fuselage and the propeller. Finally it allows for calculation of the forces and moments working on the fuselage, wing and the vertical tail. In this research this model is again being put operational by creating a Matlab program. The model was validated and accurate results where found, proving the model could be used for simulations. Its modular code, build up with different Matlab function files, allows for expansion of the program. Therefore it was adapted to use and expanded within this project.

Summarising the problem statement and motivation for this research:

1. Vertical tail design in the conceptual design phase is based on semi-empirical relations based on windtunnel measurements with aircraft geometries different from turbo-prop configurations and geometry parameters.

2. The generated sideforce of the vertical tail under a sideslip angle is strongly affected by the configuration of the aircraft, due to the interference effects of the wing, fuselage and horizontal tail.

3. The propeller slipstream has a significant effect on the directional stability of the aircraft especially in OEI conditions.

4. Slipstream effects are not or barely taken into account in the conceptual design phase only a few semi-empirical relations obtained by Mannée are currently available in open literature.

5. No low-fidelity analysis tools are available in open literature predicting the slipstream effects on the aircraft directional stability due to the complexity of the flow field.

Leading to the main research question:

Can a potential flow model be used to improve the vertical tail design in the conceptual design phase by predicting the directional stability derivatives for various propeller aircraft configurations under the influence of a propeller slipstream?

This main research question is decomposed in the following sub-questions:

Can a potential flow model accurately predict the sideforce coefficient of the vertical tail for various aircraft configurations and conditions (without the effects of the propeller slipstream)?

Can a potential flow model be used to analyse how the propeller slipstream influences the sideforce coefficient of the isolated vertical tail and the interference effects created by the fuselage, wing and horizontal tail on the vertical tail?

Can a potential flow model be used to analyse how the propeller slipstream affects the aircraft directional stability derivatives for various aircraft configurations and conditions?

1.2. RESEARCH OBJECTIVE

Being able to predict the effects and therefore have an accurate analysis of the vertical tail effectiveness under the influence of the propeller slipstream will be a first step for a more efficient vertical tail design for propeller aircraft in the conceptual design phase. To improve the vertical tail design for propeller aircraft in the conceptual design phase the objective for this research is:

To analyse and identify the effects of the propeller slipstream on the aircraft directional stability derivatives for different aircraft and empennage configurations by expanding and using a potential flow model.

This objective may be decomposed into several goals which are to be fulfilled throughout the research:

1. To verify and validate the sideforce coefficient of the isolated vertical tail under a side slip angle predicted by the potential flow model and the interference effects of the fuselage, wing and horizontal tail on the vertical tail effectiveness.
2. To verify and validate the side force coefficient of the vertical tail under a side slip angle predicted by the potential flow model for different aircraft configurations and conditions without the propeller slipstream effects.
3. To analyse and identify how the propeller slipstream affects the aircraft directional stability derivatives by assessing the propeller slipstream effects on the isolated vertical tail and on the interference effects on the installed vertical tail .
4. To analyse how the propeller slipstream affects the directional stability derivatives for various complete aircraft configurations and conditions.

1.3. RESEARCH SCOPE

To evaluate how the propeller slipstream affects the directional stability of the aircraft for various configurations, a parametric approach has been used for this research. First the sideforce coefficient of the vertical tail is evaluated without the propeller slipstream effects. To be able to verify and validate the potential flow model, the isolated vertical tail and the aerodynamic interference effects of the fuselage, wing and horizontal tail on the vertical tail will be individually evaluated. The importance of this analysis is twofold: first it shows the potential flow can accurately predict the sideforce of the isolated vertical tail and the interference effects of the different components and therefore it can accurately predict the sidefoce and yawing moment of the installed vertical tail. This functionality would already be an improvement to the current design process: the model allows to accurately predict the directional stability derivatives of the actual aircraft geometry where the semi-empirical relations use an approximation of the geometry. Secondly this analysis is important to have a reference, to study how the propeller slipstream affects the directional stability and the vertical tail effectiveness. The results of this step will be validated using the measurements of Della Vecchia who used a RANS solver.

To evaluate how the propeller slipstream influences the side force coefficient of the vertical tail and the yawing moment of the aircraft the same parametric approach is used. Doing so it can be specifically assessed what parameters and configurations are influenced by the propeller slipstream. Finally the propeller slipstream effects on the complete aircraft configuration are analysed. To simulate the One Engine Inoperative (OEI) conditions, only one propeller was installed on the aircraft at high trust setting. This is the critical condition that will drive the vertical tail design and is also the condition where the propeller slipstream effects are the most prominent because of the low speed and the high thrust coefficient.

Three effects influencing the vertical tail design were left out of scope for this research: because the model is only able to simulate inviscid flow it is not possible to simulate viscous effects. For this reason it is not possible to determine the aircraft maximum sideslip angle which is critical in the design [15].

Next, the effect of flaps is left out of scope. In the past a lot of effort was put to model the flaps however it was found the results were to inaccurate to use for the simulations. It is known from literature that the flaps can have a significant influence on the vortex field and the sidewash created at the vertical tail [24]. Finally the rudder is not modelled, which has a significant influence on the vertical tail design. The rudder, which function it is to provide the aircraft with directional control is not modelled, leaving the rudder effectiveness outside the scope of this research. The rudder design focuses on conditions where a large rudder deflection is required, creating viscous effects which can not be modelled accurately using a potential flow model.

1.4. REPORT OUTLINE

The report will first consist of an extensive overview of the background information regarding vertical tail design, its function, the requirements and current design methods, elaborated in Chapter 2. Chapter 3 will give an extensive elaboration of the propeller effects on the wing and vertical tail. How the propeller slipstream is formed and how it is affected by different parts of the aircraft.

Chapter 4 will present the model used for this research. An concise overview of the modelling techniques will be presented together with the expansion of the model. Chapter 5 will present the validation and a sensitivity analysis of the model to determine the amount of panels needed for the various parts of the aircraft. Chapter 6 gives an overview of the aircraft model used and of the configurations and conditions it is used for. The parametric analysis used for the obtain the results is explained.

Chapter 7 and 8 present the results and discussion of the parametric analysis. The results obtained without the propeller installed are presented in chapter 7 and with the propeller installed are presented in chapter 8. Finally the conclusion and recommendations are given in Chapter 9

2
CONCEPTUAL VERTICAL TAIL DESIGN

How is the vertical tail currently designed in the conceptual design phase and why? This will be elaborated upon in this chapter, in order to understand the short comings of the current design process for propeller aircraft. First the functions and driving requirements of the vertical tail will be discussed. Next the current conceptual design process of the vertical tail will discussed. Secondly the DATCOM method and the VeDSC method will be elaborated. The DATCOM and the VeDSC method will be applied to a Fokker 50 and ATR 42 aircraft to obtain the directional stability derivatives which will be later be used in the results section for comparison with the results of the potential flow model. Finally the current vertical tail design tool in the Initiator of the Flight Performance and Propulsion group will be discussed.

2.1. BACKGROUND VERTICAL TAIL DESIGN

The vertical tail is designed to give the aircraft lateral-directional static and dynamic stability and control and trim during all flight conditions. Vertical tail is a symmetric profile which is designed to create a restoring moment under a sideslip or a yawing moment when a rudder input is given. Rudder trim is used in one engine inoperative conditions to trim the aircraft for the new asymmetrical condition. The rudder design is directly related to the design of the vertical tail since it limits the height of the rudder. Maximum rudder input is required for cross wind landings, one engine inoperative conditions at low speeds and spin recovery. The size and the type of rudder as well as the type of vertical tail define its effectiveness.
The requirements for vertical tail design are: [14][15][25]

- Provide sufficient static and dynamic directional stability: Provide a force sufficient to balance the total tail-off forces
- Tail plane should not stall at high angles of attack

Requirements for the rudder are:

- To provide sufficient directional control capability, up to high sideslip and rudder deflection angles. According to the European Aviation Safety Agency (EASA) CS-25, the aircraft must be able to [26]:
  - Keep heading and manoeuvre in one engine inoperative conditions. The minimum control speed in flight, V_{mc_a} should not exceed 1.2 times the stall speed of the aircraft, V_s. The necessary rudder deflection should not exceed 25 degrees so that additional rudder deflection is possible to allow for manoeuvring.
  - Perform crosswind landings up to 30 knots or 55 km/h.
- Provide a means for achieving a steady state equilibrium (trim).
- Provide a means of counteract for disturbances, e.g. gusts.
- To have low control forces.

2.1.1. VERTICAL TAIL DESIGN PROPELLER AIRCRAFT

The only semi-empirical relations currently available in open literature regarding the influence of propeller slipstream effect, are based on the findings of J. Mannée in the Aeronautical conference of 1962 [24]. In this technical report he describes his findings for multi-engine propeller aircraft with one engine inoperative and the influence on the yawing moment of the aircraft. It is found that for propeller aircraft as compared to jet aircraft the rudder has to be a factor 'k' larger for the same configuration and thrust level. This factor k is dependent on empirical relations and changes with configuration changes of the vertical position of the wing and position of the engines. For the various design methods this factor k is however not mathematically explained but derived from empirical test conducted for various configurations. For a propeller aircraft the yawing moment N created is a factor k larger:

$$N = k \cdot T dy \tag{2.1}$$

Where dy is the distance between the propeller axis and the fuselage centre line. the k factor is introcuced to take into account the propeller slisptream effects. Mannée explains this k factor in his report: 'the propeller in front of a wing creates locally an increase in dynamic pressure over the wing which causes an increase in lift. Additionally the propeller changes the angle of attack at the leading edge of the wing, causes it to give increase in angle of attack and lift at up-going blade and decrease in angle of attack and lift in down-going blade. These trailing edge vortices create a strong sidewash at the vertical tail'. This will be elaborated upon in detail in chapter 3. Further it is described that the k factor is not only dependent on the rotation of the blades but also on the position of the wings and the flap setting of the aircraft. The flaps have a large influence since, the lift and therefore the vortex created is much stronger, increasing the sidewash at the tail.

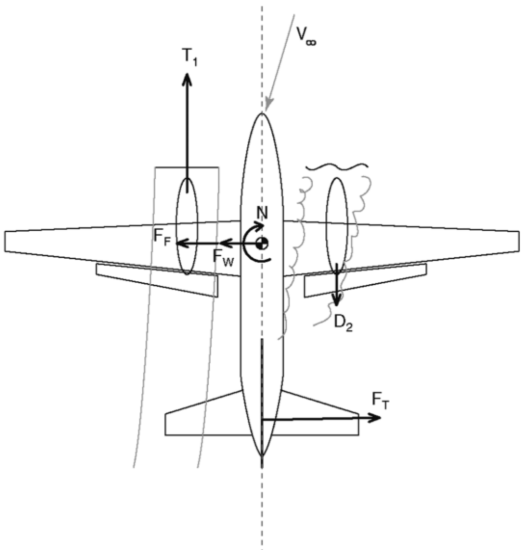

Figure 2.1: One engine inoperative conditions for a propeller aircraft including the basic forces and moments

For a propeller aircraft with one engine inoperative in take off conditions this effect is the largest, a high thrust thrust is selected with a low aircraft speed leading to a high thrust coefficient, and flaps for take-off are selected. During this situation the aircraft must a least be able to maintain its V_{mc_a} which is the minimum in flight control speed also called blue line speed (indicated by a blue line on the airspeed indicator). Due to regulations this speed can not exceed 1.2 times the stall speed of the aircraft V_s [26]. In figure 2.1 an one engine inoperative situation is given to illustrate the different forces and moments created. The force created by the rudder deflection must be of sufficient strength to balance the moment created by the thrust of the operating engine and the drag created by the failed engine.

2.2. SEMI-EMPIRICAL METHODS - DATCOM

From the '30s to the '50s the US National Advisory Committee for Aeronautics (NACA) provided a significant amount of results on the directional stability on isolated vertical tail planes, partial and complete aircraft configurations obtained through many hours of wind-tunnel tests. These results were summed up in a new design procedure reported and described in the United States Air Force Data Compendium (USAF DATCOM) by Finck [5].

The investigations were focused on the attempt to separate the effects of fuselage, wing and horizontal tail from the isolated vertical tail. Lots of geometries were tested, from the early years to the '50s, i.e. rectangular, elliptical and swept wings, symmetrical and unsymmetrical airfoils, slender bodies with rounded or sharp edges, tails of different aspect ratio and size [8][7]. Performed tests dealt with geometries quite different from the actual transport aircraft, being more similar to World War II fighter aircraft. In fact most of the work of the NACA was pushed by war and the aim of the early tests was to gain a certain knowledge on the physics of the problem of directional stability and control and on the mutual interference among aircraft components. Later tests aimed to improve stability and manoeuvrability of high speed combat aircraft [6][7][8][9].

2.2.1. DATCOM METHOD

The USAF Stability and Control DATCOM was compiled between 1960 and 1978 by the McDonnell Douglas Corporation in conjunction with the engineers at the Flight Dynamics Laboratory at Wright-Patterson Air Force Base. It is a collection, correlation, and recording of knowledge, opinion, and judgement in the area of aerodynamic stability and control prediction methods. DATCOM provides methods for estimating basic stability and control derivatives for most flight conditions and configurations and in many cases can be used in conjunction with test data.

USAF DATCOM method is valid for low speed (subsonic) in cruise configuration (low angle of attack, low angle of sideslip) and does not account for flaps or engine effects. It uses the basic equation for a lift curve slope for tapered wing and then use different correction factors [5].

In the DATCOM method the sideforce derivative due to sideslip $C_{Y_{\beta v}}$ is effected by three interference effects on the lift curve slope: body-vertical tail (due presence of the fuselage at the root of the vertical tail it causes an end plate effect), horizontal tail surface interference and the wing-body wake and side-wash effect. The first two effects affect the effective aspect ratio of the vertical tail that has to be included in the lift curve equation, Equation 2.3. The wing-body wake and side-wash effect are directly incorporated in the side force coefficient as $\frac{d\sigma}{d\beta}\eta_v$. The interference effects are further explained in Section 2.2.2. .

$$C_{Y_{\beta v}} = -k_v C_{L_{\alpha v}} \left(1 + \frac{d\sigma}{d\beta}\right) \eta_v \frac{S_V}{S} \tag{2.2}$$

Where $\frac{d\sigma}{d\beta}$ is the sidewash and wing body wake-effect created by the wing and fuselage of the aircraft on the vertical tail which causes a deviation of the inflow at the vertical tail. The ratio $\frac{S_V}{S}$ is the ratio between the surface area of the vertical tail and the surface of the wing.

The basic equation is the definition of the lift curve slope for tapered wings proposed by Diederich [27] presented in equation 2.3.

$$C_{L_\alpha} = \frac{2\pi A}{2 + \left[\frac{B^2 A^2}{\eta}\left(1 + \frac{tan^2\Lambda_{c/2}}{B^2}\right) + 4\right]^{1/2}} \tag{2.3}$$

Where A is the aspect ratio of the vertical tail. B is the Prandtl Glauert compressibility correction factor which is equal to $B = \sqrt{1 - M^2}$. The parameter η is the section lift-curve slope of the theoretical thin-section value which is equal to $C_{l_\alpha}/(2\pi/B)$. The corrected aspect ratio has to be used to found using equation 2.4.

$$A_{V_{eff}} = \frac{A_{V_f}}{A_V} A_V \left[1 + K_{VH}\left(\frac{A_{V_{(hf)}}}{A_{V(f)}} - 1\right)\right] \tag{2.4}$$

Here $\frac{A_{V_f}}{A_V}$ is the ratio of the vertical tail aspect ratio in the presence of the fuselage to that of an isolated vertical tail.

$\frac{A_{V_{(hf)}}}{A_{V(f)}}$ is the is the ratio of the vertical tail aspect ratio in the presence of the horizontal tail and the fuselage to that of the fuselage alone.

The parameter K_{VH} accounts for the position of the horizontal tail. When the horizontal tail is present at a relatively high or low position with respect to the vertical tail, this increases the effectiveness of the vertical tail. This is called the endplate effect of the horizontal tail on the vertical tail lift curve slope. The endplate effect is larger (20%) in the case the horizontal tail is placed as a T-tail.[5]
Further elaboration of the effects of the fuselage, the wing position and the position of the horizontal tail can be found in Section 2.2.2.

2.2.2. AIRCRAFT INTERFERENCE EFFECTS ON VERTICAL TAIL

The effects taken into account in the DATCOM method, the fuselage, wing and horizontal tail interference effect on the vertical tail effectiveness will be further elaborated upon in this section. The explanation here of the different effects will also be used later on to explain the found results and the correction curves will be compared to those found using the potential flow model.

FUSELAGE EFFECT

The presence of the fuselage has two effects on the vertical tail. Firstly, the presence of the fuselage causes and end-plate effect on the installed vertical tail. The flow at the bottom side of the vertical tail is prevented at a side slip angle to flow from the higher pressure side to the lower pressure side. Increasing the effective aspect ratio of the vertical tail included in Equation 2.4.

Next the fuselage causes an increase in sidewash at the vertical tail as shown in figure 2.2. The sidewash increases from a component $Vsin(\beta)$ to $Vsin(\beta-\sigma)$. The flow around an isolated fuselage can be presented schematically as in figure 2.3. A positive angle of sideslip causes a negative induced sidewash, or ($\frac{d\sigma}{d\beta} < 0$). [28]. The sidewash effect of the fuselage is included in Equation 2.2 as $\frac{d\sigma}{d\beta}\eta_v$.

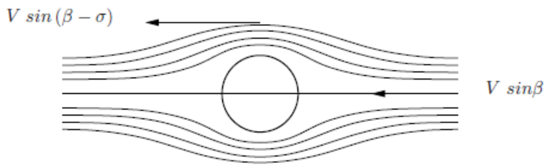

Figure 2.2: Flow around the isolated fuselage under a sideslip angle β [28]

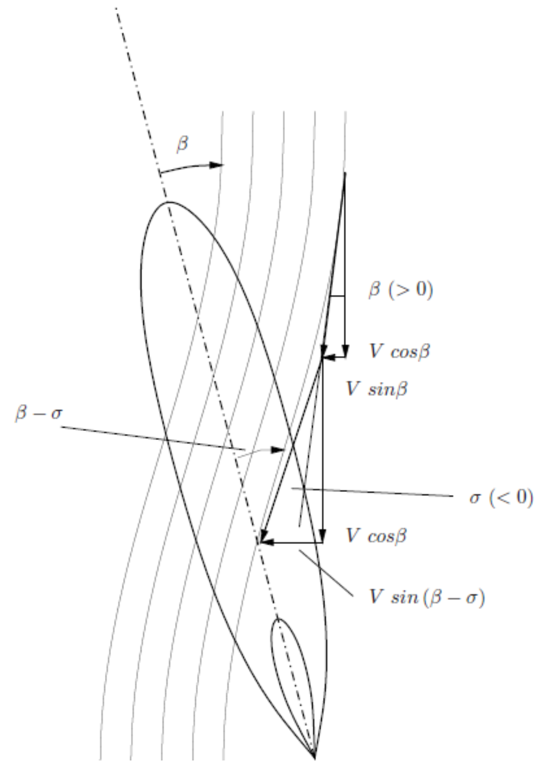

Figure 2.3: Increase in sidewash at the vertical tail due to the presence of the fuslage [28]

The correction factor obtained by Obert for the fuselage interference effect, used in the DATCOM method is presented in Figure 2.4. The complete document is added in Appendix A, together with the parameters used in the experiment.

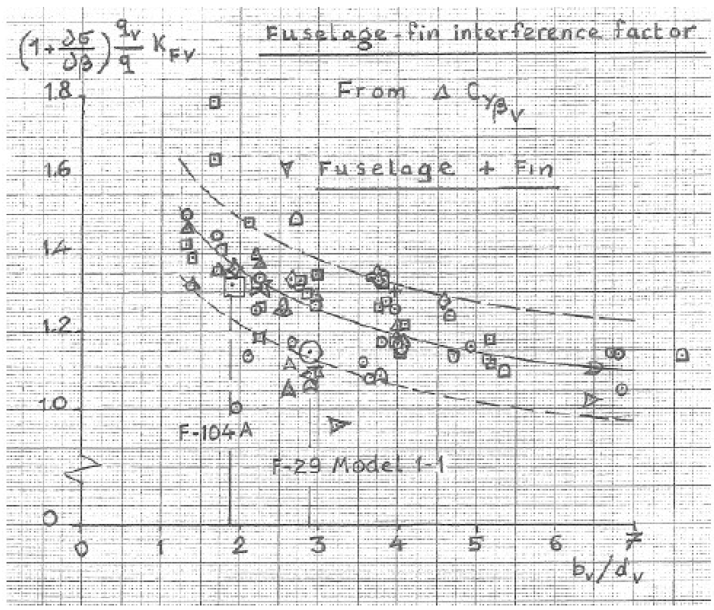

Figure 2.4: Fuselage interference effect on vertical tail updated by Obert [29]

In the figure the fuselage correction factor is plotted in function of the local thickness of the fuselage at the aerodynamic centre of mean aerodynamic chord of the vertical tail (see Appendix A for a sketch). The fuselage interference effect decreases as the fuselage becomes more slender. The local sidewash created decreases and therefore the correction factor decreases. This interference effect is later compared with the results in Section 7.2.

WING EFFECT

The wing fuselage combination has a significant effect on the vertical tail. When the fuselage-wing combination is set under a sideslip angle the position of the wing affects the lift and downwash distribution. Important for the way in which the lift distribution varies with angle of sideslip is the vertical position of the wing relative to the fuselage, see figure 2.5. The forward semi-wing of a low wing aircraft experiences a decrease in angle of attack due to sideslip. This produces a decrease in lift whereas the receding semi-wing experiences an increase in angle of attack and thus an increase in lift, due to the presence of the fuselage. For the low wing configuration the exact opposite happens.

The downwash pattern is displaced laterally along with the main flow, over an angle β with the X-axis, see figure 2.6. The main effect, however, is a circulation about the fuselage. If a low wing aircraft sideslips to the right, the circulation is counter-clockwise, figure 2.7. This circulation generates at the vertical tailplane a negative sidewash. This induced cross-flow is stabilising, generating an extra force to stabilise the aircraft. For a high wing aircraft in sideslip to the right, the sidewash is positive, the influence of the wing fuselage interaction is thus seen to be destabilising. The sidewash effect is included in the $\frac{d\sigma}{d\beta}\eta_v$ in Equation 2.2.

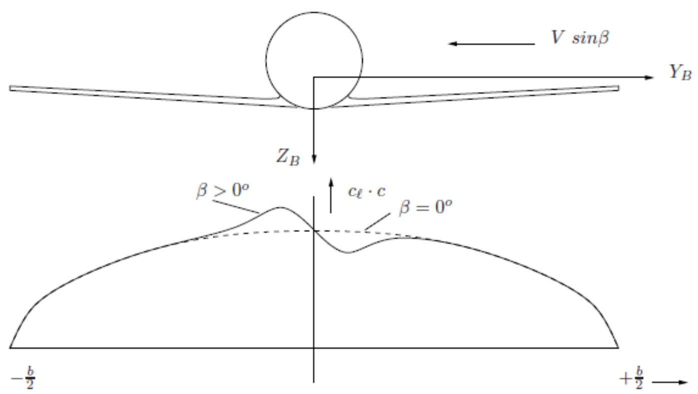

Figure 2.5: Change in lift and downwash distribution behind the wing and the fuselage due to a sideslip [28]

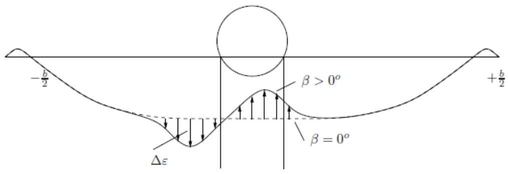

Figure 2.6: Change in lift distribution causes a shift in downwash for a low wing aircraft in side-slipping flight [28]

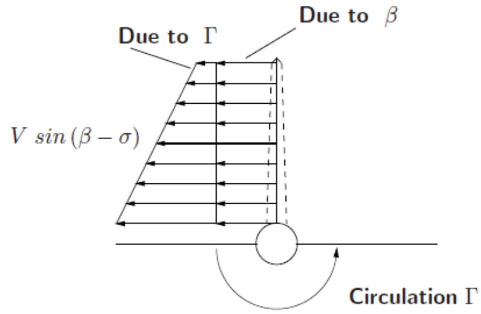

Figure 2.7: The effect of wing fuselage interaction on the sidewash at the vertical tailplane of a low-wing aircraft in sideslipping flight, increasing the effectiveness for a low-wing aircraft [28]

The correction factor for the wing interference effect obtained by Obert is presented in Figure 2.8, the complete document can be found in Appendix A. The correction factor is linear and equal in magnitude for the high and low wing. This correction curve will be later used for comparison between the DATCOM method and the results obtained.

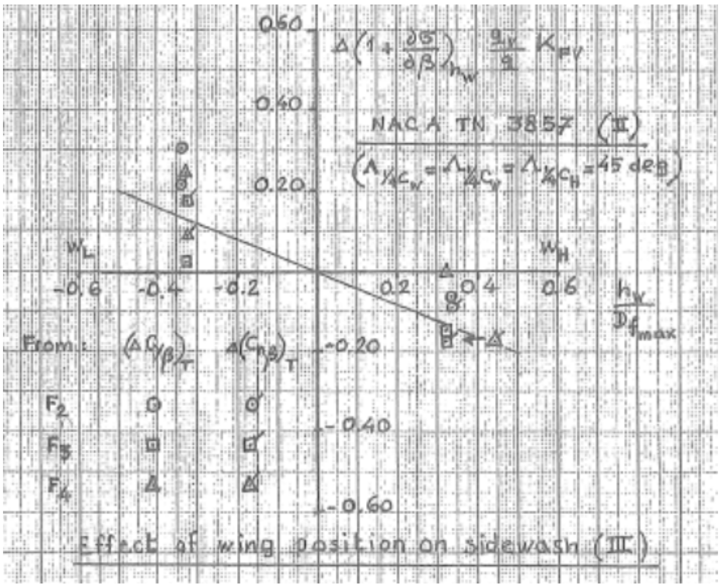

Figure 2.8: Corection curve for the wing effect obtained by Obert [29]

H-TAIL EFFECT

In the past, extensive research has been done regarding the end-plate effect of the horizontal tail on the vertical tail. The horizontal tail at the root or tip of the vertical tail works as an end-plate, obstructing the flow going from the higher pressure side to the lower pressure side and in doing so increasing the effective aspect ratio of the vertical tail [30] [5] [25].

The end-plate effect of the h-tail is significant, increasing the v-tail effectiveness at the root with approximately 10% depending on ratio of the horizontal tail surface to the vertical tail surface($\frac{S_h}{S_v}$) and up to 40% when the horizontal tail is installed as t-tail (at the tip of the v-tail). This can be seen in figure 2.9 where K_{vh} is the parameter as used before in the DATCOM method, to describe the factor of increase in effectiveness and zh/bv is the location of the horizontal tail.

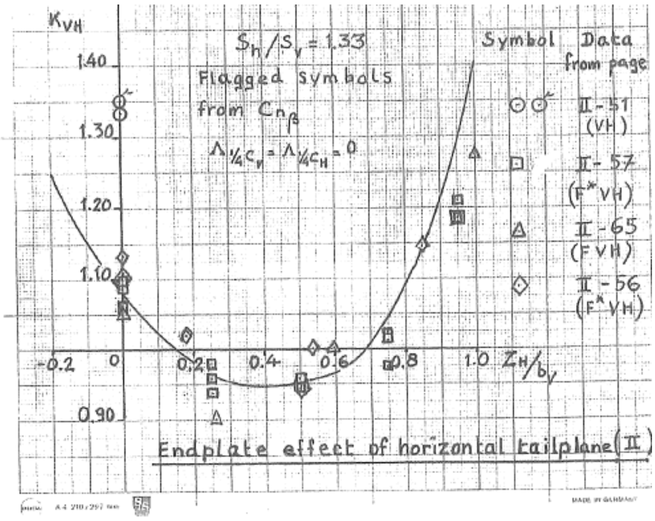

Figure 2.9: The interference effect of the horizontal tail on the vertical tail (K_{VH})

In literature it was also found that the endplate effect changes with the horizontal position of the h-tail compared to the leading edge of the V-tail.
It was found that when the horizon tail was located near the base of the vertical tail, the end-plate effect was increased by moving the horizontal tail rearward [31].

2.2.3. Application of DATCOM to Turboprop Aircraft

In order to compare, in the results of this research, two typical turboprop aircraft are analysed both by the DATCOM method. The ATR 42 and the Fokker 50 aircraft are taken as an example, for both aircraft the geometrical properties are analysed and the sideforce coefficient is calculated. Both aircraft can be seen in Figure 2.10 and Figure 2.11. For the Fokker 50 the vertical tail is assumed without the dorsal fin. Both aircraft have similar aircraft configuration properties: both have a high wing configuration and a comparable fuselage slenderness ratio. However the Fokker has a horizontal tail positioned at the bottom of the vertical tail while the ATR has a horizontal tail almost at the top of the vertical tail (T-tail configuration).

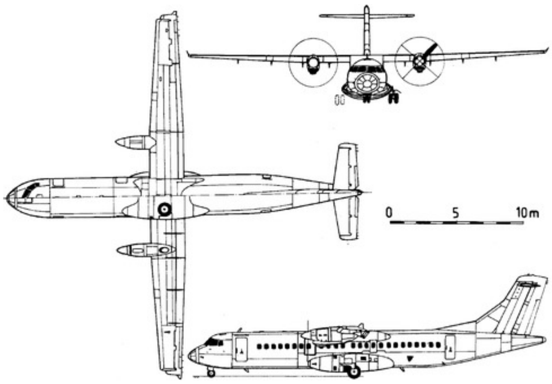

Figure 2.10: ATR 42 Dimensions

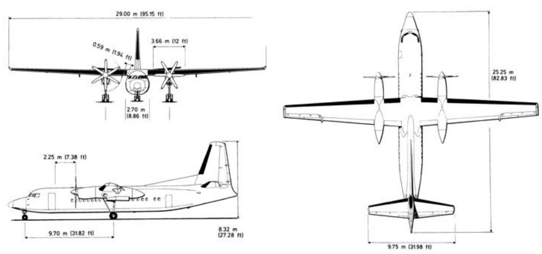

Figure 2.11: Fokker 50 dimensions

Aircraft	AR_V [-]	Λ_V [°]
ATR 42	1.6	23
F50	1.4	4

Table 2.1: Parameters influencing the $C_{L_{\alpha v}}$ curve of the vertical tail

In table 2.2 the tail derivatives can be found for the respective aircraft using the equations described above. Calculations are made for a low mach number, leading to a value of B(compressibility correction factor)=1. The lower aspect ratio of the Fokker in combination with the smaller sweep angle gives a lower $C_{L_{\alpha v}}$. For the $C_{Y_{\beta v}}$ the lower position of the horizontal tail in combination with the lower lift curve slope leads to a lower value of the derivative. The calculated values can be seen in table 2.2.

Aircraft	$C_{L_{\alpha v}}$ [rad]	$C_{Y_{\beta v}}$ [-]
ATR 42	2.243	0.669
F50	2.105	0.614

Table 2.2: Stability derivatives of the V-tail calculated using DATCOM method

2.3. VEDSC METHOD

In the recent past (2014) a new design method proposal, for conceptual vertical tail design has been made by Della Vecchia, in the Dept. of Industrial Engineering - University of Naples [32]. This new design method VeDSC, Vertical tail Design Stability and Control, is based on CFD analysis, obtained with more than 300 CFD Navier-Stokes analysis. Therefore it is suitable for regional turboprop and commuter aircraft in subsonic flow regime and cruise conditions [32] [33].

Using the CFD analysis, parametric analysis of several configurations are extremely useful for the correct estimation of aerodynamic interference among aircraft components and to highlight some useful trends that could indicate how a specific aerodynamic characteristics are linked to aircraft geometrical parameters. In his approach typical turboprop dimensions are used to focus the analysis on turboprop aircraft.

$$C_{Y_v} = C_{Y_{\beta_v}}\beta + C_{Y_\delta r}\delta_r \tag{2.5}$$

The sideforce coefficient is estimated by determining three correction factors which have a interference effect on the vertical tail.

$$C_{Y_{\beta_v}} = K_F K_W K_H C_{L_{\alpha_v}} \frac{S_v}{V} \tag{2.6}$$

For $C_{L_{\alpha_v}}$ the same equation is used as proposed by Diederich which is also used for the DATCOM method. Where K_F is the correction factor for the fuselage, K_W the correction factor for the fuselage and K_H is the correction factor for the horizontal tail. These correction factors have been determined by numerous CFD analysis determining the effects of each component on the vertical tail. Please visit the aforementioned literature to see how the correction are obtained and effect the vertical tail effectiveness.

In Table 2.3 the VeDSC method is applied for the two example aircraft for the calculation of $C_{Y_{\beta_v}}$ and is compared with the DATCOM results obtained in Section 2.2. Since the value for $C_{L_{\alpha_v}}$ is the same for VeDSC as for DATCOM only the $C_{Y_{\beta_v}}$ is presented for both methods.

	Aircraft	DATCOM	VeDSC	Δ
$C_{Y_{\beta v}}$ [-]	ATR 42	0.669	0.659	2 %
	Fokker 50	0.614	0.595	3 %

Table 2.3: Sideforce coefficient for the vertical tail calculated using the DATCOM and VeDSC method for the two example aircraft, the Fokker 50 and ATR 42

The difference between both methods is relatively small (2-3 %). This difference is mainly caused by the correction factor of the wing which is smaller for the VeDSC method for the high wing configuration of the ATR 42 and the Fokker 50.

2.4. CONCEPTUAL VERTICAL TAIL DESIGN INITIATOR

The **Initiator**, a modular design tool for preliminary sizing and design analysis, has recently been updated with a vertical tail sizing module designed by A.P. Hettema [34]. His goal was to develop a rapid aerodynamic analysis method for initial vertical tail design, based on semi-empirical relations using a optimiser to minimise the vertical tail size and weight. In his research the requirements that drive the vertical tail design can be subdivided into four requirements in three flight conditions.

The first requirement is a positive value for the yawing moment coefficient due to sideslip in all conditions ($C_{n_\beta} > 0$). For the cruise condition this is expanded to a goal value that should be met, which helps guide design until a full static and dynamic analysis has been performed. In his thesis the yawing moment coefficient, C_{n_β} is plotted against the Mach number for several classic jet engine and turboprop aircraft and a scattered plot is created. Next the value of C_{n_β} is chosen based on the design cruise mach number of the aircraft. Note that this requirement is in most conditions not the critical requirement. Also it should be noted here that it would also be more accurate if various scattered plots were made for jet-turbofan aircraft and for turboprop aircraft for different conditions. Finally there is no direct relation between the yawing moment coefficient due to sideslip and the cruise mach number of the aircraft. For this reason one could therefore argue if this is the correct approach to estimate C_{n_β}. An alternative for this approach would be to base the yawing moment coefficient on the MTOW of different aircraft and make separate plots for propeller and jet aircraft.

The second requirement in his thesis is the OEI condition at take-off. Here different drag factors are taken for the inoperative engine depending on the engine type (prop/jet). However propeller slipstream effects are not taken further into account in the complete model: how the effectiveness of the vertical tail changes under the different conditions, depending on which engine has failed. The third requirement is landing with maximum crosswind. The fourth requirement is for the vertical tail not to stall at the maximum sideslip angle.

In Conclusion, at this point the vertical tail design is based on statistical data and semi-empirical relations and almost no difference is made between the design process of a jet/turbofan and a propeller aircraft. The propeller slipstream effects in OEI conditions are not taken into account for the design of the vertical tail although it is known they have significant effects on the vertical tail effectiveness [25]. Updating the statistical data for propeller aircraft and include the propeller slipstream effects would improve the vertical tail design to a more tailored vertical tail design for a regional turbo-prop aircraft.

3
PROPELLER WING AND TAIL INTERACTION

When designing a multi-engine propeller aircraft one of the important aspects is the interaction between the propeller and the wing. Especially because modern designs incorporate high wing disk loading and increased number of propeller blades, this is to increase the cruise speed while keeping the noise production at a low level. This chapter will be elaborate upon the propeller characteristics and how the propeller influences the aerodynamics of the aircraft. A typical example of modern multi-engine high transonic propeller aircraft, the Airbus A400m, is given in figure 3.1.

Figure 3.1: Typical modern multi-engine propeller aircraft - Airbus A400M

Analysing the effects of the propeller, two major different aspects can be noticed. First , the high disk loading leads to high forces and moments on the propeller. These moments can lead to significant effects on the aircraft lateral, longitudinal and directional stability and control. Next to the moments, the propeller slipstream with high kinetic energy influences other parts of the aircraft, especially the effectiveness of the horizontal and vertical tail. This influences again the longitudinal, directional and lateral stability of the aircraft.

The high swirl velocities in the slipstream of the propeller, which follow from the high disk loading, will generate a large deformation on the lift distribution over the wing, which influences the aerodynamic behaviour and performance of the wing. Additionally, the high speed slipstream can lead to adverse effects in transonic operating speeds. Compressibility effects between the slipstream and other aircraft parts can negatively affect the aircraft aerodynamic performance.

These effects largely influence the aircraft design. For this reason, this chapter focuses on the effects of the propeller slipstream on the wing lift distribution and the directional stability of the aircraft. When a propeller configuration is chosen with the resulting propeller slipstream, the wing performance and the stability and control of the aircraft needs to be optimised. Therefore a detailed anal-

ysis of these phenomena which are closely related, is of high importance.
First the propeller forces and moments will be explained together with the main characteristics of the propeller slipstream. Next the effect of the slipstream on the wing and the vertical tail will be discussed.

3.1. PROPELLER FORCES AND MOMENTS

The main force created by the propeller is the thrust force, which gives the propulsion to the aircraft. However there is also a normal force and a torque which is generated by the propeller. When the propeller is in a non-zero angle of attack, forces and moments are generated in all three axes. The normal force gives a contribution to the aircraft lift coefficient and has a significant influence on the stability of the aircraft. The moments created are fairly small however for example in the case of OEI conditions, the moments gives a contribution to the moment created by the failed engine. It can have a significant influence when for example making a turn over the non-operative engine.

3.2. CHARACTERISTICS OF PROPELLER SLIPSTREAM FLOW

This section gives an overview of the important characteristics of the propeller slipstream, which will be used later when the modelling will be discussed. In the following subsections the main characteristics will be further explained. A simplified and often used way of representing the propeller is to see the propeller as an advancing rotating wing creating a helical vortex system.
The vortex system produces self induced velocities and the vortex wakes tend to roll up which produces a slipstream tube with strong gradients in various flow quantities in streamwise and radial direction.
The most important quantities that characterise the slipstream are listed below and will be discussed in the following subsections:

- Axial velocity profile
- Swirl velocity profile
- Pressure distribution
- Vorticity
- Helicity
- Contraction

VELOCITY PROFILE

The local velocity anywhere in the stream can be written as a vector of the forces in the 3 axes.

$$\overrightarrow{V} = \begin{pmatrix} v_x \\ v_y \\ v_z \end{pmatrix} = \begin{pmatrix} u \\ v \\ w \end{pmatrix} \tag{3.1}$$

In this notation the axial flow is the v_x component of the velocity vector. Because of the changing loading over the blade and a strong gradient in spanwise direction a maximum value is found around $\frac{3}{4}R$. An example of an axial flow distribution for a propeller with low disk loading is given in figure 3.2.
Regarding the axial flow component, it increases in streamwise direction as a result of the increased length of the vortex system at the particular reference location, see figure 3.3. This is especially important when looking at the interaction between the propeller and the wing and designing the distance between both.

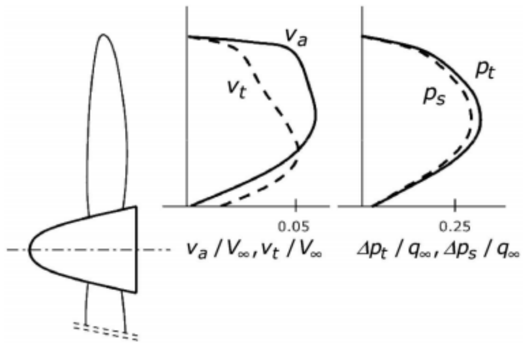

Figure 3.2: Example of axial velocity, swirl and pressure distribution for a propeller with low disk loading [3]

.

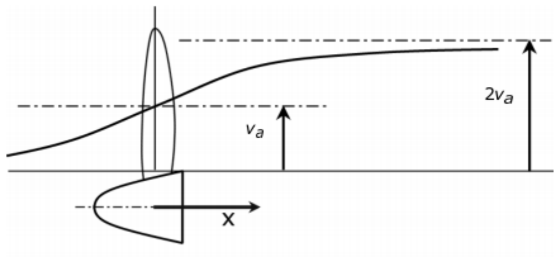

Figure 3.3: Propeller typical streamwise axial velocity increment [3]

.

3.2.1. SWIRL VELOCITY PROFILE

The tangential induced velocity is called the swirl velocity and can therefore be written as, $v_t = \sqrt{u^2 + w^2}$. A simplified representation of the swirl velocity profile is given in figure 3.4. It is found that the bound vortices , attached to the propeller blades, induce no axial velocity in the slipstream.

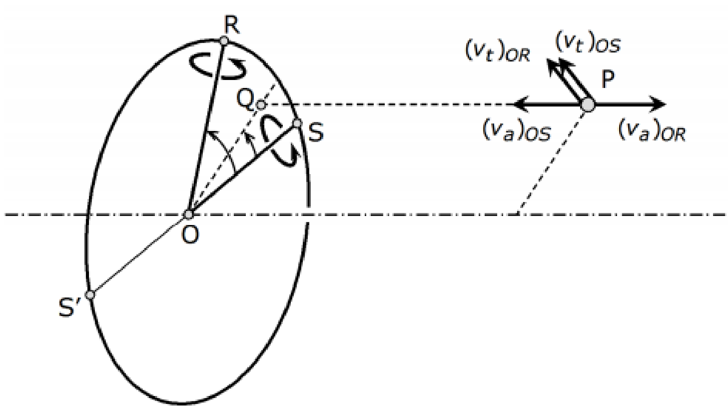

Figure 3.4: Axial and tangential velocities induced by propeller blade bound vortex[3]

.

The distribution in axial direction of the tangential velocity due to both the bound vortex system and the free vortex system is sketched in figure 3.5. By adding the effect of both systems, we see that the tangential velocity component is zero everywhere in front of the propeller; its value is w in the propeller plane and becomes 2w far behind the propeller.

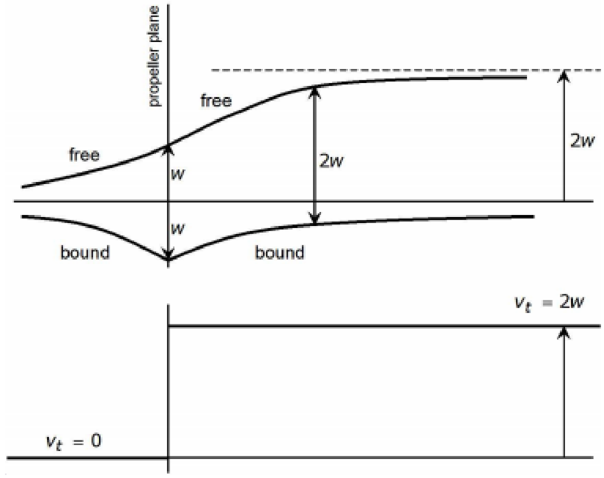

Figure 3.5: Tangential velocity distribution in the axial direction [3]

.

The swirl angle, depends both on the axial and tangential velocity component in the slipstream. The swirl angle is given in equation 3.2.

$$\theta_{sw} = tan^{-1}(\frac{v_t}{V_\infty + v_a}) \tag{3.2}$$

Looking at this equation, knowing that the axial component stays constant and the tangential does not, the swirl angle at the location of the wing becomes dependent on the distance between the propeller and the wing.

PRESSURE DISTRIBUTION

Both static and total pressure rise discontinuously across the propeller disk. The static pressure reduces to its free stream value toward infinity whereas the total pressure remains constant behind the propeller, this is sketched in figure 3.6. The small difference between the static pressure and the total pressure rise at the location of the propeller disk can be attributed to the rotational motion. The relation to the total pressure jump with respect to the static pressure jump in the propeller plane is given in equation 3.3.

$$(p_t)_s - (p_t)_\infty = \Delta p + \frac{1}{2}\rho v_t^2 \tag{3.3}$$

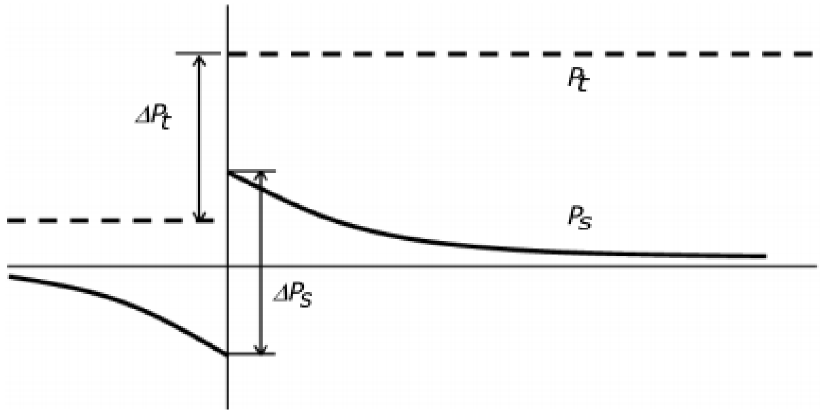

Figure 3.6: Pressure distribution along the wake of the propeller, increase of total pressure when crossing the wake. Static pressure decreases gradually back to free stream pressure [3]

.

The increase in total pressure can therefore be seen as the jump in static pressure with a contribution due to the rotational velocity caused by the propeller. Looking at equation 3.3, the small term, $\frac{1}{2}\rho v_t^2$ represents the kinetic energy of the rotational motion imposed to the fluid by the torque of the propeller.

3.2.2. VORTICITY / HELICITY

Mathematically, the **vorticity** of a three-dimensional flow is a pseudovector field, usually denoted by ω, defined as the curl or rotational of the velocity field V describing the continuum motion.

$$\omega = \nabla \times V = \begin{pmatrix} \omega_x \\ \omega_y \\ \omega_z \end{pmatrix} = \begin{pmatrix} \xi \\ \eta \\ \zeta \end{pmatrix} \tag{3.4}$$

The vorticity gives an important insight of the rotational character of the flow. The vorticity of the flow is dependent on the position of the blade in time and the blade loading.
Helicity is the dot product of the vorticity vector and the velocity vector.

$$h = \omega.V = u\xi + v\eta + w\zeta \tag{3.5}$$

Due to the characteristics of the dot product it is a measure for the alignment between the vorticity vector and the velocity vector.

3.2.3. CONTRACTION

The contraction of the propeller slipstream is caused by the velocity increase induced by the propeller slipstream. The reason for the contraction is to preserve the mass flow of the of the slipstream, as the velocity is increased through the propeller disk. It is found that the contraction is only a few percentage of the original diameter of the slipstream [35]. Only for propellers with high disk loading the slipstream contraction effect is significant when analysing the propeller slipstream. The equation according to Theodorsen and Crigler for the contraction over a distance x can be approximated as [36].

$$R(x) = R\sqrt{\frac{1+a}{1+a\left(1+\frac{x}{\sqrt{R^2+x^2}}\right)}} \tag{3.6}$$

For the fully contracted slipstream, R_∞, this equation becomes:

$$R_\infty = R_p \sqrt{\frac{1+a}{1+2a}} \tag{3.7}$$

It should be noted that this equation is only valid for a freely contracting slipstream. In figure 3.7 an example is given for the contraction effect, where A is original diameter of the slipstream and B is the contracted one.

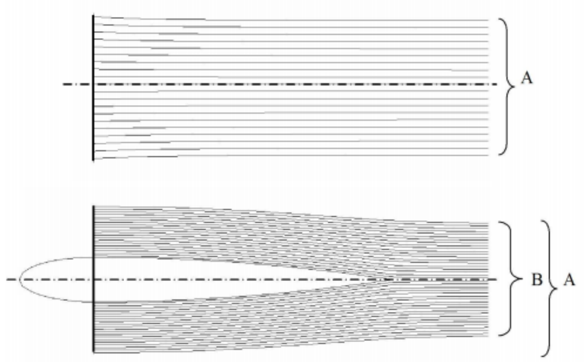

Figure 3.7: Contraction of the propeller slipstream [3]

.

3.3. PROPELLER SLIPSTREAM EFFECTS ON WING

In this section the effects of the propeller installed in front of a wing will be discussed, which is the case for most turbo-prop aircraft. As discussed earlier, for the un-installed propeller, the region behind the propeller will be affected by the propeller slipstream which induces an increase in axial velocity and a swirl component. Of course, the larger the propeller and the disk loading, the more significant the effect on the wing will be.

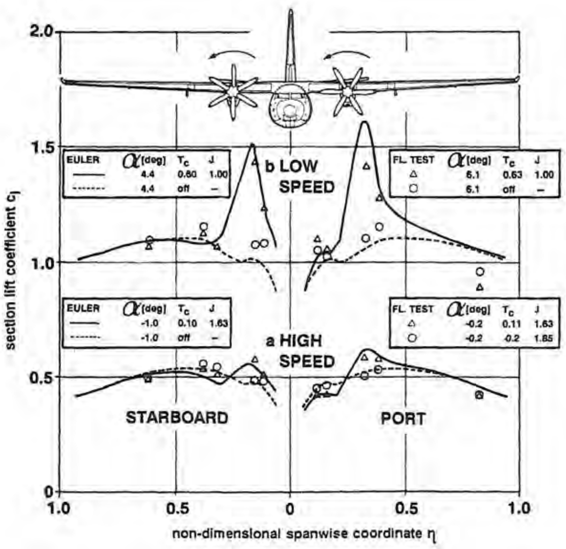

Figure 3.8: Effect of the propeller slipstream on the section lift coefficient for the F27, Fokker Friendship [37]

.

In figure 3.8 the effect of the slipstream on the wing lift distribution is given for a Fokker Friendship, F27. It can be clearly seen from the figure that the situation for the left and the right wing is not identical, especially when the speed is low and therefore the thrust coefficient is high. This is due to that the starboard propeller is turning inboard up, while the port propeller is turning outboard up. The slipstream will also affect the flow pattern outside the slipstream and therefore affects other parts of the wing as well.

The axial velocity increase results in an increased dynamic pressure, this will not change the local lift and drag coefficient of the airfoil itself, but will drastically increase the local forces and moments. As discussed in section 3.2, the axial velocity distribution along the propeller is not constant and maximum at $\frac{3}{4}$. The vertical distance plays therefore an important factor, since it depends how much the wing is affected by the changing axial velocity profile. Also in the axis of the axial velocity the velocity increases with distance behind the propeller, see figure 3.3, and the axial distance between the propeller and the wing is therefore and important parameter. The effect of the axial velocity increase by the propeller on the local lift distribution is sketched in figure 3.9. Both on the inboard and outboard side of the propeller an increase in local lift coefficient is present.

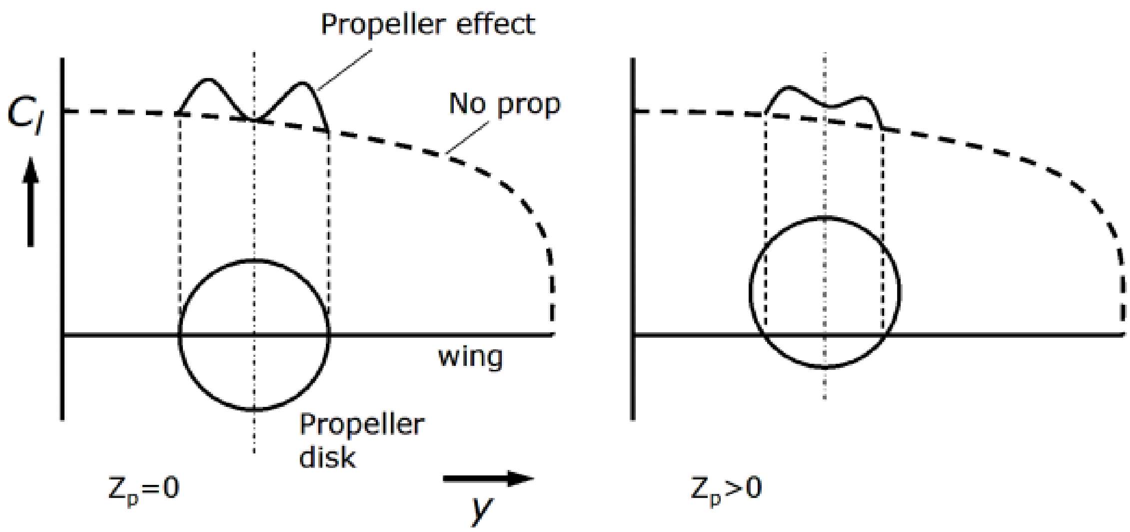

Figure 3.9: Effect of the axial increment of the velocity over the wing on the local lift coefficient. Left situation gives the propeller right in front of the wing while the right gives a situation for a high propeller position [3]

.

The other component, the swirl component of the slipstream, results in a non symmetrical effect on the wing lift distribution, this is sketched in figure 3.11. The up going blade will create an upwash over the wing submerged wing and this will result in a higher effective angle of attack and therefore a higher lift coefficient. The down going blade will have the exact opposite effect, the downwash created will result in a lower effective angle of attack and therefore a lower local lift coefficient. For this reason it's completely dependent on the direction of rotation of the propeller, this also leads to the non symmetrical lift increase for the F27 in figure 3.8

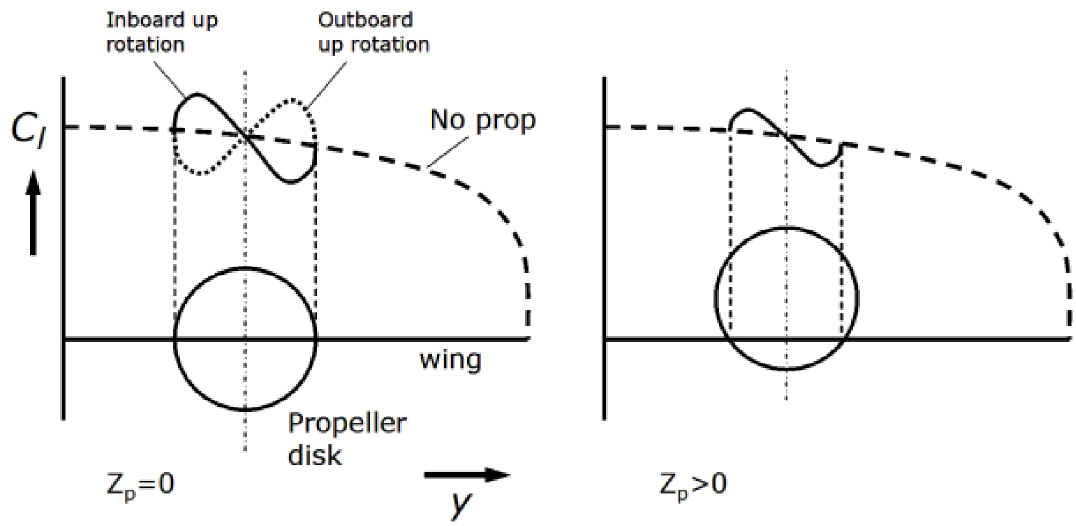

Figure 3.10: Effect of the axial increment of the velocity over the wing on the local lift coefficient. Left situation shows the propeller right in front of the wing while the right shows a situation for a high propeller position [3]

.

Finally when now these 2 effects are combined and taking the effects outside of the propeller slipstream into account, the lift distribution over the wing becomes a bit more complicated. Outside the propeller slipstream, the flow is affected by the upwash and downwash created by the propeller. This is because of the wing inflow conditions which have changed by the propeller. The lift distribution is largely effected by the propeller and this is especially the case for high thrust coefficients. In the case where the wing is under high wing loading the effect of the upwash creates a positive effect on the total lift of the aircraft, while for the case of a inside down propeller it causes a decrease of the performance of the wing.

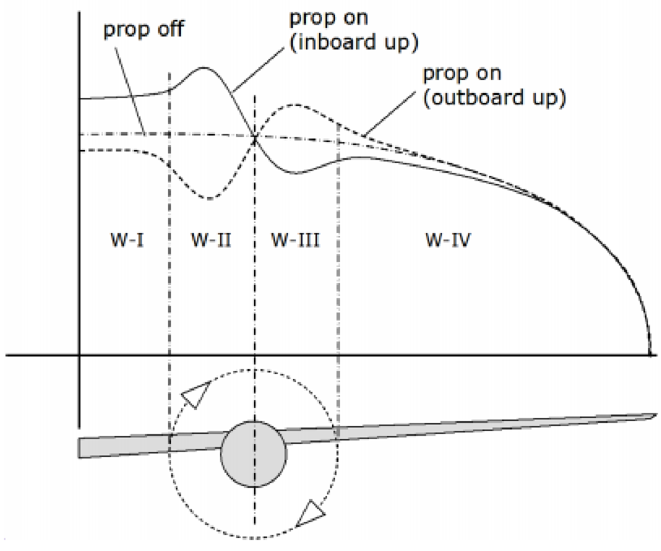

Figure 3.11: Typical lift distribution over a wing affected by a tractor propeller in front of the wing. Both effect of axial velocity increase as swirl has been included

The changed inflow over the wing causes also a change of the resultant force which is created by the wing. The upwash will create a local increase of angle of attack over the wing, this will cause to shift the resultant forward and create a negative drag force. This negative drag force is therefore creating a positive force in x-axis on the wing and can therefore seen as extra created thrust by the propeller. In figure 3.12 this is shown for the upgoing and downgoing blade situation on the local resultant.

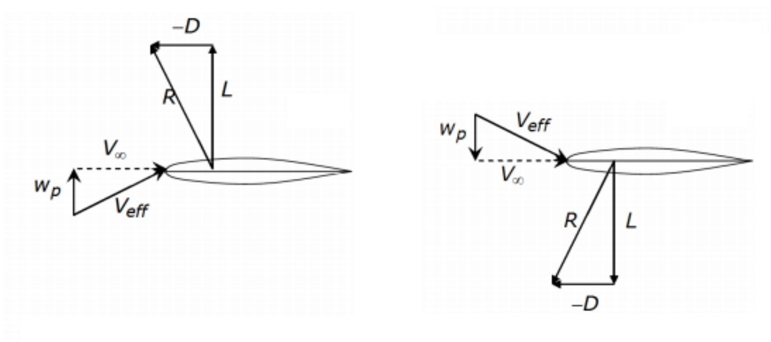

Figure 3.12: Effect of the propeller slipstream on the local airfoil for a infinite wing. Left the upwash situation is given, the local increase of angle of attack causes the resultant to shift forward. Right the situation is given for the downwash, the airfoil experiences a negative effect to local angle of attack and resultant is shifted forward again.

3.4. PROPELLER FUSELAGE-TAIL INTERFERENCE

The propeller slipstream has an effect on both the fuselage and the tail. The fuselage and tail have an additional influence on each other due to the flow modified by the propeller slipstream. The propeller slipstream can change the total pressure on one or both sides of the fuselage or tail when it directly coincides with the component. The second direct effect is the modified free stream properties by the wing trailing vortex sheet. These two disturbances result in a force and moment on the fuselage and tail separately.
The tail is placed in the influence region of the fuselage, this interference may have a significant effect on the vertical tail force. The first effect is the modification of the flow on the tail due to the lift-carry-over effect, resulting in a different lift distribution over the tail. The second effect is the increase in side wash due to the blockage effect of the fuselage.
The fuselage is placed in the influence region of the vertical tail. This results in lift carry over on the fuselage, effectively increasing the size of the tail, this effect is mentioned here as it acts on the fuselage. The second effect is the increased side wash in front of the vertical tail due to the lift on it. These four effects can increase the side force on the empennage considerably as they amplify each other.

3.5. PROPELLER SLIPSTREAM EFFECTS ON VERTICAL TAIL

Now having examined the characteristics of the propeller slipstream and its effect on the wing, the focus will be on how this slipstream will effect the vertical tail. Especially the critical case, when one engine is inoperative, an asymmetrical situation exists on the vertical tail which affects the directional stability and control of the aircraft. First, the increased dynamic pressure at one side of the vertical tail. In figure 3.13 the dynamic pressure distribution is given on the horizontal tail for the Fokker F27 with 35 degrees flap setting. It becomes clear from the figure that the left engine, rotating inboard up, creates a dynamic pressure increase closer to the vertical tail. It follows that for the case there is one engine inoperative, that the sidewash in this situation will be larger when the inboard up engine (port engine) is the operative engine. [37].

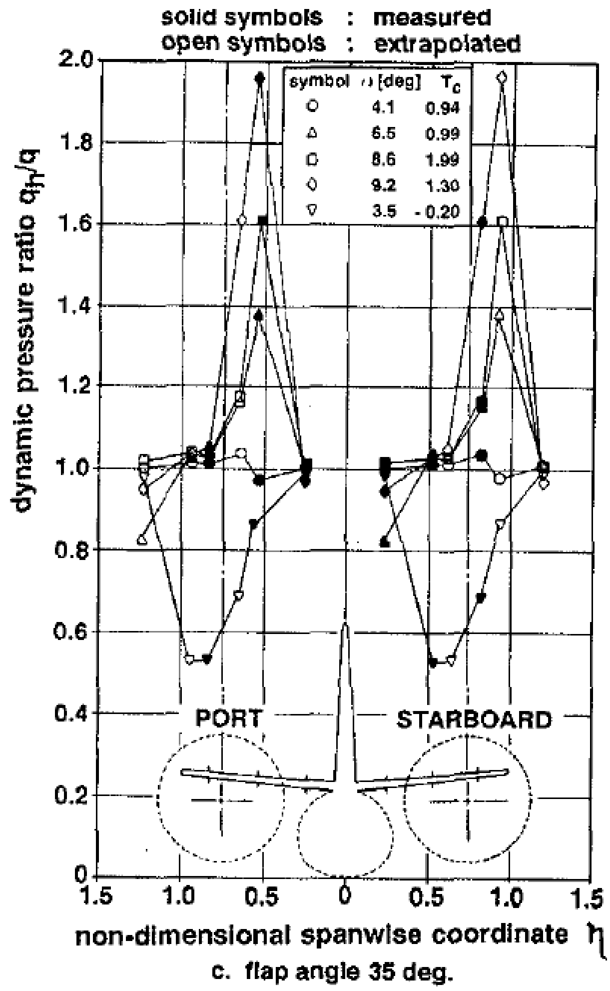

Figure 3.13: Dynamic pressure distribution on the horizontal tail, inboard up engine crease a larger increase in dynamic pressure closer to the vertical tail [37]

Secondly, and the main reason for the sideforce, is the asymmetric lift distribution created over the wing as described in section 3.3. The swirl and the increased axial velocity cause a large amount of additional lift at the side where the propeller blade moves upwards due to the local change in angle of attack creating a strong trailing vortex. The large asymmetric spanwise lift distribution over the wing fuselage combination causes a larger downwash at one side of the aircraft. This increased downwash at one side of the fuselage causes to create a circulation around the fuselage. This circulation changes the incoming flow at the vertical tail, creating a force side force.
It is found that a yawing moment of in total 1.5 times the static yawing moment is created due to the propeller installation effects, this mainly caused because of the side wash at the vertical tail due to the asymmetric lift distribution [38][25]. The creation of the asymmetric lift distribution for an IU and OU propeller and the effect on the vertical tail is sketched in Figure 3.14.

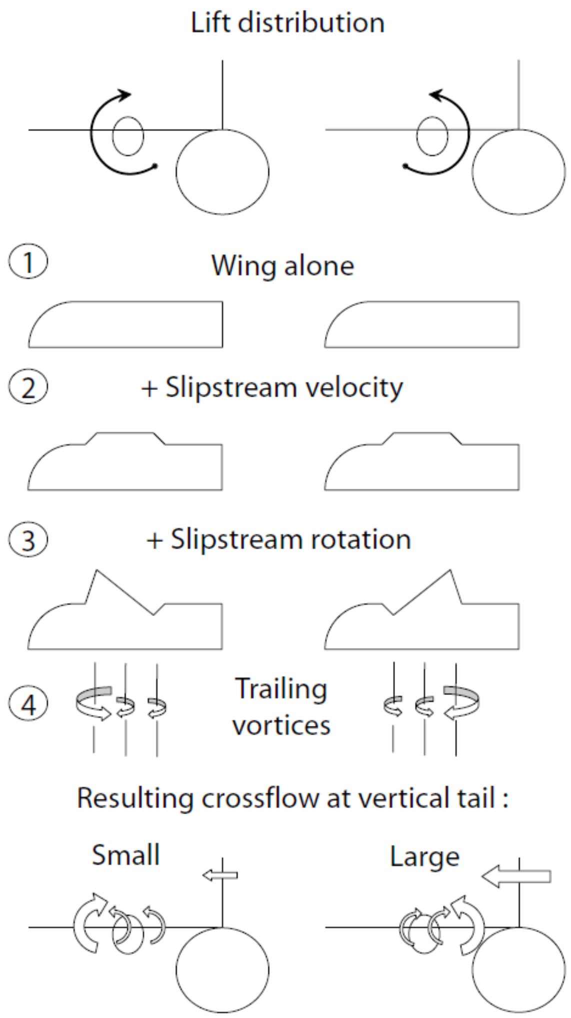

Figure 3.14: Illustration of the asymmetric lift spanwise lift distribution for a OU and IU rotating propeller and the effect on the vertical tail [25]

The inboard up rotating propeller creates a peak in lift coefficient closer to the fuselage. This causes the circulation created around the fuselage to be larger. For this reason the OU engine is the critical engine: if it fails it creates the largest adverse yawing moment on the aircraft. To compensate for this a large rudder deflection is required. If the 'inboard up' engine fails, a much smaller rudder deflection is required because the crossflow caused by the slipstream of the operating engine is much smaller. In the results section of this research in Chapter 8, the asymmetric lift distribution and the forces on the vertical tail will be analysed using the potential flow model.

4
PROPELLER SLIPSTREAM AND TAIL INTERFERENCE MODEL

The modelling of the propeller slipstream and the aerodynamic modelling of the wing, fuselage and empennage will be elaborated in this chapter. The potential flow model, previously developed by Rauhut, van Nispen and Schroijen is expanded to evaluate the directional stability derivatives of different aircraft and empennage configurations. Vertical plane design criteria depend greatly on the type of aircraft (and so the flow regime), engine numbers and position, wing-fuselage and horizontal tail position. These factors affect the estimation of stability derivatives (the variation of aerodynamic coefficients with the independent variable, the angle of sideslip). This process is complicated since it involves asymmetrical flow behind the wing-fuselage combination and lateral cross-control. For this reason the modelling of different aircraft and empennage configurations had to be expanded compared to the original model.

4.1. PROPELLER SLIPSTREAM MODEL

In this section briefly the slipstream shearing model will be elaborated. This is to give an understanding of how the propeller slipstream is modelled and how it affects the other parts of the aircraft. The model is based on a surface vorticity panel method.

4.1.1. ASSUMPTIONS

- **Steady propeller slipstream** The propeller slipstream is assumed to be steady, this is equal to a propeller with an infinite number of blades or a time averaged velocity

- **Fully contracted propeller slipstream** The propeller slipstream is directly assumed to be fully contracted. However when the propeller slipstream passes over the wing the slipstream is not yet fully contracted. This will result in a small deviation in the lift distribution caused by the propeller. It was found in literature the propeller slipstream contracts about 1 to 2 percent in comparison with the propeller diameter[39]. However the effects of the propeller slipstream are researched at the empennage where the slipstream is fully contracted.

$$R(x) = R_p \sqrt{\frac{1+a}{1+a\left(1+\frac{x}{\sqrt{R_p^2+x^2}}\right)}} \tag{4.1}$$

  When x goes to infinity, far downstream, it can be seen the that the previous equation becomes

$$R_\infty = R_p \sqrt{\frac{1+a}{1+2a}} \tag{4.2}$$

- **Concentrated vorticity** The vorticity is concentrated in a vortex at the propeller blade-root and a vortex sheet at the propeller blade-tip. To calculate the vortex strength from the vortex theory the following relation of total pressure increase is used.

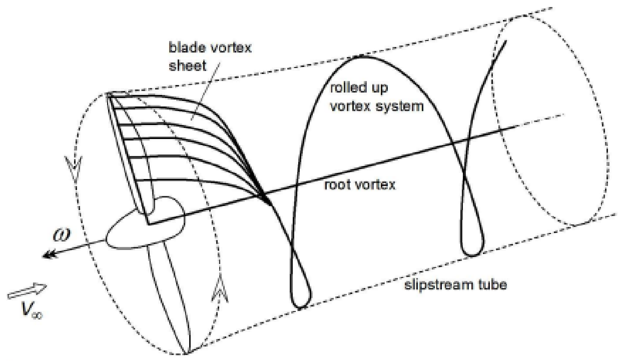

Figure 4.1: Vortex theory, flow relative to a blade element [18]

To calculate the vortex strength from the vortex theory the following relation of total pressure increase is used, where S is the surface of a panel.

$$(p_t)_s - (p_t)_\infty = p' + \frac{1}{2}\rho v_t^2 \tag{4.3}$$

$$\frac{1}{S_p}\int\int_{S_p} \Delta p_t dS = \frac{T}{S_p} + \frac{2}{S_p}\int\int_{S_p} (\Omega a' r)^2 dS \tag{4.4}$$

$$N_b\Gamma = \frac{2\pi\Delta\overline{p_t}}{\rho\Omega}\frac{R_\infty}{R_p} \tag{4.5}$$

Where $\Delta\overline{p_t}$ is the average increase in total pressure as given by the integral on the left side of the second equation.

- **Constant strength panels**. The slipstream can be divided in panels of constant strength. This assumption transforms the continues $\overrightarrow{\gamma}$ distribution in a piecewise constant function $\overrightarrow{\gamma}_{i,j}$. With a control point at the centroid of each panel.

4.1.2. UNDEFORMED SLIPSTREAM

The slipstream surface is divided in NP trapezoidal panels in circumferential direction and Mp + 1 panels in flow direction. The additional panel in flow direction is a panel to be able to simulate infinity conditions. For each panel the four corners are calculated in the local (ξ,η,ζ) panel reference frame. The origin of this reference frame is chosen to be the centroid of the panel. This point is chosen as the control point and the origin of the element coordinate system. This can be seen in figure 4.2.

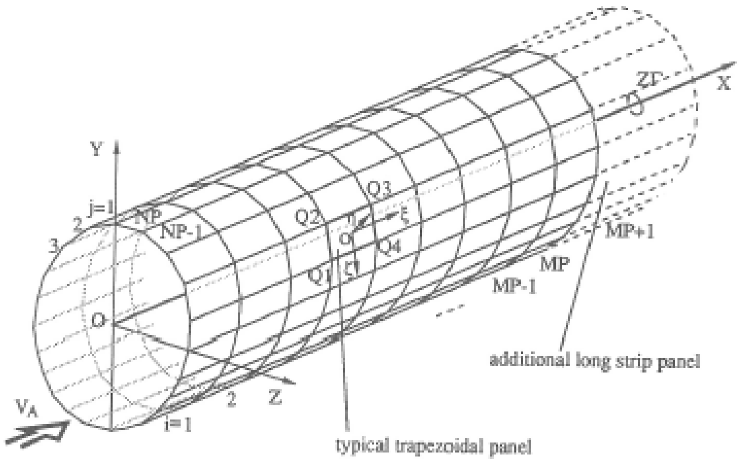

Figure 4.2: Simulated propeller non-deformed slipstream tube, divided in N_p sections in circumferential direction and M_p sections in slipstream direction

The shearing of the slipstream causes the panels at $\theta = 0, \pi, 2\pi$ to move independently of each other. The definition of shearing direction and positive reference frame on the additional panels is given in Figure 4.3. According to the Helmholtz theory vorticity cannot be created nor destroyed in ideal flow. The Vorticity in each panel is calculated in the respective axis system and then transformed back to the body axis system. For the complete shearing model and the verification please visit the research of Schroijen [23].

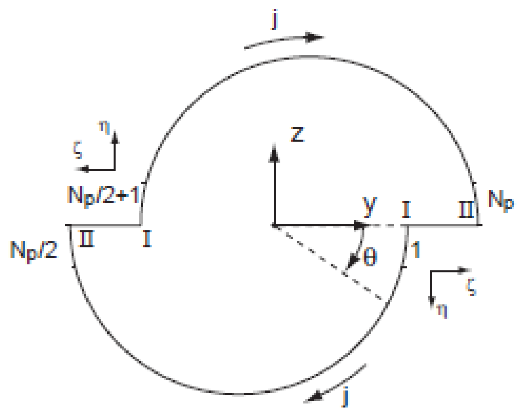

Figure 4.3: Cross section of the sheared propeller slipstream tube, indicating the positive angles and directions

4.2. PROPELLER TAIL INTERFERENCE MODEL

A short description is given of the Propeller Tail Interference Model (PTIM). This model has been developed by Rauhut, van Nispen and Renooij and is further expanded by Schrooijen, see references [23],[22], [40],[41]. For a more detailed description please visit the aforementioned references.

4.2.1. PROPELLER MODEL

The propeller model is based on the vortex theory assuming a propeller with an infinite number of blades. The model is based on the blade element theory with a correction for the induced velocities due to the propeller slipstream. The blade element lift curve is assumed linear and with this assumption an implicit function can be derived for the flow angle ϕ with respect to the propeller plane see, this can be seen in figure 4.4.

$$\frac{r\Omega}{V} = \frac{cos\phi + \frac{\sigma}{4sin\phi F}\left((\theta-\phi)C_{l_\alpha} sin\phi + C_d cos\phi\right)}{sin\phi + \frac{\sigma}{4sin\phi F}\left((\theta-\phi)C_{l_\alpha} cos\phi + C_d sin\phi\right)} \tag{4.6}$$

Where F is the Prandtl correction factor [18] for the fact the propeller blades are finite. As a blade has a suction-surface and a pressure surface, air tends to flow over the blade tip from the lower (pressure) surface to the upper (suction) surface, effectively reducing the resulting forces in the vicinity of the tip. This theory is summarised by a correction to the induced velocity field and can be expressed simply by the following equation.

$$F = \frac{2}{\pi} cos^{-1} e^f \tag{4.7}$$

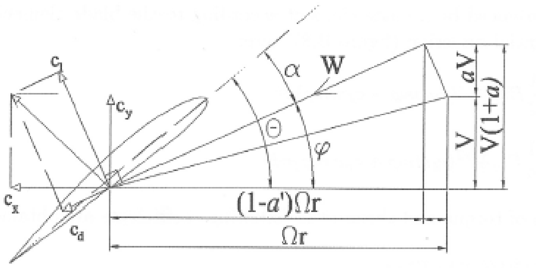

Figure 4.4: Propeller blade element definitions

4.2.2. WING MODEL

The lift on the wing is calculated by putting N_w horseshoe vortices on the quarter chord of the wing. The induced velocities due to these unit strength vortices are then calculated on N_w collocation points located at the three quarter chord. The dot product of the induced velocity with the vector normal to the wing surface is taken, this results in an influence matrix $\widehat{A}$. The velocity distribution at the collocation points consists of a contribution of the free stream, propeller induced velocities and upwash due to the fuselage. The component of the 'free stream' velocity normal to the wing surface should be cancelled by the wing induced velocities to fulfil the zero velocity through the wing boundary condition (Potential Flow).

$$\overrightarrow{v_\infty} \cdot \overrightarrow{n} + \widehat{A}\overrightarrow{\Gamma} = 0 \tag{4.8}$$

where the vortex distribution $\overrightarrow{\Gamma}$ over the wing is the only unknown. To include the effect of the fuselage on the wing lift distribution the effect of the mirror vortices is included in the influence matrix $\widehat{A}$. Where the location of these mirror vortices is given by

$$\begin{bmatrix} 0 \\ y \\ z \end{bmatrix}_M = \frac{{R_F}^2}{y^2+z^2} \begin{bmatrix} 0 \\ y \\ z \end{bmatrix} \tag{4.9}$$

4.2.3. WING DRAG CALCULATION

The induced drag is calculated differently from a wing in undisturbed flow. This is due to the fact that the propeller slipstream locally modifies the inflow angle of the wing. The velocities on the wing are given in Figure 4.5.

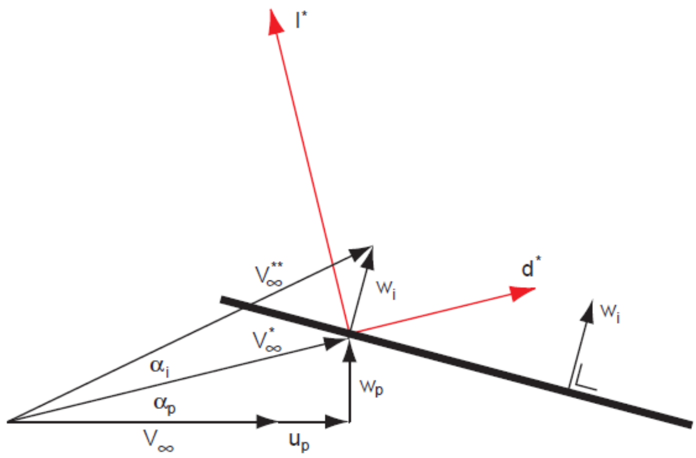

Figure 4.5: Velocities on a wing profile under influence of propeller-slipstream

From Figure 4.5 the following relations can be deduced.

$$V_{\infty}{}^{*} = \sqrt{(V_{\infty} + u_p)^2 + w_p{}^2} \tag{4.10}$$

$$V_{\infty}{}^{**} = V^{*} + w_i sin(\alpha_w + \alpha_p) + w_i cos(\alpha_w + \alpha_p) \tag{4.11}$$

$$\alpha_i = tan^{-1} \frac{V^{*} + w_i sin(\alpha_w + \alpha_p)}{V_{\infty}^{*} + w_i sin(\alpha_w + \alpha_p)} \tag{4.12}$$

$$d = -l^{*} sin(\alpha_i + \alpha_p) + d * cos(\alpha_i + \alpha_p) \tag{4.13}$$

Here l^* is the lift as calculated in the non-uniform flow field and d* is calculated from the profile drag variation with the lift coefficient.

4.2.4. FUSELAGE

The fuselage flow is influenced mainly by the wing trailing vortex sheet. The fuselage is divided in sections. On these sections the wing trailing vortex effect is calculated at 4 points on the fuselage surface and averaged to acquire the mean induced velocity in the centre of the fuselage section see Figure 4.6. With this mean velocity a pitch angle and side wash angle are calculated and the resulting moments on one section are given by equation 4.14.

$$\begin{aligned} dM &= \pi \rho R_f^2 \alpha (V_{\infty} + \vec{v_x})^2 \Delta x \\ dN &= \pi \rho R_f^2 \beta (V_{\infty} + \vec{v_x})^2 \Delta x \end{aligned} \tag{4.14}$$

The total moment that is generated by the fuselage in M an N direction is calculated by summing the moments of all the sections.

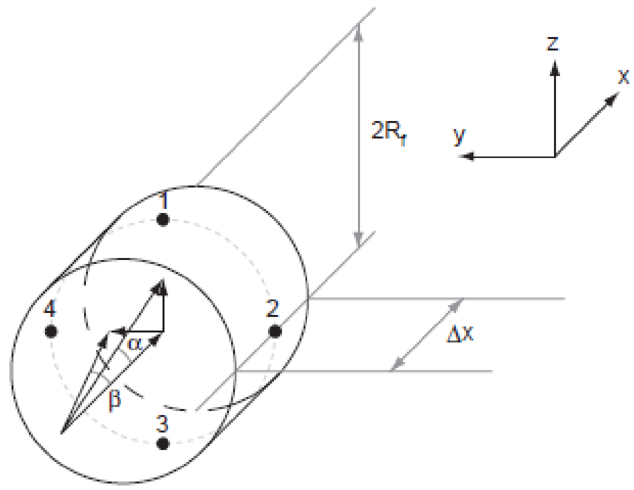

Figure 4.6: Fuselage section and definition of positive angels

4.2.5. WING TRAILING VORTEX SHEET

The trailing vortex sheet is calculated by a time stepping method. The position of the vortex in the next step is calculated by equation 4.15.

$$(x, y, z)_n = \left(x + dx, y + \frac{v_y}{v_x} dx, z + \frac{v_z}{v_x} dx\right) \tag{4.15}$$

The induced velocities are calculated from the influence of three components

1. The wing trailing vortex sheet on itself
2. The propeller slipstream
3. The fuselage induced velocities, mirror vortex and upwash

The trailing vortex sheet is calculated for each step in the y-z plane in the body-axis system, depending on the amounts of steps defined. The location of the mirror vortices are recalculated for every step as the trailing vortex sheet position and fuselage radius change with x position. The velocity induced by the vortex on a point y,z from the vortex core is given by equation 4.16 where $d\Gamma$ is the vortex strength of the trailing vortices.

$$d\vec{v} = \frac{d\Gamma}{2\pi(x^2 + y^2)} \begin{bmatrix} 0 \\ -z \\ y \end{bmatrix} \tag{4.16}$$

The influence of the propeller slipstream is calculated by searching for vortices inside the slipstream contour and determining the induced velocity at the location of the wing vortex sheet in the y,z plane. The slipstream position is also recalculated for every step so that it moves with the local velocity vector.

4.2.6. VERTICAL TAIL

The vertical tail is modelled in the same way as the wing, with the addition that the vortices are on the vertical tail. The 'freestream' velocity consists of effects of

1. the trailing vortex sheet

2. the propeller slipstream

3. the fuselage upwash

4. undisturbed flow

The effect of the trailing vortex sheet is calculated by taking the coordinates as calculated in the wing trailing vortex sheet model and assuming linear segments between them. The propeller slipstream position at the tail is also taken from the wing trailing vortex sheet model. The collocation points on the tail positioned inside the slipstream are determined. For these points the slipstream induced velocities are calculated.
The fuselage is included in the same way as in the wing model, by including mirror vortices and including the upwash due to the fuselage under an angle of attack.

4.3. EXPANSION TO GEOMETRY MODELLING

The model was originally developed to examine the yawing moment coefficient in OEI conditions at zero degree angle of sideslip for a fixed configuration. The wing position was fixed as a high wing configuration modelled as a rectangular wing, the fuselage was symmetric round the x-axis and the tail section only consisted of a vertical tail with a fixed geometry. To evaluate for this research the interference effects and the influences of the propeller slipstream effects on the directional stability of the aircraft, the model has been expanded such that it can evaluate a wide range of aircraft and especially empennage configurations. This has been achieved by expanding the wing, fuselage and and empennage modelling. The propeller slipstream model and the wing lift distribution under the influence of the propeller has not been modified however it has been expanded such that multiple propellers can be installed.

4.3.1. WING GEOMETRY AND POSITION

The wing was originally modelled as a straight wing modelled at a high wing position. The wing needed to be modified in two ways for the research. It must be able to give taper to the wing planform, affecting the spanwise lift distribution and secondly the wing position needed to be adjustable over the aircraft both in X and Z direction.

The taper of the wing was introduced by making the panels from constant to variable in length (chordwise) over the wing span. The circulation, directly affected by the chord length, decreases as the chord length reduces. However the spanwise lift distribution becomes more elliptical as the taper ratio goes to 0.4-0.5 as the downwash of each element changes with the chord length.
The downwash at any span position on the wing can be found by integrating the influence of individual elements of the trailing sheet [42].

$$w_i = \frac{1}{4\pi}\int_{\frac{-b}{2}}^{\frac{+b}{2}} \frac{1}{(y-y_i)} d\Gamma \tag{4.17}$$

Where $(y - y_i)$ is the distance across the span between the vortex element and the point at which downwash is being calculated.

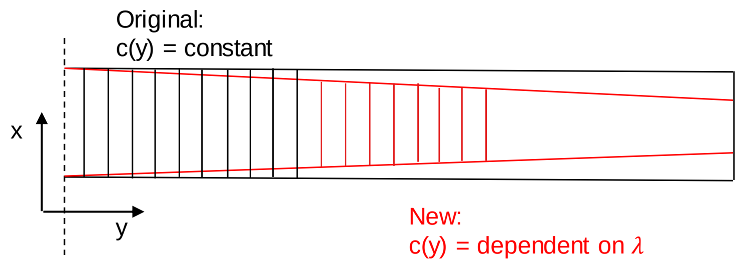

Figure 4.7: Expansion of the wing model by making the spanwise chord length variable

The wing position was made adjustable, shifting the wing at any location in x and z direction. Since the wing position shifts, also the wing trailing vortex sheet shifts with its location. Finally the position of and the number of propellers was made adjustable independent of the wing. Allowing to shift the propeller in X and Z direction with respect to the wing location. Changing the propeller location with respect to the wing influences the inflow angle at the wing [3]. The variation of the wing position is shown in Figure 4.8 where the wing position is varied from a high to a low wing configuration, together with the vortex field created behind the wing.

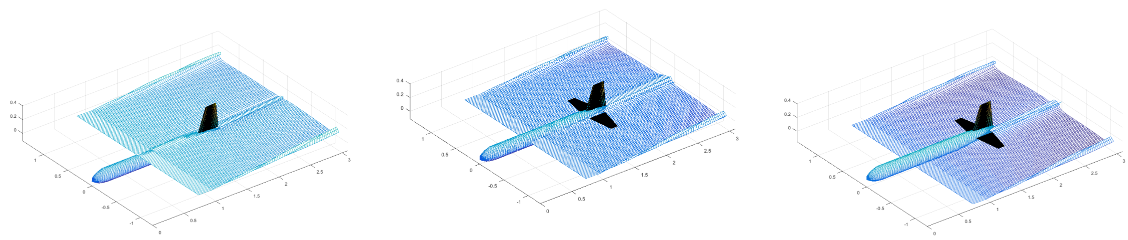

(a) (b) (c)

Figure 4.8: Variation of the wing position, a): high wing position, b): mid wing position, c): low wing position

4.3.2. FUSELAGE GEOMETRY

The fuselage model consisted of a cylindrical tube which was symmetrical round the aircraft x-axis. It consisted of circular sections which could vary in diameter to create the aft and front fuselage section. To this modelling a z-component has been added, allowing for the creation of a front and aft fuselage section with the fuselage centre placed lower or higher compared to the main fuselage centre. Especially the aft fuselage section of which the centre of the fuselage normally shift up, is important since is will be later evaluated in the results section when the interference effect of the fuselage on the vertical tail is examined. The fuselage dimensions used for the simulations are presented in Table 6.6.

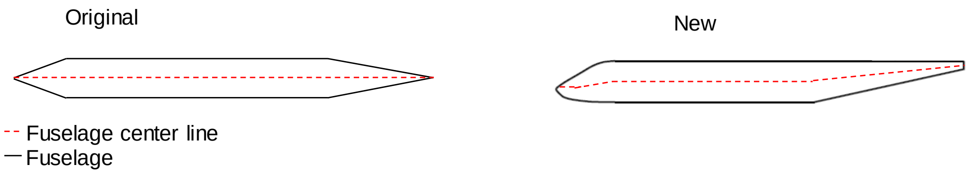

Figure 4.9: Expansion to the fuselage modelling making the centre line adjustable in z-direction

4.3.3. HORIZONTAL TAIL

Last the horizontal tail is added to the empennage to examine the interference effect of the horizontal tail on the vertical tail. The modelling of the horizontal tail is done in the same way as the vertical tail, it's created as a lifting surface, divided into panels on which the vorticity is calculated. As for the vertical tail, it calculates the lift with the 'free stream' velocity influenced by the trailing vortex sheet, the propeller slipstream, the fuselage upwash and the undisturbed flow. The collocation point are placed at 3/4 of the chord over the horizontal tail.

5

Model Validation and Sensitivity Analysis

In this chapter the validation and the model sensitivity, determination of the number of panels used for the simulations, will be discussed. This has been done to show that it is valid to use the model for the results obtained and additionally how the model is used for the results.
The validation will first be done for the wing plus propeller combination, Section 5.1. The results of the isolated propeller model are not validated in this report, since that has been done thoroughly in [22], showing reliable results. By first excluding the fuselage it can be checked if the model shows accurate results solely for the influence of the propeller on the wing.

Next the fuselage is added to the model and validation is done for the complete configuration, Section 5.2. Here first the validation is done for the condition the propeller is not operative and next the same conditions are used with the propeller operative. Finally the complete model, including empennage is used to show the accuracy for the yawing moment coefficient, Section 5.3.
In Section 5.5 a sensitivity analysis is made and the number of panels used for the simulations is determined.

5.1. Validation Wing-Propeller

To validate the wing-propeller combination the data has been used obtained by the PHD of Veldhuis [3]. The Propeller Wing Model (PROWIM) has been used for verification and experimental results obtained in the PHD are used for validation. The properties of the PROWIM model and the experimental research executed are extensively described in [3]. Due to this extensive description of the model is was possible to precisely determine the conditions and geometry of the propeller and wing. In Figure 5.1 and Figure 5.2 the results of the verification and validation are shown. Figure 5.1 shows the results of half the wing span (b/2) at $\alpha = 0°$ and Figure 5.1 is at $\alpha = 4\circ$.

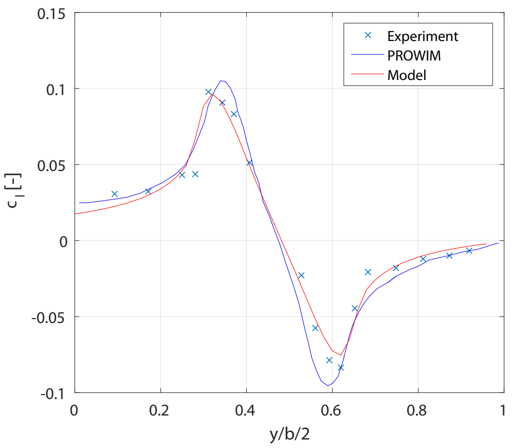

Figure 5.1: Validation Prowim and experiment[3], $\alpha = 0°$

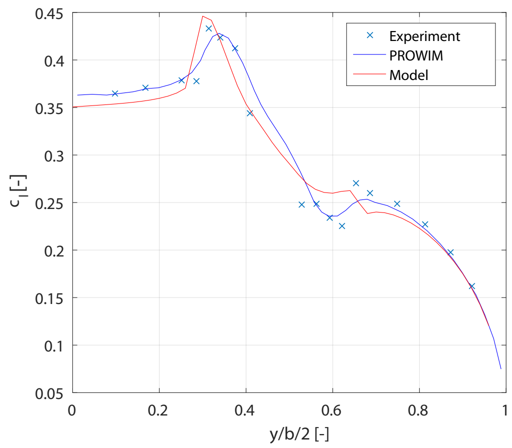

Figure 5.2: Validation Prowim and experiment[3], $\alpha = 4°$

The agreement is very acceptable for both angles of attack and a clear deformation of the elliptic shape as a result of the slipstream swirl velocity component is found. Nevertheless, for the case (α = 0), the lift coefficient on the propeller inboard side is somewhat overestimated by the VLM-code and more accurately for the model. For both situations, the 0 and the 4 degree AoA the lift coefficient at the root is predicted slightly to low while the lift coefficient outside the propeller slipstream at the outboard side is predicted more accurate for both cases.

Finally it can be seen that the down-going blade in case the propeller is under the 4 degrees AoA, is overestimating the lift coefficient. The down-going blade experience a increased angle of attack however this effect seems to be slightly overestimated by the model. However this effect, looking at the experimental results, seems to be under estimated by the Prowim model.

5.2. VALIDATION WING-FUSELAGE AND WING-FUSELAGE-PROP

The results of model are compared to flight test results and are compared with the results obtained from the VLM-method of Veldhuis[3].The flight tests are performed on the Fokker 50 aircraft. During these test the lift distribution over the wing was obtained by performing pressure measurements in chordwise direction using pressure belts. During the test 2 typical conditions were examined, a Low Thrust Condition (LTC) at -0.2° angle of attack, a T_c of 0.11 and an advance ratio of 1.63 and a High Thrust Condition (HTC) at 6.1° angle of attack, T_c of 0.63 and a advance ratio of 1.0 . The conditions are summarised in Table 5.1.

Table 5.1: Conditions of the flight test Fokker 50

Condition	α [°]	T_c [-]	J [-]
LTC	-0.2	0.11	1.63
HTC	6.1	0.63	1.0

To arrive at an accurate prediction of the characteristics it is important to model both the fuselage and the nacelle adequately since they tend to lower the local lift coefficient considerably. The nacelle is approximated from a CAD drawing as a cylindrical tube and is then scaled to the model. For the fuselage especially the fuselage slenderness ratio is important as is the size of the fuselage compared to the wing span. The properties to model the wing are given in table 5.2. Since the validation is specific about the lift distribution concerning the wing the correct parameters are essential [3]. Both are co-rotating, the left propeller is turning inboard up while the outboard propeller is turning outboard up.

Table 5.2: Fokker 50 wing properties

Wing Properties	Symbol	Value	Unit
Wing Aspect Ratio	A	12	[-]
Taper Ratio	λ	0.4	[-]
Incidence Angle Root	i_w	3.27	[°]
Zero lift AoA (Airfoil)	α_0	-3.382	[°]

Wing Fuselage Nacelle

In Figure 5.3 and Figure 5.4 the lift distribution can be seen for the wing, fuselage and nacelle combination. It follows from the figures that the fuselage and the nacelle have a remarkable influence on the lift distribution.

It can be seen that the model results are very close to the results of the flight test and the VLM model by Veldhuis. Especially in the LTC case ($\alpha = -0.2°$) the model and the VLM model give almost the same result. For the HTC case ($\alpha = 6.1°$) it can be seen that the lift distribution is different between the model and the VLM model for the fuselage section. However in this region no flight-test measurements have been done so no clear conclusion can be given which model is more accurate for the high angle of attack situation. In general, panel methods tend to be more inaccurate for high angle of attack situations since the viscous effects can not be modelled. However for the research conducted the angle of attack is kept at zero degrees.

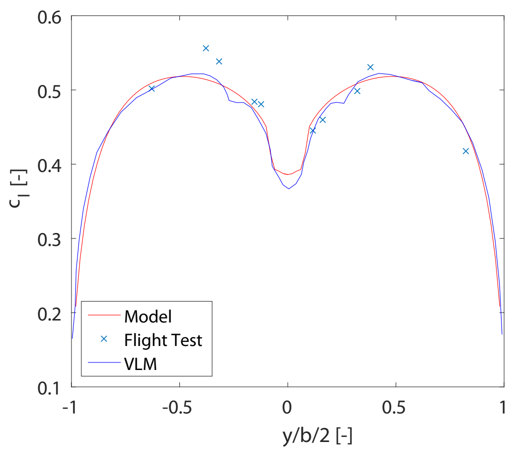

Figure 5.3: Wing-fuselage lift distribution, LTC

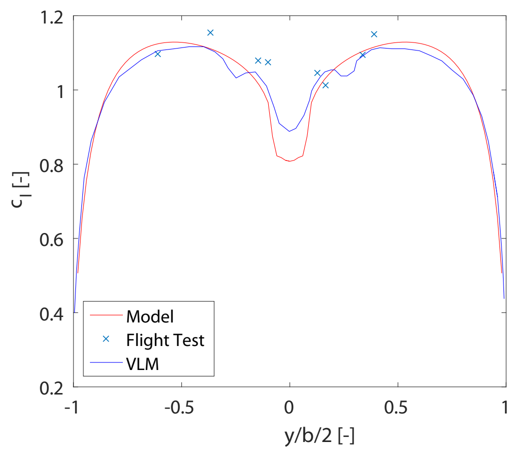

Figure 5.4: Wing-fuselage lift distribution, HTC

Wing Fuselage Nacelle Propeller

In Figure 5.5 and Figure 5.5 the lift distribution can be seen for the wing, fuselage,nacelle and propeller combination. As can be seen in both figures the propeller slipstream generates a significant disturbance of the spanwise lift distribution.

Although the associated flow over the real aircraft in flight is very complex, the model and the VLM method, predicts the local lift coefficient remarkably well for the LTC condition. Both models clearly follow the flight test results, however again only measurements have been done at 10 locations. A broader spectrum of measurements especially around the fuselage and propeller region would allow for a better conclusion. It can be seen that for the inboard-up propeller(left) the down-going blade is modelled more accurate then the VLM model, showing a slight increase again after the propeller position in the lift coefficient.

For the HTC case is can be seen that there is quit a remarkable difference between the 2 models and the flight test results. First again as in the LTC case, the lift coefficient for the fuselage is again lower for the model as compared to the VLM method. However in this region again no flight measurements are available.

It can be seen that the model overestimates the lift coefficient for the down-going blade in the high angle of attack case. The down-going blades experiences in this situation an extra increase in angle of attack but it seams to be overestimated especially for the inboard-up going propeller. For the outboard up going propeller also the flight measurement shows a slight increase in lift coefficient for the downgoing propeller in comparison to the VLM model.

For the research conducted, the angle of attack in most cases is kept at 0 degrees and for some cases raised until max 5 degrees making the LTC case more relevant for which the model shows accurate results, however the thrust coefficient ($T_c = 0.63$) of the HTC condition is more representative for the simulations.

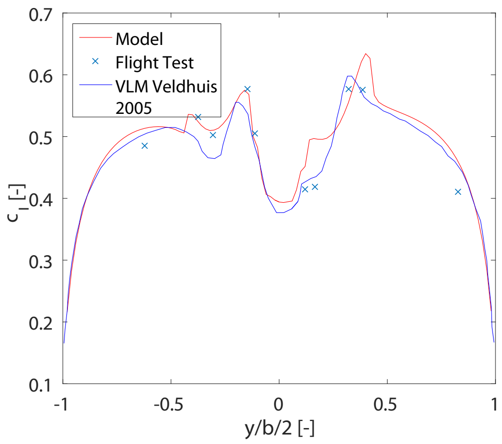

Figure 5.5: Wing-fuselage-propeller lift distribution, LTC

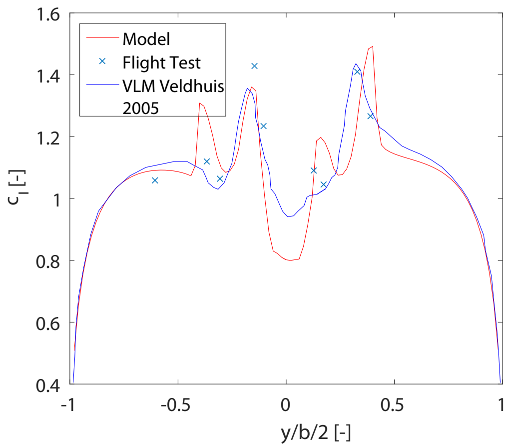

Figure 5.6: Wing-fuselage-propeller lift distribution, HTC

5.3. VALIDATION YAWING MOMENT COEFFICIENT OEI

The lift distribution over the wing and fuselage, influenced by the propeller slipstream is of great importance for the tail effectiveness as already described before in Section 3.5. However this last step of the validation is to check the yawing moment coefficient in OEI and check for the correct modelling of the wing vortex sheet. As in the description of the modelling of the empennage there are four factors that influences the force generated by the empennage, the free stream, the wing vortex sheet, the upflow from the fuselage and the propeller slipstream tube. Additionally it will be shown that the flaps model doesn't give accurate results and therefore will not be used in further analysis. For the validation the work of Schroijen has been used which is validated by the windtunnel measurements of Mannée[23][24]. In Figure 5.7 and Figure 5.8 the results are shown for both a Inboard Up (IU) and a Outboard Up (OU) rotating propeller for the fuselage, wing, propeller and empennage configuration. In Figure 5.8 the results are shown with a flap deflection of 30°.

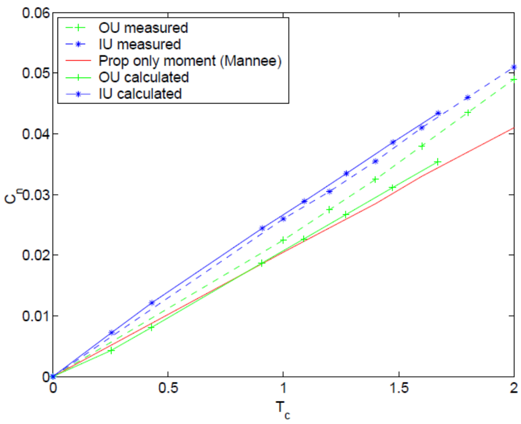

Figure 5.7: Yawing moment coefficient for the wing, fuselage, propeller and empennage combination with flaps retracted

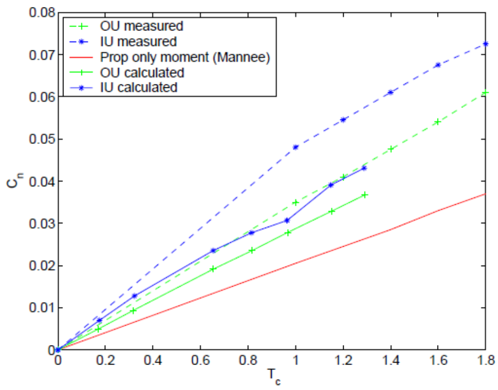

Figure 5.8: Yawing moment coefficient for the wing, fuselage, propeller and empennage combination with flaps at 30°

It can be seen from Figure 5.7 that the model predicts the yawing moment for the inboard up rotating propeller accurate for the whole regime of thrust coefficients while for the OU the error at Tc=1.5 is 6%.

From Figure 5.8, condition with flaps, it can be clearly seen that the error for the OU has significantly grown and that the error especially for the IU rotating propeller is very large (50,4 % at Tc=1.2). For both the IU and the OU situation the yawing moment is underestimated by the model. The large error from the IU rotating propeller with flaps can be explained by the irregular wing vortex sheet. This results in a wing trailing vortex sheet with incorrect vortex strength distribution, which affects the vortex movement. The induced velocities are therefore incorrect at the vertical tail. For this reason it is chosen not to use flaps in the model for the results. Since a lot of effort have been made in the past to model the flaps and because of the complexity of the modelling of the flaps (viscous effects) is has been chosen to leave the flaps out of the scope of research.

5.4. CONCLUSION ON MODEL VALIDATION

From the validation of the spanwise lift coefficient the following conclusions can be made. When validating the individual wing and the propeller the error between the model and the experimental data for the spanwise lift coefficient is within 2% for the condition where $\alpha = 0°$ For the condition where $\alpha = 4°$ the error is within 3% except for the region of the downgoing blade, here an overestimation of the lift is found. While the experimental data shows a small decrease the model predicts a small increase in lift. The error in this region equals 13% compared to the experimental values.

From the verification of the fuselage-wing-nacelle combination it is found that the model shows predicts the spanwise lift coefficient with a small error (1-2%) for the complete span in comparison with the VLM model for the $\alpha = 0°$ condition. For the $\alpha = 6.1°$ condition it is found that the lift is predicted similar to the VLM only the lift created in the fuselage section is under predicted by 12%. Only a few experimental data points are available which makes the validation more difficult. The model shows similar trends to the experimental data for both $\alpha = 0°$ and $\alpha = 6.1°$ condition. The maximum error found with a experimental data point is 10%. Finally the propeller-wing-fuselage combination was verified and validated. It was found that for the HTC the lift coefficient behind the downgoing blade is overestimated compared to the experiment and the VLM method. This increase in the model is caused by an overestimation of the angle of attack the downgoing blade is experiencing. Especially for the propeller turning inboard up, at the port side, a large peak is estimated while the experiment only shows a slight increase. The VLM method doesn't show this increase at all but predicts a decrease in lift. For the LTC the error between the experimental data and the model is relatively small and the same trend can be seen in the data.

Finally from the validation of the complete aircraft model on the yawing moment coefficient it was found that the for the simulation whiteout flaps only a small error is found. The error for the IU condition is round 1% and for the OU condition it increases to maximum 6%. For the condition with flaps, it can be clearly seen that the error for the OU has significantly grown and that the error especially for the IU rotating propeller is very large (50.4 % at Tc=1.2). For both the IU and the OU situation the yawing moment is underestimated by the model. From the validation of the model it is concluded that the model shows sufficient accuracy for the prediction of the spanwise lift coefficient of the wing-fuselage-propeller combination with low angles of attack. Additionally the model shows sufficient accuracy of predicting the yawing moment coefficient for a low to a high thrust coefficient for the condition without flaps. It was found that deploying the flaps leads to a significant error up to 50% for the yawing coefficient of the complete model. Therefore the flap model is not used in the analysis of the directional stability of the aircraft.

5.5. PANEL SENSITIVITY

In this section a sensitivity analysis is performed to determine the amount of panels needed for the simulations. The amount of panels determines the accuracy of the model within the numerical assumptions made to predict this complex flow which acts around the aircraft due to the numerous parts of the aircraft and the propeller. As the amount of panels increases it can be seen that the re-

sults converge. The convergence point is taken when the difference between the next step is smaller than 0.01% of the previous value. This convergence point has been determined for the various panels and will be used later for the results.
The amount of panels used for the propeller, wing and fuselage have an effect on the lift distribution and vortex field. Next the amount of panels used on the model the vortex field and fuselage in x-direction (longitudinal) influence the vortex field. Finally the amount of panels used on the stabilo and vertical tail influence the prediction of the lift over these parts.
Below an overview is given of the different panel parameters:

- N_p: Number of transversal stations on the propeller slipstream grid
- N_w: Number of panels used on wing
- N_v: Number of steps in vortex field
- N_e: Number of panels used on the horizontal and vertical tail
- N_f: Number of panels on the fuselage
- N_s: Number of sections of the fuselage behind the wing

Propeller - N_p: The propeller model is insensitive to the number of spokes chosen to model the disc. This shows that the linear interpolation over the disc is a good approximation, and calculation time can be increased by decreasing the number of spokes used.

Wing - N_w: The amount of panels on the wing influence the prediction of the lift coefficient. It is chosen to show the lift coefficient, however since the drag coefficient is also directly linked it is assumed that the other wing parameters converge for the same amount of panels. It is chosen to have a equal distribution of panels over the wing to have sufficient panels both at the root and propeller section but also at tip. For the determination of the panels the configuration of describe in Section 5.1 has been used at 4 degree angle of attack, OU rotating propeller. In table 5.3 an overview is given of the amount of panels on the wing and the effect on the lift coefficient of the wing. It can be seen that the lift coefficient converges at 100 panels on the wing (complete wing span, 50 per wing section).

Table 5.3: Variation of the amount of panels on the wing and the effect on C_L

Parameter								
N_w [-]	20	30	40	50	100	200	500	1000
C_L [-]	0.2880	0.2987	0.3040	0.3072	0.3136	0.3140	0.3141	0.3141

Vortex Field - N_v Number of steps in vortex field. To show the convergence in the vortex field, the yawing moment coefficient has been used as a reference. In this way the vortex field can be evaluated by the moment it creates on the fuselage and tail. An OEI situation has been chosen with a high wing configuration with a inboard up rotating propeller for all the simulations.

Table 5.4: Variation of the amount of steps in the vortex field and the effect on C_n

Parameter					
N_v [-]	25	50	75	100	125
C_n [-]	0.0225	0.0224	0.0223	0.0223	0.0223

Empennage - N_e For the empennage it is assumed that the lift distribution over the vertical tail and the stabilo will converge at the same amount of panels as has been used for the wing. Leading to a equal spread of panels over the stabilo and vertical tail of 100 panels.

Fuselage - N_f It was found that changing the mesh of the fuselage in a section has only a very little effect on the results. This is because of the assumption when calculation the properties of the fuselage the average of the fuselage is taken at 4 points. Varying the mesh between those 4 points has therefor little effect. In Table 5.5 the results are shown for varying the mesh on the yawing moment coefficient.

Table 5.5: Variation of amount of panels on a fuselage section

Parameter						
N_f [-]	8	20	40	60	80	100
C_n [-]	0.0222	0.0222	0.0223	0.0223	0.0223	0.0223

N_s determines the amount of panels in longitudinal direction of the fuselage. The more panels are taken the better the vortex field can be estimated for due to the fuselage upwash.

Table 5.6: Variation of the amount of sections of the fuselage

Parameter					
N_s [-]	10	20	40	60	100
C_n [-]	0.0224	0.0222	0.0223	0.0223	0.0223

It can be seen from Table 5.6 that changing the amount of sections spanwise has only little effect on the yawing moment coefficient of the aircraft, C_n converges at 40 panels. This is also the value that has been chosen for N_s for the simulations.

Overview of selected panels For all parameters the number of panels has been chosen until convergence of the results is obtained, in Table 5.7 an overview is given for all the parameters.

Table 5.7: Overview of the number of panels for the different sections of the model

Parameter	No. of panels
N_p	8
N_w	100
N_v	75
N_e	100
N_f	20
N_s	40

6
AIRCRAFT MODEL AND APPROACH

In this chapter first the model is described used for the simulations and next an overview is given of the approach to analyse the effects on the vertical tail. The aircraft model consist of a model of the wing, fuselage, empennage and the propeller. The general layout of the aircraft model will be discussed and followed by the description of the individual aircraft components. Next the propeller model will be described. The approach for analysis consists of a parametric analysis, to see the isolated effects of the different aircraft components on the vertical tail. Finally in Section 6.5 an overview is presented of all the different simulations.

6.1. TURBOPROP TYPICAL DIMENSIONS

To evaluate the directional stability characteristics for a turbo-prop aircraft the model have been given the characteristics of modern turbo-prop aircraft. The fuselage, wing and empennage parameters of the Fokker 50 and the ATR 42 have been determined and can be seen in table 6.1, table 6.2 and table 6.3. Also the parameters for the fuselage, wing and empennage of the simulated model are given. These are the standard values used when they are not evaluated for, e.g. the aspect ratio of the wing is fixed at 10 as the position of the horizontal tail is varied.

Table 6.1: Fuselage parameters of regional turbo prop aircraft and the used model

	l_f/f_d [-]	x_{we}/l_f [-]	l_f/l_c [-]
ATR 42	10.3	0.41	3.2
Fokker 50	9.35	0.36	2.9
Model	10.5	0.39	3.9

Table 6.2: Vertical tail parameters of regional turbo prop aircraft and the used model

	A_v [-]	λ_v [-]	Λ_{vLe} [°]
ATR 42	1.56	0.61	32
Fokker 50	1.21	0.68	24
Model	1.5	0.5	27

Table 6.3: Horizontal tail parameters of regional turbo prop aircraft and the used model

	A_h [-]	λ_v [-]	Λ_{hLe} [°]
ATR 42	4.1	0.6	7
Fokker 50	4.9	0.45	9
Model	5	0.5	7

6.2. AIRCRAFT MODEL DIMENSIONS

Below the 'general' aicraft model will be shown that is used for the simulations, the model shows the original configuration parameters, these are of course changed for the different simulations. For example when the effects of the horizontal tail are studied, the parameters shown in Figure 6.1 are used for the fuselage and wing and the parameters of the position of the horizontal tail is variable.

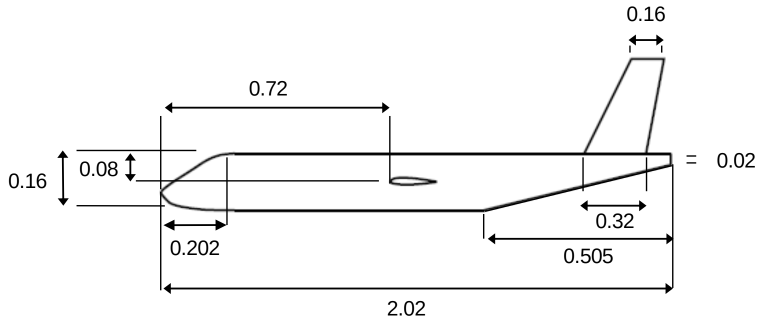

Figure 6.1: Side view of the aircraft model used for the simulations

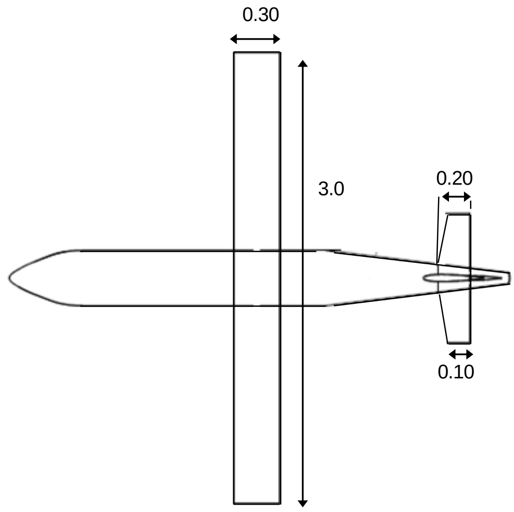

Figure 6.2: Top view of the aircraft model used for the simulations

6.2.1. WING PROPERTIES

The wing has as been discussed modelled as a rectangular wing. In Table 6.4 the properties of the wing are presented.

Table 6.4: Aircraft model - Wing parameters

Parameter	Symbol	value	Unit
Taper ratio	λ_w	1	[-]
Tip chord	c_{w_r}	0.3	[-]
Root chord	l_w	0.3	[-]
Span	S	3	[-]
Twist	ϵ	0	[°]
Sweep angle	Λ_w	0	[°]
Incidence angle	i_w	-1	[°]
Wing zero lift coefficient	α_0	-2.05	[°]
Wing aspect ratio	AR_w	10	[-]

6.2.2. FUSELAGE PROPERTIES

For this research the fuselage model has been expanded, allowing to shift the fuselage sections in z-direction. The fuselage has been modelled as circular section in longitudinal direction. The fuselage has been modelled by 14 sections, the fuselage properties are presented in Table 6.6. Since the fuselage is a cylindrical tube between x = 0.202 and x = 1.400 most sections are placed at the nose and aft section of the fuselage to correctly model the decreasing fuselage diameter in these areas. The fuselage properties are presented in Table 6.5. The centre of gravity of the fuselage in z-direction is assumed to be at the centre of the main fuselage diameter.

Table 6.5: Aircraft model - fuselage properties

Parameter	Symbol	Value	Unit
Fuselage length	f_l	2.02	[m]
Fuselage main diameter	f_d	0.08	[m]
Fuselage main radius	f_r	0.04	[m]
Fuselage cg in x-direction	$x_{cg_{fus}}$	0.768	[m]

Table 6.6: Fuselage x,y and z component for every section

Sections														
Fuselage X	0.00	0.01	0.1	0.202	1.400	1.605	1.710	1.780	1.840	1.880	1.925	1.970	2.000	2.02
Fuselage Z	-0.045	-0.03	-0.03	-0.02	-0.01	0.000	0.000	0.000	0.01	0.015	0.02	0.025	0.028	0.03
Fuselage radius	0.00	0.025	0.07	0.080	0.080	0.080	0.070	0.060	0.050	0.040	0.030	0.020	0.010	0.00

6.3. PROPELLER MODEL

In this section the propeller model will be discussed. First the propeller model installation on the aircraft will be discussed and next the properties of the propeller itself.

6.3.1. PROPELLER INSTALLATION ON AIRCRAFT

The horizontal location of the propeller is of great importance. It determines the interaction between the propeller and the fuselage and the effect of the propeller on the vertical tail. For the propeller installation 2 parameters are of main importance, the distance of the center of the propeller to the fuselage and the propeller diameter, as shown in figure 6.3.

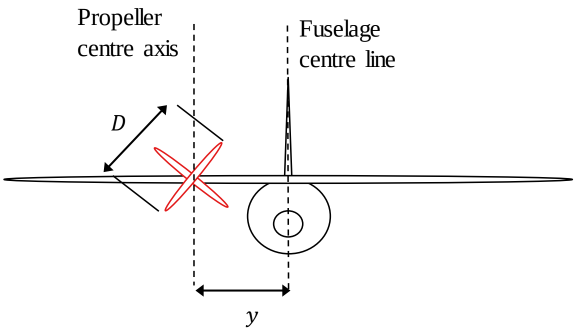

Figure 6.3: Parameters used to define the propeller location on the wing

In table 6.7 the typical propeller distance is shown of the reference aircraft and the model's propeller position when it is not the variable parameter.

Table 6.7: Parameters to describe the propeller instalment on the aircraft

	y[m]	D[m]	y/D [-]
ATR 72	4.6	3.9	1.18
Fokker 50	3.77	3.66	1.03
Model	0.275	0.262	1.05

In Figure 6.4 the location of the propeller with respect to the wing is illustrated. From literature it was found that both the horizontal and the vertical location of the propeller have a large influence on the inflow over the wing and thus the lift coefficient created. It was chosen to centre the propeller axis and the wing centre axis in z direction such that the propeller is placed directly in front of the wing. The propeller is placed 0.2 m in front of the wing.

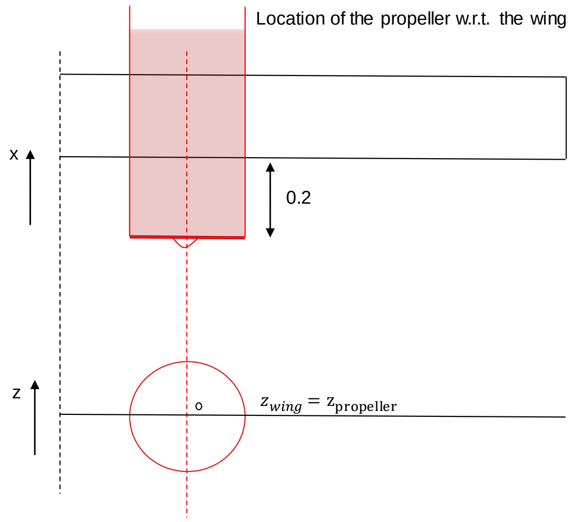

Figure 6.4: Propeller location w.r.t. the wing location

6.3.2. PROPELLER BLADE ANGLE CALIBRATION

The calibration of the propeller has been done to obtain the same thrust coefficient to advance ratio ($T_c - J$) as been used in the windtunnel measurements by Mannée . Doing so the simulated propeller represents an actual propeller and the simulations with a propeller installed can be checked with the windtunnel tests.

The precise propeller shape cannot be determined from the literature, the propeller is therefore roughly calibrated on a given Tc - J graph given in the report of Mannée. Because in different literature (design vs propeller) thrust coefficient is defined differently, Tc is the non-dimensional thrust coefficient

$$T_c = \frac{T}{\frac{1}{2}\rho V^2 D^2} \tag{6.1}$$

While the thrust coefficient for propeller normally is defined as:

$$C_T = \frac{T}{\rho n^2 D^4} \tag{6.2}$$

For the calibration of the thrust the high-wing configuration with vertical tail,with and without is used. To achieve the correct thrust setting for a given advance ratio the 0.75R blade angle is modified by an extra blade angle:

$$\theta = \theta_{geo} + \beta_p \tag{6.3}$$

The geometric blade angle (θ_{geo}) variation is shown in Figure 6.6 . The values for which the blade angle is varied is given in Table 6.8.

Table 6.8: Calibration of the propeller blade angle

n [RPM]	7034	8240	10883	11771	12539	13414	14068
β_p [°]	6.5	5.85	4.50	4.00	3.75	3.30	3.30

Using the adjusted blade angles results in the following thrust coefficient as a function of advance ratio graph (Figure 6.5), plotted together with the experimental set-up of Mannée.

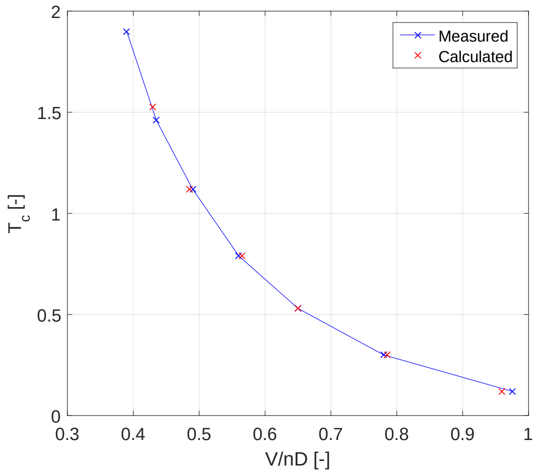

Figure 6.5: Thrust coefficient plotted against the advance ratio for the used propeller in the simulations

From the graph it can be seen that blade angle is adjusted such that the thrust coefficient to advance ratio matches those of Mannée.

6.3.3. PROPELLER PROPERTIES

The propeller properties are summarised in Table 6.9. Here the various parameters are shown to model the propeller. The propeller properties are based on the work of Mannée. The blade angle (θ_{geo}) and chord of the propeller blade vary spanwise and are given in Figure 6.6.

Table 6.9: Properties of the propeller used for the simulations

Description	Parameter	Value	Unit
Number of Propellers	N_p	1	[-]
Number of blades	N_b	2	[-]
Propeller diameter	D	0.305	[m]
Propeller radius	R	0.1525	[m]
Number of radial stations	r_i	7	[-]
Propeller chord	c	$c(r)$	[m]
Geometric blade angle	θ_{geo}	$\theta_{geo}(r)$	[°]

In Figure 6.6 the spanwise chord and blade angle are given for the propeller.

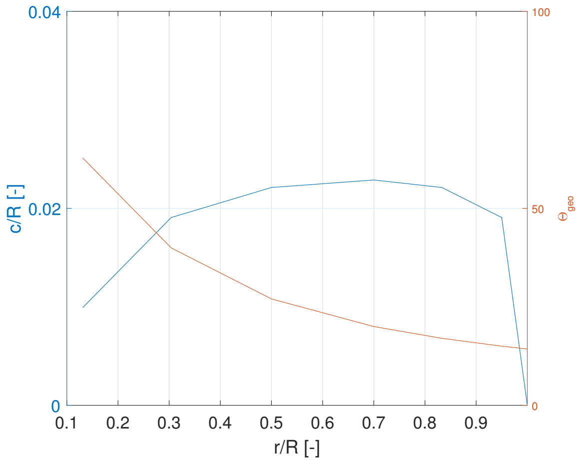

Figure 6.6: Propeller chord and blade angle over the span of a blade

6.4. PARAMETRIC ANALYSIS

In order to see the effects of the different parts of the aircraft on the installed vertical tail a parametric analysis has been performed. This is done to see the isolated effect of an added parameter while the other parameters are kept constant. In this way it is able to clearly see for example the effect of adding a horizontal tail on the effectiveness of the vertical tail. The parametric approach is first applied on the aircraft model without the propeller. It is verified and validated if the aerodynamic model is able to predict the side force coefficient for different configurations of the aircraft and empennage. Once the individual effects are validated the complete aircraft configuration is analysed. Next the same analysis is performed with the propeller installed and compared to the situation without the propeller. In this way it is possible to identify what the effects of the propeller are on the isolated vertical tail and the interference effects and finally on the complete aircraft configuration.
The analysis has been performed in the following order, in which the aircraft is 'build up' in four steps.

1. The isolated vertical tail is evaluated. The sideforce coefficient of the vertical is examined for a negative to a positive sideslip angle. This step is very important because in the following three steps it will be evaluated how the various aircraft parts influence the vertical tail.

2. To evaluate the fuselage interference effect, the fuselage is added to the vertical tail. The results are compared to the isolated vertical tail to see the interference effect of the fuselage. Different slenderness ratios are used for the aft fuselage section

3. Next the wing is added to the fuselage and tail combination. The results are evaluated, comparing them to the fuselage and the vertical tail combination. The position of the wing is varied and the aspect ratio of the wing at the different vertical positions of the wing.

4. Finally the horizontal tail is added. As for the previous situations, now it is compared with the v-tail-fuselage-wing situation. The position of the horizontal tail is varied both chordwise as vertically.

After the analysis of the isolated vertical tail and the individual interference effects the directional stability derivatives of the complete aircraft model are evaluated.
In Figure 6.7 the four different different steps are presented.

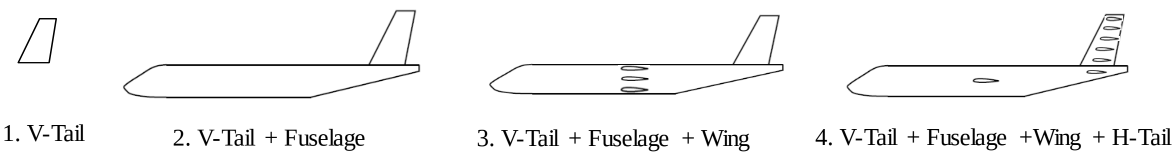

Figure 6.7: Parametric analysis to identify the interference effects of the various aircraft parts

6.5. OVERVIEW OF SIMULATIONS

In this Section an overview will be given of all the simulations. These scheme is very useful when evaluating the results section, giving a clear overview of all the simulations for the results.

No propeller installed
As described before, in total three effects are evaluated for in the case there is no propeller installed, the effect of the fuselage,wing and horizontal tail. The sideslip angle is kept constant at five degrees. For the fuselage in total five different configurations are evaluated for, for the wing four different aspect ratios and three different wing positions. Finally for the horizontal tail the vertical position of the horizontal tail is evaluated at six different vertical positions. The horizontal position of the horizontal tail is again evaluate at three different chordwise positions (x/c= -0.25, 0, 25) at all six vertical positions.

Propeller Installed
For the propeller operating situation it was chosen to perform the tests in one engine inoperative situation for most simulations. This gives the largest effects of yawing moments and sidewash at the vertical tail and is the critical condition for the vertical tail design. From literature it was already known that the inboard up rotating propeller generates the largest yawing moment, for this reason a OEI condition is used with the propeller rotating inboard up. However, because of the asymmetric conditions the situation changes for a positive or negative sideslip angle. This can be seen in Figure 6.8 and Figure 6.9. For the positive sidelsip angle, Figure 6.9 the propeller slipstream tube flows in direction of the freestream and is displaced in direction of the fuselage. This increases the propeller slipstream effects on the fuselage and the vertical tail because the presence of the slipstream is more dominant then in the case where the propeller slipstream is displaced away from the fuselage, see Figure 6.8.

An additional comment to this condition is that the aircraft, in case of an engine failure is operated with a sideslip angle, towards the 'living' engine. In other words, in the situations described earlier, the situation as shown in Figure 6.9. This is because, in this situation the vertical tail already generates a corrective force for the asymmetric thrust. Doing so the amount of rudder deflection, needed to counteract the asymmetric thrust, decreases and the drag of the aircraft decreases, allowing to achieve better aerodynamic properties. From my own experience I, the author and a licenced pilot, know that it is unable to achieve a climb rate with a PA-44 (Piper Seminole) in OEI conditions when it is not flown with this sideslip angle.

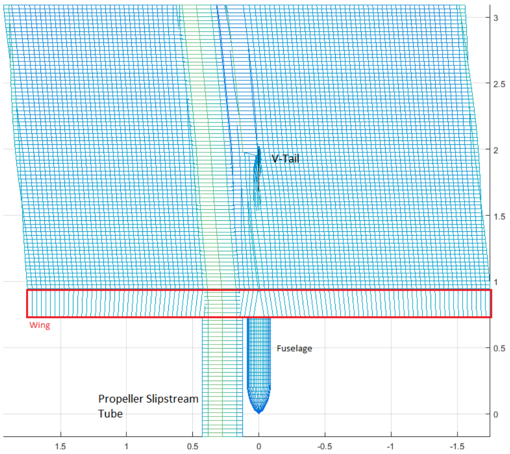

Figure 6.8: Potential flow model showing the fuselage, wing and tail combination (top view) for a sideslipping flight at -5°

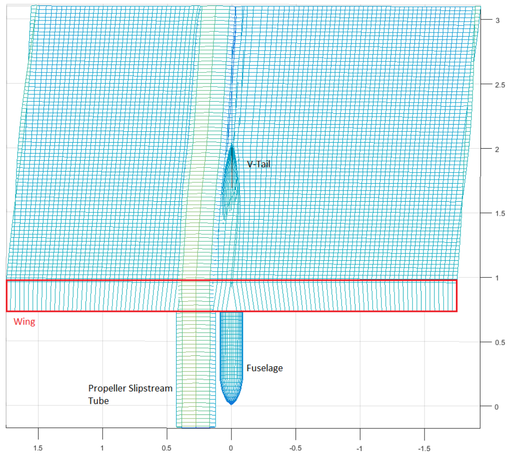

Figure 6.9: Potential flow model showing the fuselage, wing and tail combination (top view) for a sideslipping flight at 5°

Additionally, to research the wing interference effect under influence of the propeller slipstream, the simulations are performed at 0 degree of sideslip. This has been done to also show the effects of the rotating propeller on the yawing moment of the aircraft whiteout the effects of a side slipping flight. It can be seen that the location of the wing and thus the propeller significantly influences the tail effectiveness. In Figure 6.10 an overview is given for the simulations.

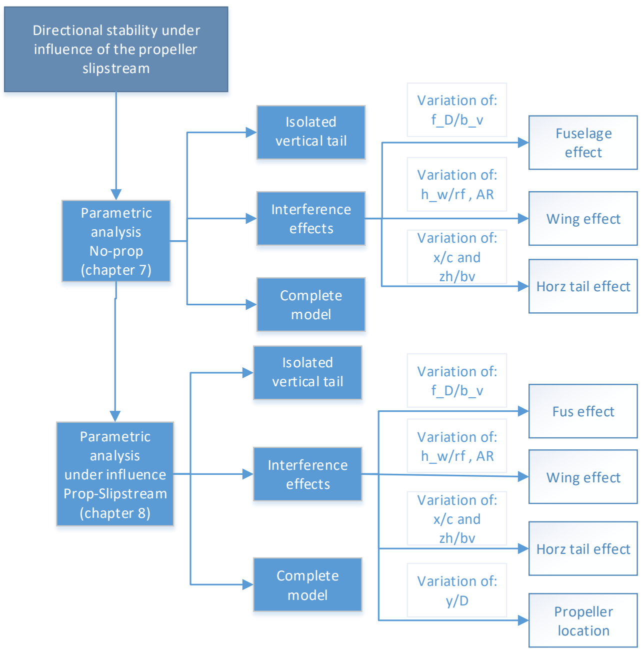

Figure 6.10: Overview of the simulations performed for the different configurations

7

Analysis of Directional Stability Using a Potential Flow Model

In this chapter the sideforce coefficient generated by the vertical tail under a side slip angle will be verified and validated. The side force coefficient of the vertical tail is dependent on the shape of the vertical tail itself and the interference effect created by the other parts of the aircraft. To show that the potential model is able to predict the sideforce coefficient of an installed vertical tail for different configurations, these two dependencies will be evaluated. First the individual vertical tail will be evaluated and next the different interference effects. If both dependencies are validated and show accurate results it can be assumed that the model predicts the sideforce coefficient of the installed vertical tail with sufficient certainty matching validated models. Finally for two complete aircraft models, the sideforce coefficient will be evaluated and compared to the results obtained with the semi-empirical methods.

The results are obtained using the aircraft model and conditions described in Chapter 6, with a side-slip angle of 5 degrees. For the various situations also the results obtained by Della Vecchia are shown, who performed the same measurements with a comparable model using a Navier-Stokes solver. This is plotted in the results with the legend 'CFD'.

7.1. Isolated Vertical Tail

In figure 7.2 the sideforce coefficient of the vertical tail is shown. The analysis of the isolated vertical tail is of great importance: to provide the vertical tail lift curve slope C_{Y_V}. Later the results will be used to estimate the interference effects created by the fuselage, wing and horizontal tail. For the isolated vertical tail, three different geometries are evaluated, see Figure 7.1, with three different aspect ratios and taper ratios. The analyses performed with the above mentioned shapes allow for the estimation of variation of lift curve slope versus aspect ratio. The results are plotted together with the CFD results of the isolated vertical tail with the same AR of Della Vecchia [32].

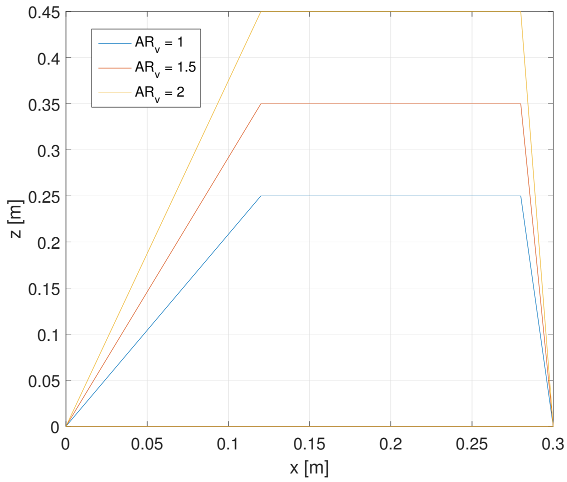

Figure 7.1: Sideview of the three vertical tail surfaces

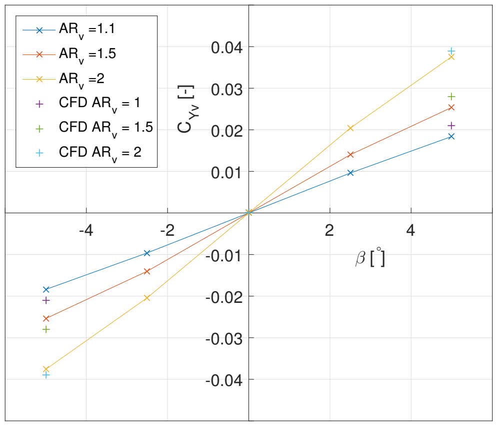

Figure 7.2: Sideforce coefficient for isolated vertical tail C_{Y_V} plotted vs. sideslip angle

The results show very comparable results to the CFD-results, the maximum error is found for AR=1. and equals 2%. For all aspect ratios there is a slight underestimation of the side-force. Since the model is symmetrical the error is the same for the -5 and +5 degrees angle of sideslip. As the aspect ratio of the vertical tail increases also the sideforce coefficient increases. In the next sections the interference effects on the installed vertical tail of an aircraft will be discussed. Finally after the interference effects are discussed, it can be judged if the model predicts the side force coefficient of the installed vertical tail accurately for different aircraft configurations.

7.2. INTERFERENCE EFFECT OF THE FUSELAGE ON THE VERTICAL TAIL

The first interference effect that has been studied is the fuselage effect on the installed vertical tail. The fuselage influences the vertical tail in a sideslip in two ways as already discussed in Section 7.2: it has an endplate effect on the vertical tail, prohibiting the flow at the root region of the vertical tail to go from the higher pressure side to the lower pressure region. Secondly increasing the sidewash over the vertical tail: the fuselage acts as a cylinder at the lower side of the vertical tail, accelerating the flow and increasing the sideforce on the vertical tail root region close to fuselage junction.

In Figure 7.3 the parameters used to vary the fuselage dimensions are shown, here b_v is the tail height. f_D is the fuselage diameter at quarter chord of the aerodynamic centre of the vertical tail. The fuselage diameter in front of the aft fuselage section is kept constant. The aft fuselage diameter can be altered in three different ways, it can be done by changing the upper fuselage angle (θ_1), by changing the lower aft fuselage angle (θ_2) or by changing both angles at the same time. This is illustrated in Figure 7.4. It is chosen for this research to modify both θ_1 and θ_2 since it represents the situation for most turbo-prop aircraft.

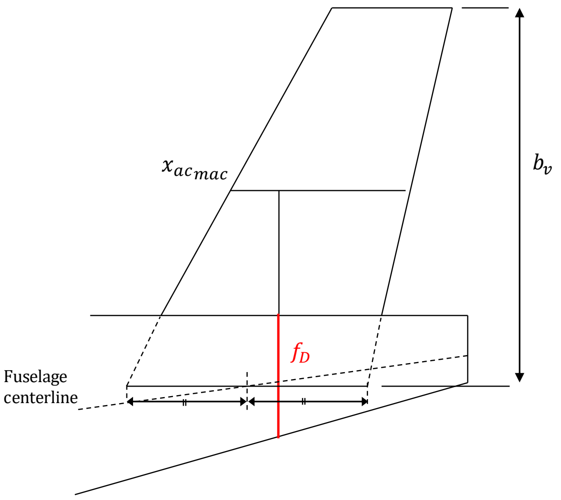

Figure 7.3: Parameters used to describe fuselage-tail effects

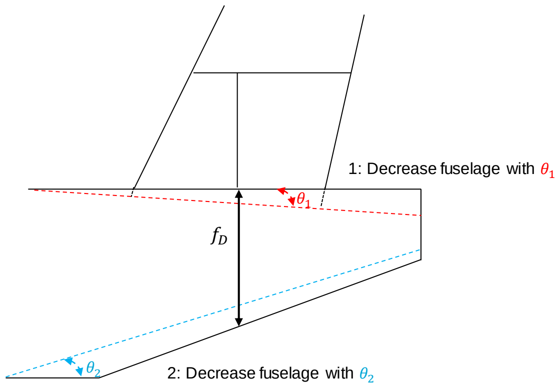

Figure 7.4: Methods to decrease the aft fuselage diameter

In Figure 7.5 the approach used to show the effect is illustrated: the side force coefficient of the vertical tail under influence of the fuselage ($C_{Y_{V_{FV}}}$) is divided by the side force of the isolated vertical tail (C_{Y_V}), previously obtained. Normally the decrease in the aft fuselage diameter would cause the centre of gravity to shift forward. However, because this shift is very small, it assumed the centre of gravity of the fuselage is kept constant at its original position.

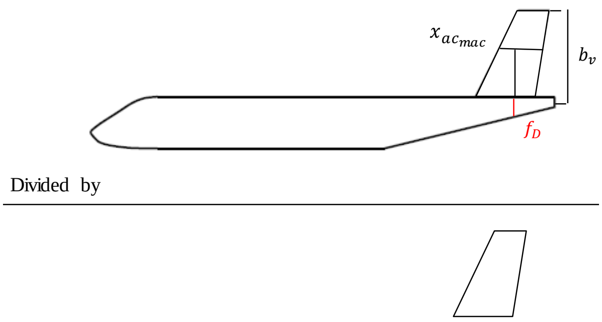

Figure 7.5: Force created by the fuselage plus vertical tail is divided by the force created by the isolated vertical tail

The results of the simulations are shown in Figure 7.6 where the side force coefficient is presented and Figure 7.7 where the yawing moment coefficient is shown for the fuselage (F) and the fuselage and vertical-tail combination (FV). The results are plotted together with the correction factor used for the DATCOM method obtained by windtunnel measurements (added in Appendix A) and the correction curve obtained by CFD by Della Vecchia [32].

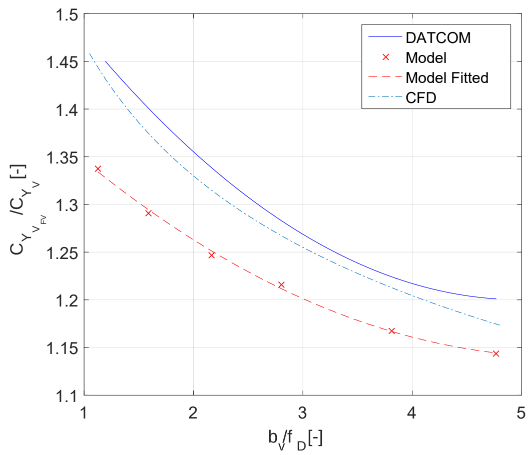

Figure 7.6: Fuselage effect, effect of changing fuselage slenderness on V-tail effectiveness, $\beta = 5°$

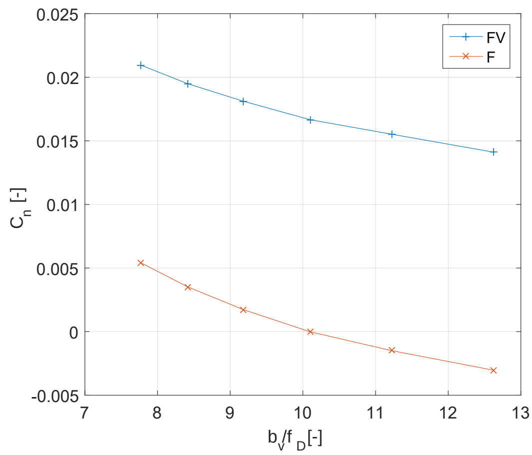

Figure 7.7: Fuselage effect, yawing moment decreases as fuselage becomes more slender, $\beta = 5°$

As the aft fuselage becomes more slender, the effect of the fuselage becomes smaller as expected. It can be seen that for a low ratio of b_v/f_d the tail effectiveness increases with 35 %. Especially the effect of the extra side-wash created $\frac{d\sigma}{d\beta}$ becomes smaller as the fuselage diameter is decreased. The results are underestimated for the tail effectiveness compared to the DATCOM correction factor and the correction curve obtained by CFD measurements [25]. The lower prediction of the model is possibly caused by different modelling of the decrease of the aft fuselage diameter at the vertical tail position which was not extensively described in the sources. In this research the position of the vertical tail was kept constant and the angles causing the decrease in fuselage diameter (θ_1 and θ_2) were varied equally. Possible other modelling of the decrease or increase of the aft fuselage is possible by only changing θ_1 or change θ_1 and θ_2 with different angels, leading to different results. When looking at the yawing moment, Figure 7.7, it becomes clear that not only the yawing moment created by the vertical tail decreases as the aft fuselage becomes more slender, but also the yawing moment by the fuselage decreases.

7.3. SIDEWASH EFFECT CREATED BY THE WING

The second interference effect that has been evaluated is the wing effect, the position of the wing in comparison with the fuselage and the wing aspect ratio on the sideforce created by the installed vertical tail. This has been done by placing a rectangular wing on the fuselage at three different positions (h_w/r_f), low-wing ($h_w/r_f = -1$), mid-wing ($h_w/r_f = 0$), and high-wing ($h_w/r_f = 1$). The aspect ratio of the wing has been varied from 5 to 15 by increasing the span, while keeping a constant shape, constant chord ratio and doing so also increasing the surface of the wing.

The wing fuselage combination has a significant effect on the vertical tail as discussed in Section 2.2.2.

The effect has been measured by the ratio between the vertical tail contribution to sideforce coefficient of the wing-fuselage-vertical tail combination with the fuselage-vertical tail combination previously obtained in Section 7.2. This is illustrated in Figure 7.8, the aircraft including the wing is divided by the aircraft without a wing, isolating the aerodynamic effect of adding the wing.

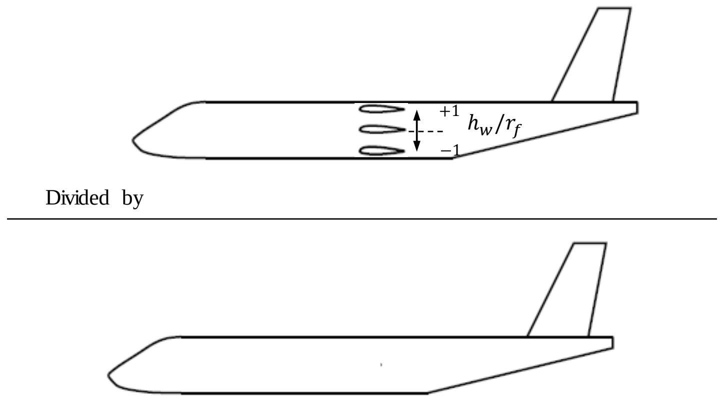

Figure 7.8: Approach to isolate the effect of changing wing configuration

Again all the results are obtained with a sideslip angle of 5 degrees. The results can be seen in Figure 7.9 where the ratio of side force coefficients is shown for the various aspect ratios and Figure 7.10 where for a Aspect ratio of 8, the results are shown together with the CFD results and the correction factor used by Obert, obtained by windtunnel measurement. Note that Obert does not make a distinction between different aspect ratios.

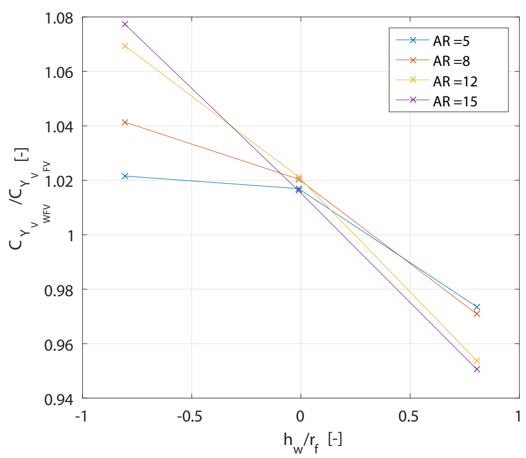

Figure 7.9: Change in vertical tail effectiveness with changing wing position and AR, $\beta = 5°$

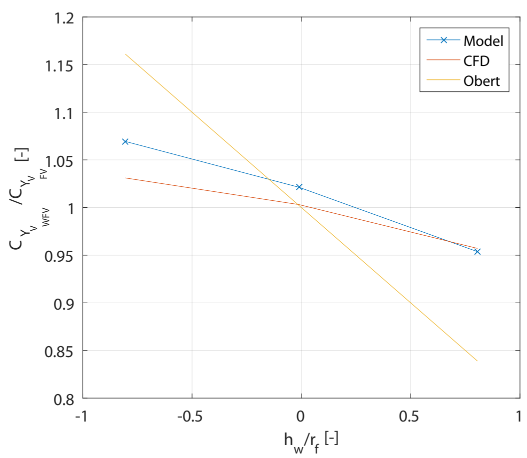

Figure 7.10: Comparison model with CFD results of Della Vecchia [32] and wind-tunnel measuremetns of Obert

From Figure 7.9 it can be seen that the tail effectiveness decreases as the wing is shifted upwards as expected, see the explanation of the wing effect. For a low wing position the circulation created by the change of lift coefficient over the wing causes an extra force on the vertical tail in the direction of the existing force caused by the sideslip, having a stabilising effect on the aircraft. The variation of circulation for a wing with an aspect ratio of 8 has been plotted in Figure 7.11. It is very clear from the figure that an asymmetric circulation is created for a high and low wing.

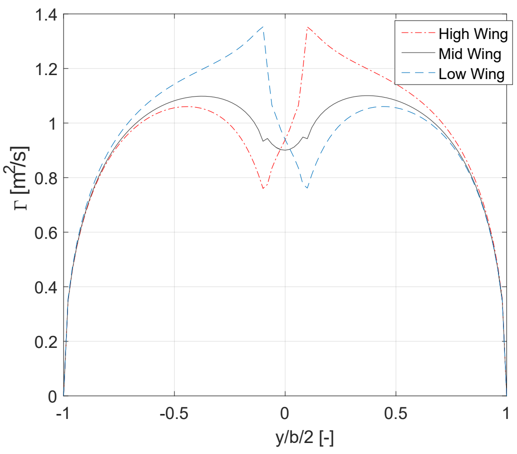

Figure 7.11: Change in circulation distribution for a high/mid/low wing configuration in sideslipping flight, $\beta = 5°$

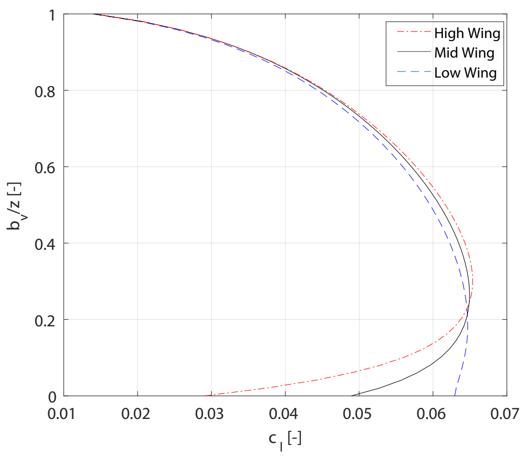

Figure 7.12: Spanwise lift distribution over the vertical tail under the influence of the sidewash created by the wing for a low,mid and high-wing position, $\beta = 5°$

Around the mid-wing position the effect is zero (the ratio $C_{Y_{V_{FWV}}}/C_{Y_V} = 1$) for all aspect ratios. This also is made very clear in Figure 7.11 since the circulation distribution is symmetrical over the complete wing span and is not causing a increase of circulation at the vertical tail.

In Figure 7.12 the spanwise lift distribution is given over the vertical tail. It can be seen as explained in Section 2.2.2 that the circulation created by the low wing increases the lift created at the root of the vertical tail and the circulation created by the high-wing adversely effects the vertical tail by decreasing the lift coefficient. It can also be seen that this effect is not symmetrical. This can be explained by the fact that the trailing vortex sheet of the wing under influence of the downwash and side-slip angle for a low wing is further away from the vertical tail compared to a high wing configuration.

The results obtained show good correlation with the CFD results, see Figure 7.10. The effect for a high wing is slightly over-estimated (4.5%) while the effect for a low wing shows the same result. It is very noticeable that the correction factor obtained by Obert overestimates the wing-effect significantly, having a 20% increase or decrease for a low and high wing configuration.

Finally for the wing interference effect the focus is put on the yawing moment coefficient of the complete aircraft model. In Figure 7.13 the yawing moment coefficient ratio is plotted of the complete model (wing-fuselage-vertical tail combination $C_{n_{WFV}}$) divided by the yawing moment coefficient of the complete model at mid-wing position (C_{n_0}). In Figure 7.14 the yawing moment coefficients of the various parts of the aircraft have been plotted at all three wing positions to explain the effect of Figure 7.13.

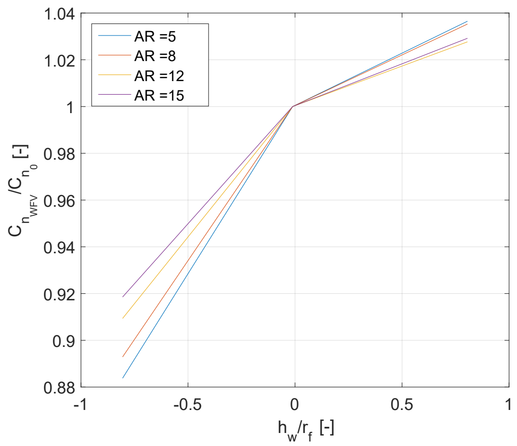

Figure 7.13: Change of yawing moment compared to a mid-wing position, $\beta = 5°$

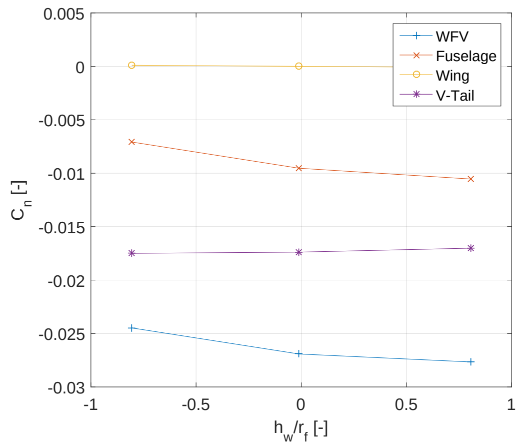

Figure 7.14: Build up of the yawing moment coefficient (WFV= Wing-Fuselage-V-tail) for AR=12, increasing in yawing moment is mainly caused by the fuselage

As the wing position increases to a high wing position the yawing moment of the aircraft increases. This is quite contradictory to the tail effectiveness, which decreases with as the wing position shifts up. This can be explained by Figure 7.14 where the yawing moment coefficient of the individual components (wing, fuselage, V-tail) are plotted. It can be seen that indeed the yawing moment of the vertical tail decreases but that the moment generated by the fuselage increases significantly. This can be explained again by the shift in circulation around the fuselage caused by the change in wing position. The high-wing situation creates a circulation which causes an extra force created by the fuselage in the same direction as the force caused by the sideslip, increasing the yawing moment coefficient of the fuselage.

7.4. HORIZONTAL-TAIL EFFECT

Last interference effect that will be discussed is the effect of the position of the horizontal tail on the vertical tail. A tapered horizontal tailplane, of constant size and aspect ratio, is mounted in five positions on the vertical tail and one on the fuselage, at the quarter chord position of the vertical tail. The dimensions of the horizontal tail can be found in Chapter 6. Next the horizontal tail position is also shifted horizontally (in x-axis direction). The horizontal tail is shifted a quarter chord forward (x/c= -0.25) and a quarter chord backwards (x/c =-0.25). All the positions with regarding to the vertical tail position are sketched in Figure 7.16.

The approach used to isolate the effect of the horizontal tail is sketched in Figure 7.15. The same approach has been used as in the previous sections, the side force coefficient of the wing-fuselage-Vertical tail and horizontal tail ($C_{Y_{V_{WFVH}}}$) is divided by the side force coefficient calculated in the previous part for a mid-wing aircraft without the horizontal tail ($C_{Y_{V_{WFV}}}$).

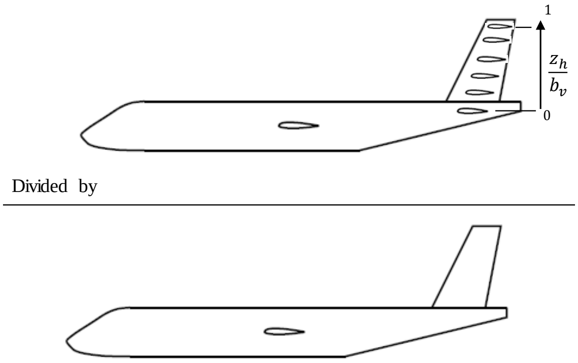

Figure 7.15: Approach to isolate the H-tail effect on the vertical tail effectiveness

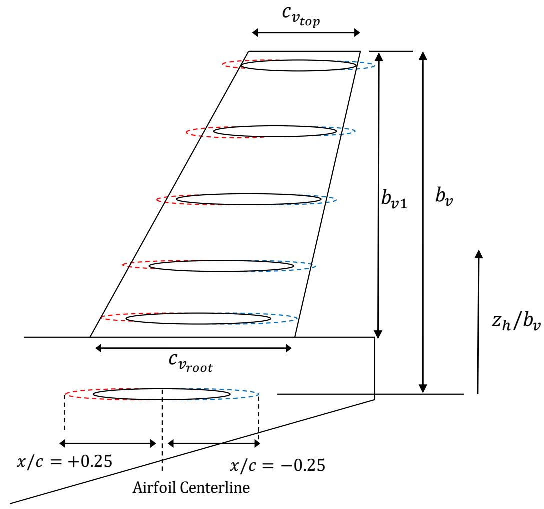

Figure 7.16: Parameters used to describe the position of the H-tail

An example of a simulation of the vertical tail and the horizontal tail is presented in Figure 7.17. To have accurate calculations of the forces and moments generated by the horizontal and vertical tail a mesh with a higher refinement is used than for the vortex field. The horizontal tail in this example is modelled at the middle of the vertical tail ($z_h/b_v = 0.4$) and is shifted a quarter chord forward ($x/c = +0.25$).

When a horizontal tail is installed on a vertical tail, it has one main effect on the vertical tail effectiveness: it prevents the flow of over the vertical tail tip or root from the higher pressure to the lower pressure side, known as the end-plate effect. Therefore increasing the effective aspect ratio of the vertical tail as a winglet does for a wing [25] [31]. Results of the simulations of shifting the horizontal tail over three horizontal positions and six vertical positions are presented in Figure 7.19.

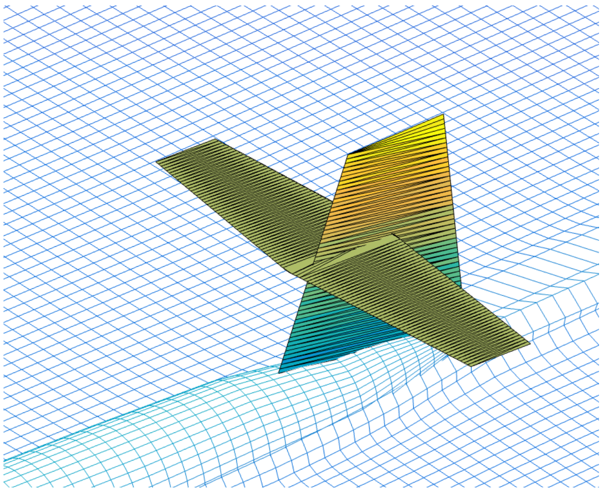

Figure 7.17: Example of simulation with the horizontal tail at mid position shifted forward with 0.25 x/c. The difference between the mesh of the V-tail and H-tail and vortex field can be seen

In Figure 7.18 the spanwise lift distribution of the vertical tail is plotted for the six different vertical tail positions at a chordwise position of $x/c = 0$. Results of the simulations of shifting the horizontal tail over three horizontal positions and six vertical positions are presented in Figure 7.20.

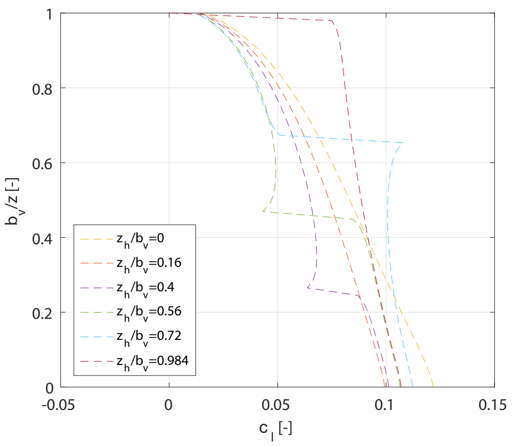

Figure 7.18: Spanwise lift coefficient of the vertical tail for the different H-tail positions with $x/c = 0$, $\beta = 5°$

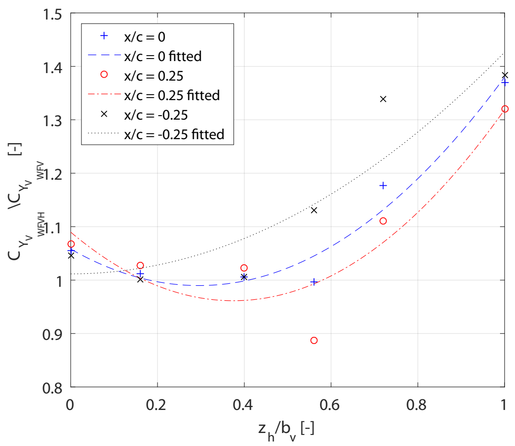

Figure 7.19: Change in vertical tail effectiveness with changing H-tail height for 3 different chord-wise positions, $\beta = 5°$

It is clear from the results that the end-plate effect is the most prominent at the extreme positions of the horizontal tail. It is also clear that the end-plate effect is significantly stronger when the horizontal tail is placed at the top of the vertical tail (T-tail) position. A conventional tail gives a increase of 4-10 percent while the T-tail configuration results in an increase of effectiveness of 30-40 %. This was also as expected since the fuselage already works as an end-plate on the vertical tail and therefore this effect is the strongest for a T-tail configuration. In Figure 7.18 the lift distribution is given for the vertical tail with the horizontal tail at the six different locations at the $x/c = 0$ position. In the figure the location of the horizontal is very clear as is causes a 'bump' in the lift distribution. Is is also very clear that when the horizontal tail is placed at the top position the spanwise lift generated by the vertical tail is maximum.

Additionally it can be seen that the effect is the strongest when the horizontal tail is shifted aft and decreases as the tail is shifted forward. This can be explained by the fact that when the tail is at its aft position the end-plate effect is the largest, the horizontal tail covers almost the entire vertical tail chord.

Validation with the DATCOM correction factor obtained by windtunnel measurements (Appendix A) and the correction curve obtained by CFD by Della Vecchia are presented in Figure 7.20[32]. Note that the CFD curves contains of two parts, causing the kink in the curve. When validating the results of the model with the windtunnel measurements and the results of the CFD analysis, it can be seen that the end-plate effect for both extreme conditions is fairly well predicted. Also the trend of the results is the same for all three, increase of the effectiveness at the bottom and top and a decrease in between. It can be seen however that the model over-predicts the effectiveness increase in the middle section. The lowest point of the graph is at z_h/b_v=0.3, while this is at z_h/b_v=0.4 for the DATCOM graph and at z_h/b_v=0.52 for the CFD correction curve. An explanation compared with the windtunnel data is that the aspect ratio of the vertical tail used for the experiment is not given. Another explanation is that the spread of both the model and the windtunnel measurement is relatively large, leading to a fitted curve with a error percentage that can not be neglected.

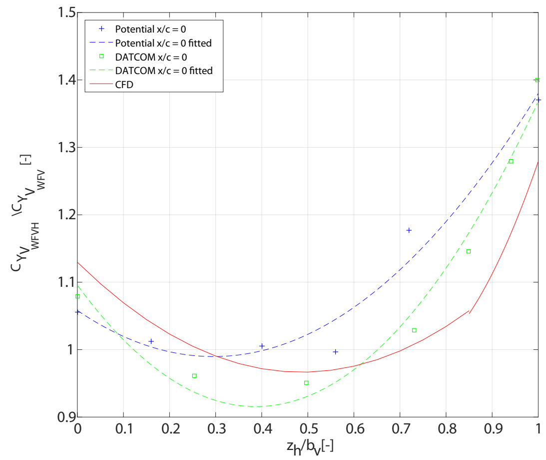

Figure 7.20: Effect of H-tail on V-tail validated with windtunnel measurement obtained for the DATCOM method and the curves obtained by CFD analysis by Della Vecchia [32] [25] x/c =0

7.5. COMPARISON POTENTIAL FLOW MODEL TO DATCOM AND VEDSC

After the analysis of the isolated vertical tail and the interference effects working on the vertical tail, without the propeller slipstream effects, it is now interesting to see how the complete model is affected for different configurations in sideslip conditions. The side force coefficient of the vertical tail of two example aircraft, the ATR 42 and the Fokker 50, are compared between the model and the results obtained using the DATCOM and VeDSC method. This is presented in Table 7.1. The simulated models are presented in Figure 7.21 and 7.22. Both models have been modelled without the dorsal fin. Also for the DATCOM and VeDSC method no additional correction factor has been applied for the dorsal fin to predict the influence on C_{Y_β}. This assumption is valid since the dorsal fin mainly influences the maximum sideslip angle [15].

Table 7.1: Comparison between the side force coefficient obtained using DATCOM and the model

		DATCOM[5]	VeDSC[32]	Model [rad]	Δ DATCOM-Model	Δ VeDSC-Model
$C_{Y_{\beta_v}}$ [-]	ATR 42	0.669	0.659	0.614	9 %	7%
	F50	0.614	0.595	0.553	11 %	8%

For both aircraft, the model predicts the side force coefficient lower for both the VeDSC and the DATCOM method. Both aircraft consist of a high wing configuration however the empennage configuration between both aircraft is quite different. The Fokker consist of a conventional tail while the ATR has a T-tail ($z_w/b_v = 0.9$) configuration. Also the aft fuselage of the ATR is more slender compared to the Fokker aircraft. Additionally the ATR consist of a vertical tail with a higher AR (1.56 - 1.21), neglecting the dorsal fins.

Since the fuselage and wing effect were already predicted significantly lower by the model it was expected that for both aircraft the yawing coefficient would be predicted lower. The difference for the ATR aircraft is smaller because for its T-tail the model predicts a larger interference effect than for the DATCOM method (Figure 7.20). For the Fokker 50 aircraft the opposite is true, the effect of the conventional tail is under predicted causing even a larger difference.

When comparing the results of the potential flow Model and the VeDSC method the differences are smaller. The VeDSC method based on CFD simulations of turboprop aircraft configurations, estimates the interference effect of the wing and fuselage closer to the model used in this research. This causes the difference between the side force coefficient of the complete model to be smaller compared to the DATCOM method.

With respect to the DATCOM method it is important to note, as already stated in the problem statement in the introduction, that the correction factors are based on windtunnel measurements for jet aircraft from the 30' until the 50'. For this reason the results in the VeDSC method, based on CFD measurements of turboprop configurations, is assumed to be a more accurate prediction method at this point. To have a better understanding about the accuracy it is recommended to perform new windtunnel measurements and analyse the different effects by studying the sideforce coefficient of the vertical tail and the yawing moment of the aircraft.

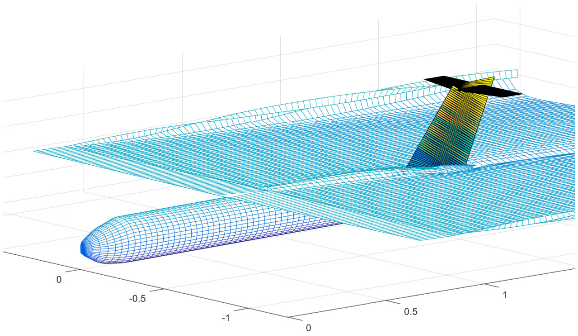

Figure 7.21: Modelling of the ATR42 aircraft: high wing, with T-tail configuration with a swept vertical tail. Wing taper ratio of 0.8.

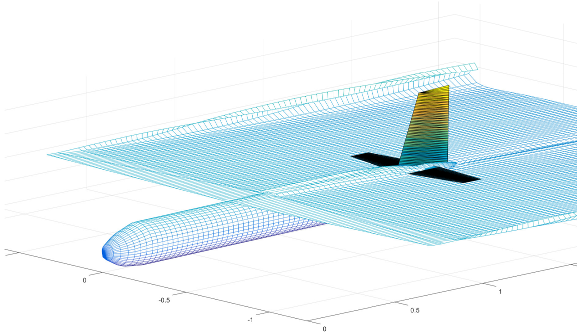

Figure 7.22: Modelling of the Fokker 50 aircraft: high wing with a conventional horizontal tail position. Tail is not swept. Wing taper ratio of 0.5

7.6. CONCLUSION ANALYSIS OF DIRECTIONAL STABILITY USING A POTENTIAL FLOW MODEL

From the verification and validation of the sideforce coefficient of the vertical tail several conclusions can be drawn. The sideforce coefficient of the vertical tail, dependent on the lift curve slope of the vertical tail itself and the inference effects have been validated and verified. If both the isolated vertical tail and the different inference effects are validated it can be assumed that the model can predict the sideforce coefficient for aircraft with different fuselage, wing and empennage configurations accurately.

The validation of the isolated vertical tail with the CFD data showed similar trends and sideforce coefficient values, an error of 2-3% for all three different vertical tail aspect ratios, showing the potential flow model can be used to predict the lift generated by the isolated vertical tail. Next the different interference effects on the installed vertical tail have been studied and validated. For all interference effects the potential model shows the same trends as the CFD data and the correction curves used for the DATCOM method. Only for the fuselage the interference effect a under prediction was found for the whole range of aft fuselage models. The error between the model and the CFD results ranges from 7% for the 'thickest' aft fuselage section to 5.5% for the most slender aft fuselage. However the reason for this could be found in the modelling of the aft fuselage which is not extensively described in the sources possible leading to incorrect modelling of the aft fuselage section in this research. When finally comparing the installed vertical tail for the two example aircraft used with the semi-empirical methods, the side force coefficient is under estimated comparing to both the DATCOM and the VeDSC method. Comparing to the DATCOM method the underprediction is 9% and 11% and comparing to the VeDSC 7% and 8% for respectively the ATR 42 and Fokker 50 aircraft. The VeDSC method, recently derived from measurements using a RANS solver, developed for turbo-prop aircraft geometries, seems to be the most reliable to compare with. The underestimation of the potential flow model can be explained by the under-prediction of the fuselage and the for the Fokker 50 aircraft additionally the under prediction of the H-tail interference effect. The short computational time of the potential flow model, ≈25 seconds without modelling the propeller, shows promising functionality of the model to operate in a conceptual design tool.

8

Analysis of Propeller Slipstream Effects on Directional Stability

In this chapter the results will be presented and described to analyse the effects of the propeller slipstream on the aircraft's directional stability. This will be done by first analysing the results of the isolated vertical tail and the interference effects of the fuselage, wing and horizontal tail on the installed vertical tail and finally evaluate the directional stability derivatives for two example aircraft. The approach and the aircraft and propeller model as described in chapter 6 is used and the mesh for the simulations is used as described in chapter 5. Additionally the effect of shifting the propeller along the wing will be discussed for various wing positions. Unless stated differently for the specific simulation, simulations are executed with a sideslip angle of 5 degrees in an OEI situation where the starboard propeller is rotating IU.

In Figure 8.1 an example of a simulation is given for an OEI condition to obtain the results for the wing interference effect for a mid-wing configuration. On the left side of the figure, the fuselage vertical tail combination can be seen, the horizontal tail is left out at this point. On the right side of the figure the propeller slipstream tube is visualised, leaving the right wing, for a propeller rotating inboard up (clockwise). It can be seen that the propeller slipstream tubes follows the downwash created by the wing and is shifted downwards at the vertical tail position. Finally also the influence of the fuselage can be seen since near the fuselage the lift and therefore the downwash created decreases.

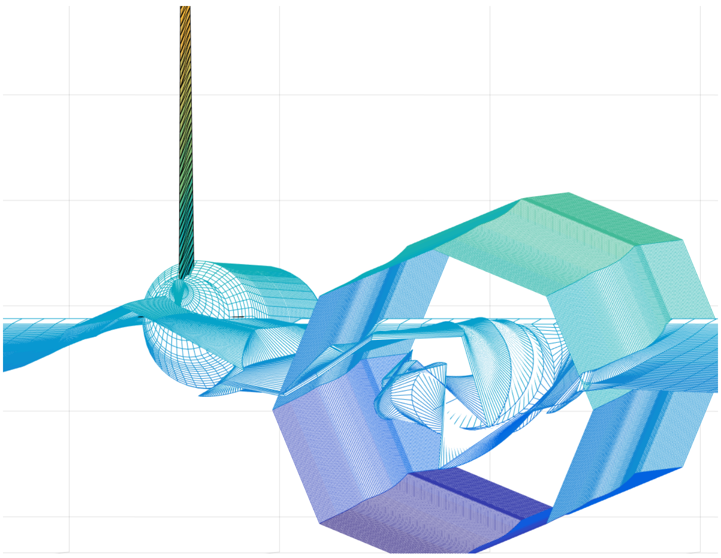

Figure 8.1: Example of a simulation for the wing interference effect under influence of the propeller slipstream. In the centre of the figure the fuselage and vertical tail combination can be seen. On the right side, the propeller slipstream tube is presented for inboard up rotating propeller. It can be seen that the slipstream tube follows the downwash created by the wing and is displaced towards the fuselage

8.1. ISOLATED VERTICAL TAIL UNDER INFLUENCE OF PROPELLER SLIPSTREAM

First the isolated vertical tail under the influence of a propeller slipstream will be discussed. This is done to verify how the propeller influences the vertical tail compared to the no-propeller condition. The isolated vertical tail is analysed to have a baseline to see in the end how all the interference effects affect the side force created by the installed vertical tail under influence of the propeller slipstream. In Figure 8.3 the results are shown for the three vertical tails presented in Figure 7.1 together with the results in the no-prop condition. The propeller has been modelled at the mid-wing position in front of where the wing normally should be and at the same location the propeller will be placed when investigating the interference effects. Both negative and positive side slip angles have been evaluated for the condition where two propeller are active both co-rotating and with one propeller operating, rotating IU positioned at the starboard side of the aircraft. The results have been plotted together with the results obtained previously without the propeller slipstream effect.

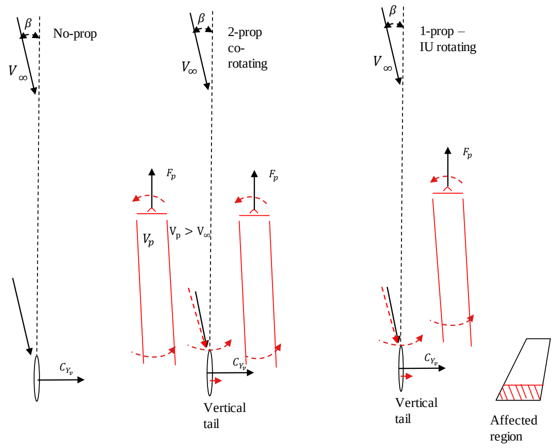

Figure 8.2: Illustrated effect of the propeller on isolated vertical tail under a sideslip angle

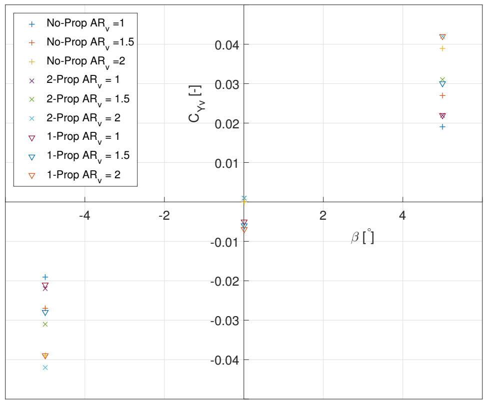

Figure 8.3: Comparison between side force generated by the vertical tail between no-propeller and propeller condition

Table 8.1: Side force coefficient created by the vertical tail for the various conditions

$\beta[°]$			-5	0	5
$C_{Y_v}[-]$	No-Prop	AR =1	-0.019	0	0.019
		AR =1.5	-0.027	0	0.027
		AR =2	-0.039	0	0.039
	1 - Prop IU	AR =1	-0.021	-0.005	0.021
		AR =1.5	-0.028	-0.005	0.027
		AR =2	-0.039	-0.006	0.037
	2 -Prop	AR =1	-0.022	0	0.021
		AR =1.5	-0.030	0	0.026
		AR =2	-0.041	0	0.038

From the results it can be seen that for all three vertical tails the side-force created increases slightly for a positive and a negative sideslip angle with the propeller installed. However the effect is found to be small for the isolated vertical tail, max 4%. What directly can be noticed is that for the one propeller case, the sideforce at the vertical tail is not zero at zero degree angle of sideslip, because of the asymmetric condition. This effect for the isolated vertical tail is still not very significant, however this effect will increase once the wing and fuselage are installed, presented later in this research. An explanation of this condition can be seen the left illustration in Figure 8.4

The small effect of the propeller on the vertical tail is mainly caused due to the fact the propeller slipstream only affects the root of the vertical tail. A sketch of the different situations is presented in Figure 8.2. The first situation represents the vertical tail under a side-slip angle. The second situation represents the second situation where two co-rotating propellers are operating. The circulation created by the propeller causes the inflow angle at the root of the vertical tail to be increased slightly compared to the free stream. This increase of inflow angle at the root causes the lift generated at the root to be slightly increased, creating a larger side force coefficient by the vertical tail. Also it was found that at the root of the vertical tail the inflow velocity was slightly increased under influence of the propeller slipstream. For the one propeller condition the same was found regarding the inflow angle. For a negative sideslip angle as shown in Figure 8.2 the inflow angles slightly increases at the root creating a larger side force coefficient. It can be concluded that the force generated by the vertical tail because of the sideslip dominates the force created by the vertical tail, as the sideforce is only increased 3% to 4% for the different vertical tails.

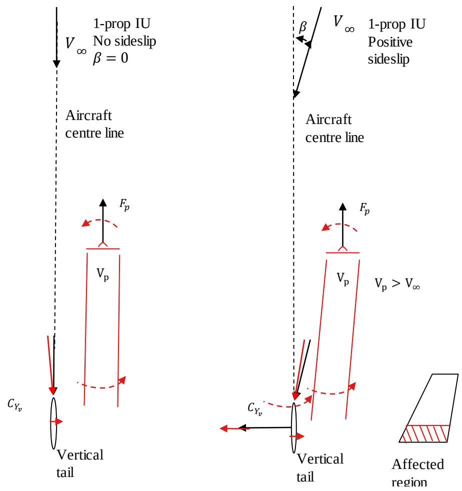

Figure 8.4: Effect of the propeller on isolated vertical tail. First situation represents the OEI condition under zero degree angle of sideslip. The second situation is the OEI condition with a positive sideslip angle

In the right of Figure 8.4 the situation is sketched for the OEI condition, rotating inboard up with a positive sideslip angle. It was found that the propeller slipstream under influence of the side slip angle moves towards the vertical tail. The propeller slipstream tube causes an increase in velocity of the flow at root of the vertical tail, increasing the side force created. However the circulation of the propeller on the other hand also decreases slightly the inflow angle, decreasing the net increase of the sideforce. It can be concluded that the force generated by the vertical tail because of the sideslip dominates the force created by the vertical tail, as the sideforce in only increased 3 to 4% for the different vertical tails.

8.2. FUSELAGE INTERFERENCE EFFECT ON THE VERTICAL TAIL UNDER INFLUENCE OF A PROPELLER SLIPSTREAM

After the isolated tail is evaluated, the interference effects under influence of the propeller slipstream on the installed vertical tail will be assessed. As discussed before, the fuselage influences the vertical tail in two ways: increase of sidewash over the vertical tail and an end-plate effect on the lower side of the vertical tail. Now it will be evaluated for how these effects are influenced by the propeller slipstream. The side force coefficient of the fuselage-vertical tail and propeller combination have been compared with the side force coefficient for the isolated vertical tail without the propeller installed, obtained previously. Having executed the same simulation without a propeller allows for good comparison how the effect is influenced. The propeller slipstream effect on fuselage interference effect has been illustrated in Figure 8.5. The additional sidewash created by the fuselage ($Vsin(\beta-\sigma)$) is now increased with the extra velocity created by the propeller slipstream (ΔV_p). The propeller slipstream increases the crossflow the vertical experiences as compared to the no-propeller situation. The increase of this crossflow increases the lift force created at the root of the vertical tail, increasing the sideforce of the vertical tail.

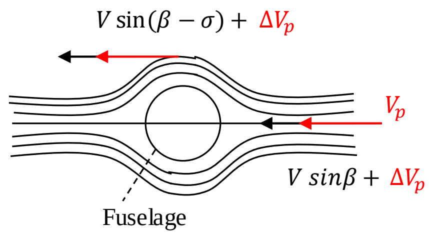

Figure 8.5: Illustration to sketch the influence of the propeller slipstream on the fuselage interference effect

The propeller has been modelled at mid-wing position, at its location in front of the wing at spanwise location (y/D= 1.05) without the wing being present. A sketch of the approach to obtain the effectiveness ratio can be seen in Figure 8.6. The propeller has been modelled rotating IU positioned at the starboard side of the aircraft.
In Figure 8.7 the results are presented for the fuselage interference effect with the propeller installed (prop-on) plotted together with results obtained previously in Section 7.2. For the prop-on condition the results are plotted both for a sideslip angle of 5 or -5 degrees, to show that the asymmetrical thrust and the propeller slipstream are influenced depending on the sideslip angle.

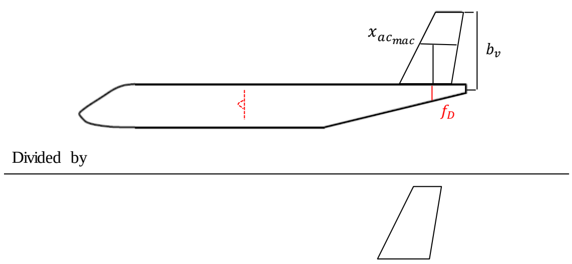

Figure 8.6: Approach to isolate the effect of the fuselage-propeller combination - OEI condition, starboard propeller installed turning IU

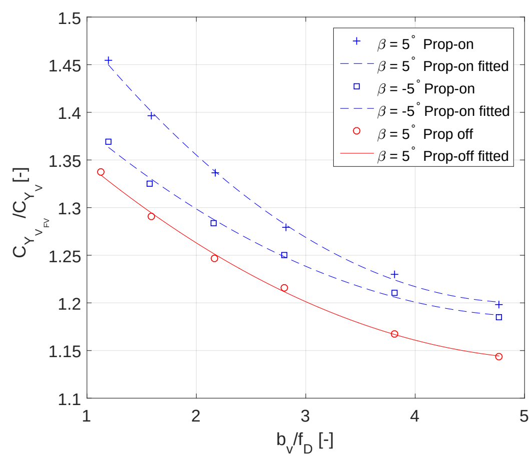

Figure 8.7: Fuselage effect, comparison between the fuselage interference effect between the prop-off and prop-on condition. Propeller rotating IU, $T_c = 1.2$. Comparison of the results for the $\beta = 5$ and $\beta = -5$ for the prop-on condition.

Propeller-Fuselage Effect: First it can be seen that the propeller has increased the fuselage effect when compared to the no-propeller situation for both the positive and the negative sideslip angle. The end-plate effect of the fuselage is assumed to constant however this increase can be explained by the increase of sidewash at the vertical tail ($\frac{d\sigma}{d\beta}$). The propeller slipstream tube consisting of higher pressure and velocity then the free stream increases the sidewash and the force generated by the vertical tail.

From the results it can be seen that the increase of effectiveness of the vertical tail is different for the positive and the negative sideslip angle as expected. For the situation where the propeller slipstream shift towards the fuselage the fuselage interference effects increase as expected. The difference between both situations is approximately 10 % for b_v/F_D close to 1 and decreases to 5%.

8.3. WING INTERFERENCE EFFECT ON VERTICAL TAIL UNDER INFLUENCE OF A PROPELLER SLIPSTREAM

The second interference effect discussed under the influence of the propeller slipstream is the wing interference effect. This has been done using the same approach as for the situation there was no propeller installed. The wing position and aspect ratio influence the lift distribution and the flow over the fuselage, changing the circulation and sidewash at the vertical tail. First the wing interference will be discussed under the influence of a propeller for a side slipping flight ($\beta = 5°$). Secondly the effect of the propeller and wing position on the vertical tail and aircraft will be discussed without a sidelslip angle ($\beta = 0°$).

The spanwise axial velocity behind the propeller is presented in Figure 8.8 for a thrust coefficient (T_c) of 1.2. It can be seen that the axial velocity increases significantly behind the blade section for both the up and down-ward going blade. Because the lift coefficient is directly related to the speed (Kutta–Joukowski theorem), the effect of the axial velocity increase can directly be seen in Figure 8.10 where the spanwise lift coefficient for the various wing positions is presented. Round zero a small bump can be seen in the velocity profile induced by the presence of the fuselage.

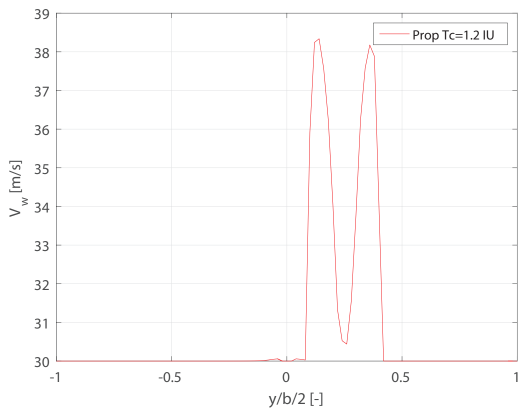

Figure 8.8: Axial velocity of the flowfield behind the propeller blade, $V_\infty = 30[m/s]$

The position of the wing is varied from a low to a high wing position, additionally the wing aspect ratio is varied between 5 and 15. This has been done by placing a rectangular wing on the fuselage at three different positions (h_w/r_f), low-wing ($h_w/r_f = -1$), mid-wing ($h_w/r_f = 0$), and high-wing ($h_w/r_f = 1$). It must be noted that the propeller position is varied with the wing position, the z-location of the propeller centre axis is placed at the same height as the wing. The propeller is modelled at y/D of 1.05 on the starboard side, rotating IU.

In Figure 8.9 and Figure 8.10 the spanwise circulation and lift coefficient are given under influence of the sideslip and the propeller slipstream. When comparing the circulation distribution to circulation distribution without the propeller installed, Figure 7.11 the effect of the propeller can be clearly seen. The increase in circulation on the upward going side and the decrease in circulation for the downward going side of the propeller. For the high wing position the combination of the sideslip angle, causing a increase in circulation in the forward semi-wing, and the propeller cause a strong peak in the circulation distribution. As stated before the lift coefficient is directly dependent on the velocity of the stream and the circulation. Combining therefore the velocity distribution of Figure 8.8 and the circulation of Figure 8.9 results in the lift coefficient distribution presented in Figure 8.10. The sharp peak in of the high wing can be seen again as expected. The increased lift coefficient at the starboard side of the fuselage, causes also a strong downwash behind the wing. The circulation created round the fuselage, causing the wing interference effect on the installed vertical tail (Figure 2.5), is increased. Therefore the wing interference effect is stronger as compared to the no-prop condition.

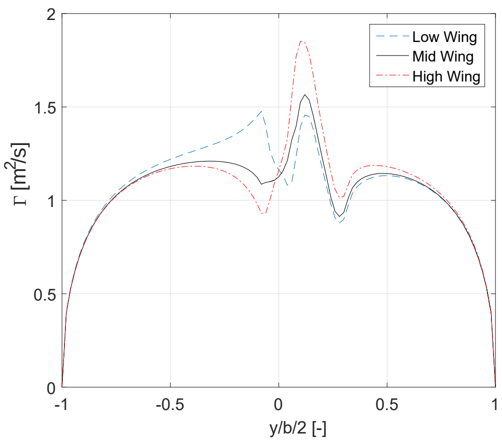

Figure 8.9: Circulation distribution over the wing (AR=12) and fuselage under a 5 degree sideslip under influence of a inboard up rotating propeller (T_c = 1.2) for a low, mid and high wing position

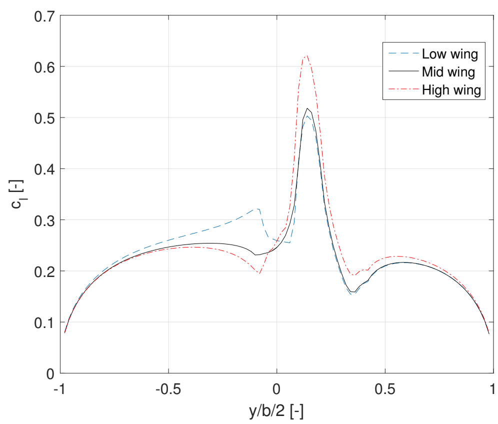

Figure 8.10: Lift distribution over the wing (AR=12) and fuselage under a 5 degree sideslip under influence of a inboard up rotating propeller (T_c = 1.2) for a low, mid and high wing position

The increase of wing interference effect under the influence of the propeller slipstream has been illustrated in Figure 8.11. The increased lift and therefore downwash at the starboard side caused by the propeller slipstream, increases the circulation round the fuselage in clockwise direction. This causes a decrease of the inflow angle at the root region of the vertical tail, decreasing the lift created. This can be seen in Figure 8.12. Here the lift distribution of the vertical tail has been plotted for the three wing positions. In the root region of the vertical tail, up till 20%, a significant difference can be seen in the lift created. Compared to the mid wing position, the lift created by the vertical tail of the low wing is slightly increased however a significant decrease can be seen for the high wing position.

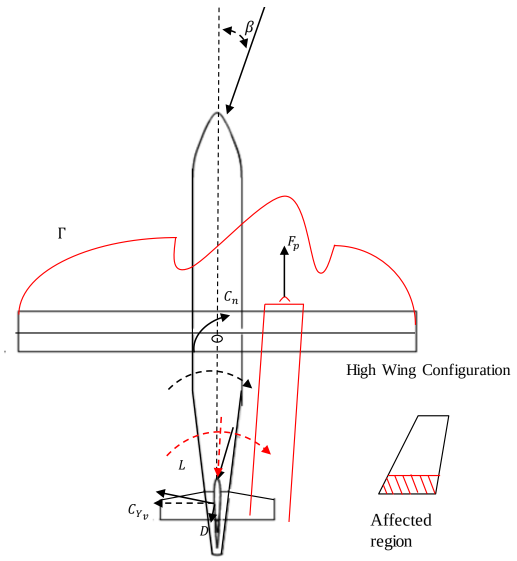

Figure 8.11: Illustration to show the effect of the high wing position with the propeller installed on the vertical tail

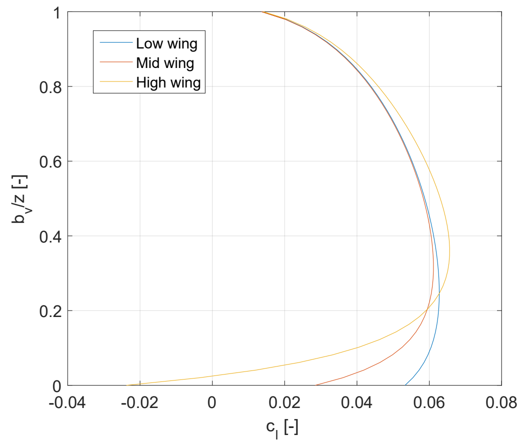

Figure 8.12: Tail lift distribution with a wing moddeled with a AR of twelve and fuselage under a 5 degree sideslip under influence of a inboard up rotating propeller ($T_c = 1.2$) for a low, mid and high wing position

The side force coefficient of the vertical tail at mid-wing position has been chosen as reference point ($C_{Y_{V0}}$) and the high-wing and low-wing position have been compared with this reference point to see the effect of changing the wing and propeller position on the side force created by the propeller. Therefore the graphs show the side force coefficient of the vertical tail under influence of the wing-fuselage-vertical tail combination ($C_{Y_{V_{WFV}}}$) relative to this reference point ($C_{Y_{V0}}$), this is illustrated in Figure 8.13. Where the first graph shows the effect under a five degree sideslip.

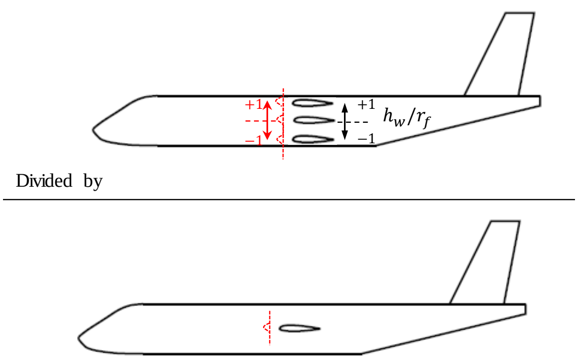

Figure 8.13: Approach to isolate the effect of changing the wing position with the propeller installed

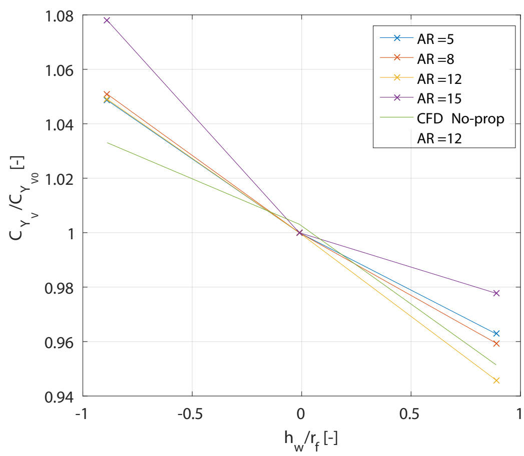

Figure 8.14: Vertical tail side force coefficient ratio plotted for a low ($h_w/r_f = 0$) to a high wing ($h_w/r_f = 1$) configuration for 4 different wing aspect ratios ($\beta = 5°$)

As for the case with no propeller installed, the tail effectiveness decreases as the wing shifts from a low to a high wing position, see Figure 8.14. This effect is mainly caused by the change in circulation distribution over the wing-fuselage combination as explained above. This circulation is now additionally affected by the propeller causing a steep increase a the upward going side and a small decrease at the down-going side of the propeller.

The circulation created round the fuselage causes the tail to become more effective for a low wing configuration and less effective for a high wing configuration. It can be seen from Figure 8.9 that the difference in circulation due to the presence of the propeller is more significant, where the circulation is plotted for a wing aspect ratio of 12 at low, mid and high-wing position. It most be noted however that the results have been plotted in comparison to the mid-wing position.

Yawing moment coefficient created by propeller slipstream under zero degree angle of sideslip

The simulations performed at zero degrees sideslip is an expansion to the work previously performed with the potential flow model and was recommended by one of the previous authors, to evaluate the yawing moment coefficient for different wing configurations for an aircraft in OEI conditions. Since the propeller location changes with the wing position, the flow round the aircraft is changed. In comparison to the previous section, where it was found that the vertical tail becomes less effective for a high wing configuration under a sideslip angle, it is now shown in the next 4 figures that the yawing moment coefficient of the aircraft increases as the wing is shifted from a low to a high wing position when there is no sideslip angle for an OEI condition. As the wing and the propeller are shifted up, the influence of the propeller on the vertical tail increases. The IU rotating propeller causes a clockwise circulation distribution at the root of the vertical tail. This causes a crossflow over the vertical tail creating a side force. This sideforce is creating a negative yawing moment in the same direction as the starboard propeller is creating, destabilising the aircraft. The effect of the propeller on the aircraft and vertical tail have been illustrated in Figure 8.15.

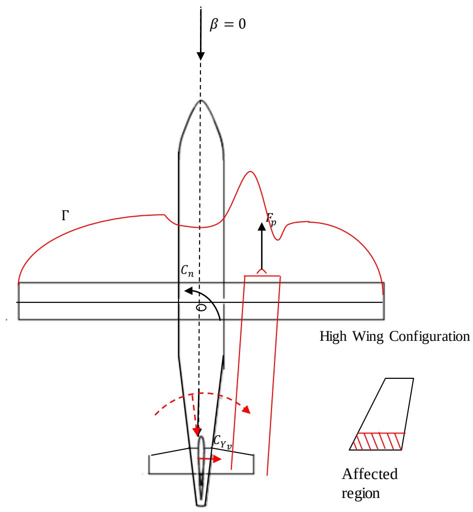

Figure 8.15: Illustration of the simulation with OEI condition at starboard side turning inboard up at zero degrees angle of sideslip ($\beta = 0$). Crossflow at the vertical tail causes a destabilizing sideforce to be created by the vertical tail

In Figure 8.16 the crossflow over the vertical tail (V_y/V_∞) is plotted and in Figure 8.17 the lift coefficient created by the crossflow is presented. It can be seen that the crossflow is especially present in the root region of the vertical tail. From the lift coefficient graph it can be seen that the effect is significant for the high wing position, since the propeller has a greater influence.

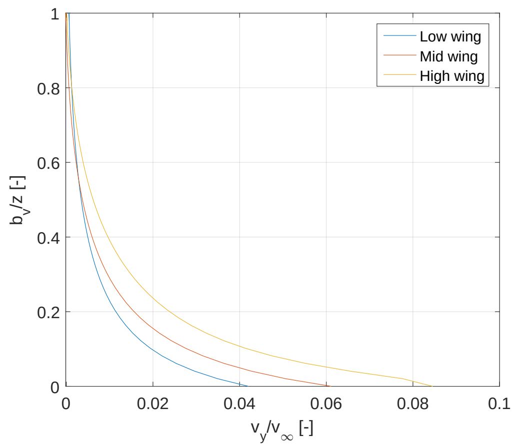

Figure 8.16: Crossflow at the vertical tail for low, mid and high wing position for an IU rotating propeller ($T_c = 1.2$) placed at the starboard position at zero degrees sideslip ($\beta = 0°$)

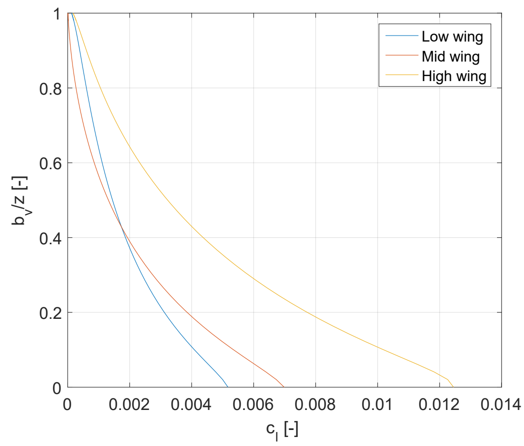

Figure 8.17: Lift at the vertical tail for low, mid and high wing position for an IU rotating propeller ($T_c = 1.2$) placed at the starboard position at zero degrees sideslip ($\beta = 0°$)

In Figure 8.18 and Figure 8.19 the results are shown for a zero degree angle of sideslip. In Figure 8.18 the yawing moment coefficient of the complete model ($C_{n_{WFV}}$) is divided by the yawing moment of the complete model at mid-wing position (C_{n_0}). To analyse how the yawing moment coefficient changes as the wing position is shifted up from a low wing to high wing configuration. In figure 8.19 the yawing moment coefficient generated by the various parts for the different wing locations is shown to explain the results.

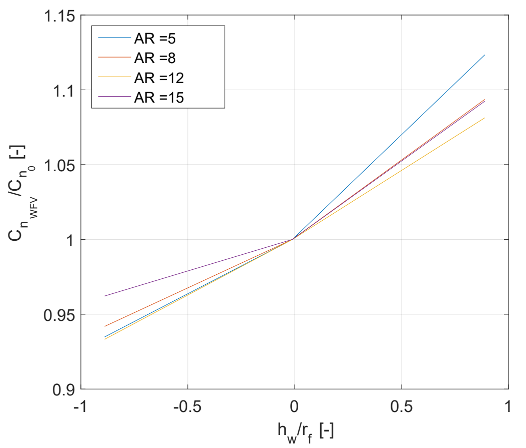

Figure 8.18: Yawing moment coefficient ratio in OEI condtion, IU rotating propeller ($T_c = 1.2$), made non-dimensionless with the mid-wing position at a sideslip of 0 degrees

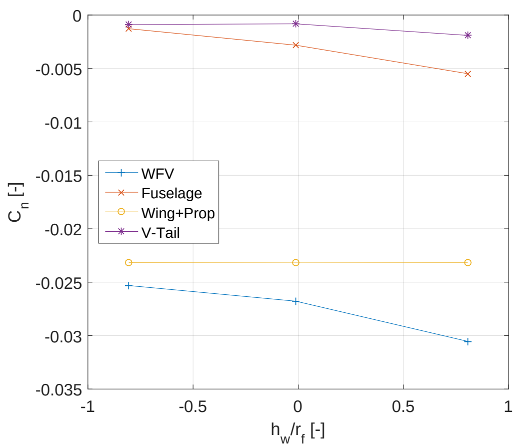

Figure 8.19: Build up of the yawing moment coefficient for AR=12 plotted for a low to a high wing configuration, IU rotating propeller ($T_c = 1.2$)

As the wing shifts up it can be seen that the yawing moment coefficient increases, this was also found in literature [24]. The change of yawing moment is significant and is around 20% for all aspect ratios. It can be seen that the effect is not symmetrical and is twice as large for the high wing position compared to the low wing position. This was also already found in the lift distribution over the vertical tail.

At zero degree angle of sideslip the moment created by the propeller on the fuselage and tail works in the same direction as the propeller itself, see Figure 8.18. The forces created on the fuselage and vertical tail thus adversely affect the aircraft directional stability in OEI situation. As the propeller, attached to the wing, shifts up, especially the yawing moment coefficient created by the fuselage increases (Figure 8.19). Note that this yawing moment coefficient is only induced by the rotating propeller since the sideslip angle is zero. The propeller slipstream tube causes an increase in crossflow over the fuselage and vertical tail, especially at the root section of the vertical tail. In case of a high wing position the downwash behind the wing causes the propeller slipstream tube to be nicely aligned next to the fuselage causing the crossflow created to be larger. Concluding that a high wing position in an OEI conditions results in a 20 % increase of the yawing moment coefficient generated by the aircraft as compared to a low wing position. To cope with the increased yawing moment, the aircraft shall need extra rudder input to be able to maintain directional control in this condition.

8.4. HORIZONTAL-TAIL INTERFERENCE EFFECT UNDER INFLUENCE OF A PROPELLER SLIPSTREAM

In this section the interference effect of the horizontal tail on the installed vertical tail will be explained under the influence of a propeller slipstream. The same approach has been used for the situation where there was no propeller installed. A tapered horizontal tailplane, of constant size and aspect ratio, is mounted in six positions on the vertical tail and one on the fuselage, at the quarter chord position of the vertical tail.
Next the horizontal tail position is also shifted horizontally (in x-axis direction). The horizontal tail is shifted a quarter chord forward (x/c= -0.25) and a quarter chord backwards (x/c =-0.25). All the positions with regarding to the vertical tail position are sketched in Figure 7.16. All measurements are done with an OEI condition, starboard propeller rotating IU, under a sideslip angle of 5 degrees.

The approach used to isolate the effect of the horizontal tail is sketched in Figure 8.20. The side force of the complete model including the horizontal tail, thus including the fuselage, wing and vertical tail and propeller ($C_{Y_{V_{WFVH}}}$) is divided by the side force coefficient calculated in the previous part for a mid wing aircraft without the horizontal tail ($C_{Y_{V_{WFV}}}$).

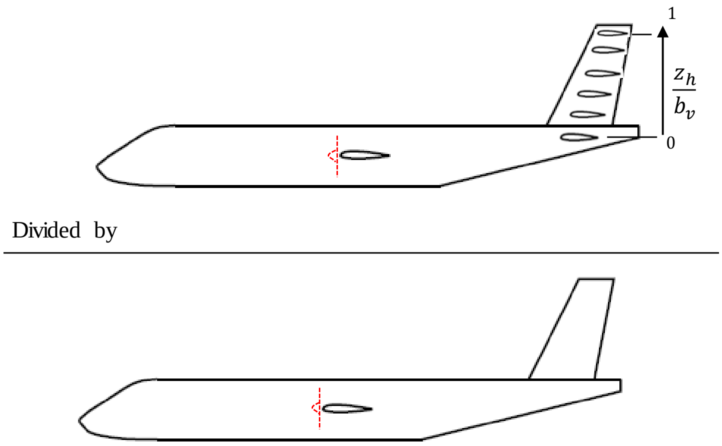

Figure 8.20: Approach to isolate the effect of changing the position of the horizontal tail. The side force coefficient including the H-tail is divided by the model whiteout the H-tail.

As stated in in Section 7.4 the horizontal tail has one main effect on the vertical tail: the horizontal tail prevents the flow from going from the higher pressure side to the lower pressure side, increasing the 'lift' generated by the vertical tail, effectively increasing the effective aspect ratio of the vertical tail. This effect is known as the end-plate effect and can be compared to the effect of a winglet on a wing.

The results of shifting the horizontal tail over six positions vertically, from a conventional tail to a T-tail, and three positions horizontally are shown in Figure 8.21. The results are again generated with a OEI condition, the propeller turning inboard up at a T_c of 1.2 and with a sideslip of 5 degrees.

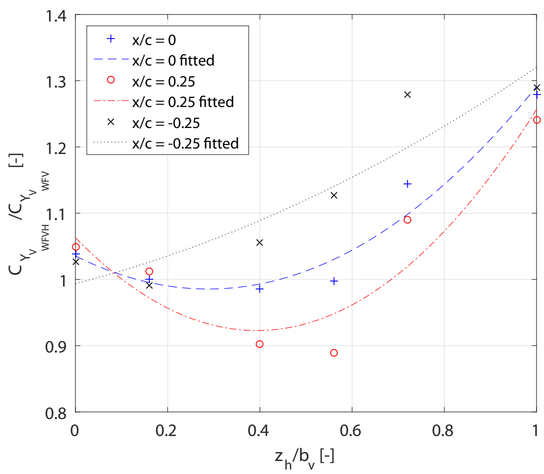

Figure 8.21: Side force coefficient ratio showing the effect of adding a horizontal tail on the side force created by the vertical tail. Shifted from a conventional tail ($z_h/b_v = 0$) to a T-tail configuration ($z_h/b_v = 1$), $T_c = 1.2$, $\beta = 5°$.

The results show a similar trend to the no-propeller situation. The horizontal tail increases the effectiveness of the vertical tail at its two outer positions with a slight decrease at the middle position. Again it is found that the end-plate effect at the top position (T-tail) configuration is stronger (24% to 32%) than its effect at the bottom (0 to 6%). This is due to the presence of the fuselage already working as an end-plate at the bottom position.

Regarding the chordwise position of the horizontal tail again the same trends can be seen as for the situation with no propeller. When the horizontal tail is shifted a quarter chord backwards (x/c =-0.25) the interference effect is larger. At this location the horizontal tail is placed at the middle of the vertical tail, almost covering the complete vertical tail chord span, preventing cross-flow over the vertical tail. The opposite happens when the horizon tail is shifted forward. Less chordwise span of the vertical tail is 'covered' by the horizontal tail. It must be noticed that the spread of the data points can not be neglected and there is an error in the fitted curve, especially for the x/c=0.25 line.

When the results are compared to the no-propeller situation it can be seen that the results show the same trend, see Figure 8.22. The biggest difference (9%) that can be noticed is the interference effect of the T-tail configuration (z_h/b_v =1).

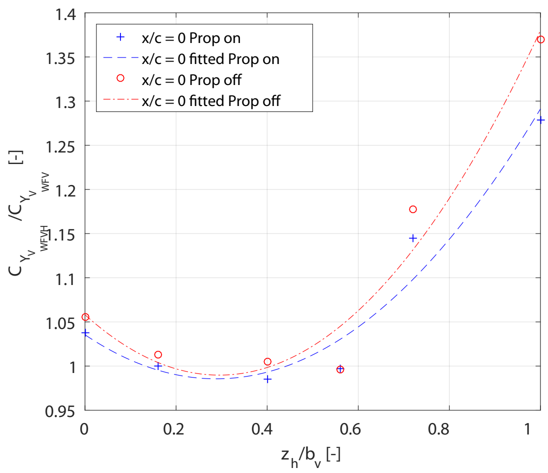

Figure 8.22: Comparison of H-tail interference effect for prop-off and prop-on condition

8.5. EFFECT SPANWISE PROPELLER LOCATION ON DIRECTIONAL STABILITY

To make this research complete, not only the effect of configuration changes is examined but also the location of the propeller itself. The propeller location, its spanwise position on the wing, has been modified to see the effects on the yawing moment coefficient (C_n. To make this location again non-dimensionless, the ratio has been taken between the distance between the location of the propeller centre axis and the fuselage centre axis (denoted as y) and the propeller diameter (denoted as D). This is shown in Figure 8.23. The wing and propeller location have been shifted over three positions, low,mid and high-wing configuration to see the effect of changing the wing and propeller position vertically.

Changing the propeller's spanwise position has two mayor effects. First the moment arm increases as the propeller shift more outboard increasing the moment generated. Secondly when the propeller is placed more closely to the fuselage, interference effects between the propeller and the fuselage and the vertical tail occur. To examine these effects the wing position has been evaluated at three positions, low-,mid- and high-wing position.

In Figure 8.24 the results are shown for the simulations and are validated with the windtunnel measurements of Mannée. To be able to compare the yawing moment coefficient to the windtunnel measurement of Mannée the model has been adapted. The configuration as described by Mannée has converted to a new aircraft geometry model and has been used for the simulations. The results are generated for an OEI condition with the propeller rotating IU at zero degree angle of sideslip. The configuration and results of Manée can be found in Appendix B.

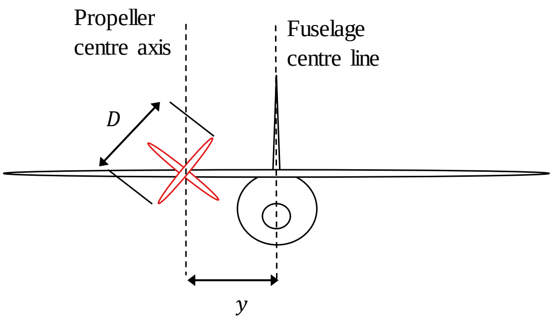

Figure 8.23: Parameters used to define the propeller location on the wing

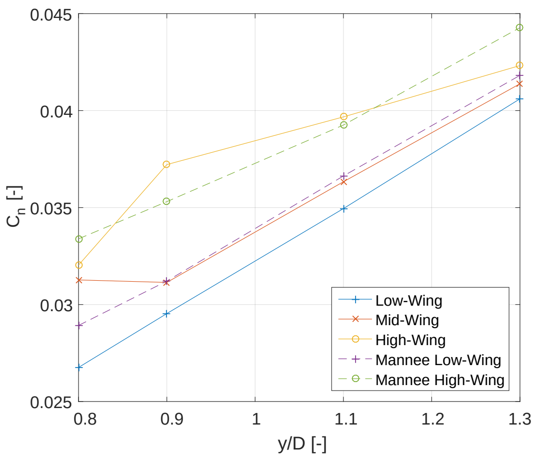

Figure 8.24: Yawing moment coefficient plotted against the propeller location on the wing for three wing positions

As expected the yawing moment increases as the propeller is moved more outboard. The linearly increased moment arm causes a linear increase in yawing moment as expected. Regarding the wing position it can be seen that as the wing shift up the yawing moment increases. This was also already found when investigating the wing interference effect in Section 8.3, confirming the results found previously. Especially when the propeller is placed at the wing root the wing position has the biggest influence on the yawing moment coefficient. This is a logical effect since when the propeller is placed more inboard the interference effects become more significant. At the low wing position the downwash of the wing causes the vortex field to be underneath the fuselage lowering the interference effects compared to the high wing configuration. When comparing the results to the measurement it can be seen that the model and the measurement have the same trend. For both the model and the measurements the high-wing generates the largest moment and the moment increases as the propeller is moved more outboard. The prediction for the low-wing is underestimated from the inboard to outboard position however for the high-wing it fluctuates round the measurement data. The model seams to over-predict the interference effect at the more inboard positions while the measurement data increases linearly as the propeller arm increases linearly.

8.6. DIRECTIONAL ANALYSIS COMPLETE AIRCRAFT CONFIGURATION

After the isolated tail and the individual interference effects have been analysed under the influence of the propeller slipstream, the model is now used to analyse the complete aircraft model. Again the two example aircraft, the Fokker 50 and the ATR 42, will be used and the directional stability coefficients are evaluated with the results obtained without the propeller been installed. First the sideforce coefficient of the vertical tail is discussed in a sideslipping flight and secondly the yawing coefficient created in OEI conditions with zero degrees angle of sideslip will be discussed.

Evaluation C_{Y_β}; Finally to compare the effects of complete aircraft on the side force coefficient of the vertical tail under a sideslip angle ($C_{Y_{\beta_V}}$), which is one of the most important coefficients in preliminary design of the vertical tail, a comparison is made between the side force coefficient of the vertical tail with and without the propeller installed. This is presented in Table 8.2. The simulation with propeller is done with an OEI condition with the starboard propeller turning IU with a thrust coefficient of 1.2.

Table 8.2: Comparison between the side force coefficient of the vertical tail under a sideslip angle between the propeller installed and no-propeller installed condition

	Aircraft	No-Propeller	Propeller	Δ
$C_{Y_{\beta_V}}$ [-]	ATR 42	0.592	0.627	6 %
	Fokker 50	0.572	0.609	7 %

Analysing the isolated vertical tail and the interference effects working on the installed vertical tail, it was found that the propeller influences the side force created. Especially for the fuselage and wing effect it was found that the side force coefficient is significantly influenced depending on the configuration of the aircraft. For both example aircraft, consisting of a high wing configuration and similar fuselage shape the increase therefore is almost equal (6 and 7%). This increase in yawing force created by the propeller, for which now a better understanding is created, should be used towards a more efficient design in the conceptual design phase.

Evaluation of C_n for $\beta = 0$; Next the yawing moment coefficient (C_n) for the two example aircraft are evaluated in OEI conditions. The yawing moment coefficient of the aircraft in OEI is an important parameter in the conceptual design of the vertical tail of turbo-prop aircraft and driving the vertical tail design (Section 2.1). The yawing moment coefficient created in OEI conditions by the propeller and aircraft must be balanced by a restoring moment created by the rudder. Having a more accurate prediction of the yawing moment coefficient in OEI conditions in the conceptual design phase will lead to a more efficient design of the vertical tail. It was already found in literature that the IU rotating propeller has largest effect on the yawing coefficient [23] [25]. To see the difference of the rotating direction on the complete configuration both inboard and outboard up conditions are now evaluated.

For both aircraft the same propeller shape and geometry have been used has been used to evaluate the different aircraft configurations. The yawing moment for both aircraft are given in Table 8.3.

In Figure 8.25 the lift distribution is given for the OU and the IU rotating propeller for the Fokker 50 aircraft configuration at zero degrees angle of attack and sideslip. The peaks created by the propeller can be clearly seen. For the IU rotating propeller the peak is more inboard ($y/b/2 \approx 0.2$) compared to the peak for the OU rotating propeller ($y/b/2 \approx 0.4$). It can also be seen that the lift coefficient peak created for the OU rotating propeller is slightly higher compared to the IU rotating propeller (0.625 - 0.6). This is to the fact, the peak of the IU rotating propeller already experiences the effect of the fuselage decreasing the lift coefficient.

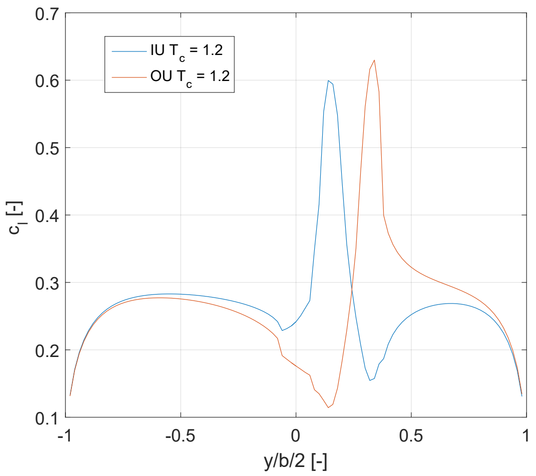

Figure 8.25: Spanwise lift distribution for the modelled Fokker 50 aircraft, $\alpha = 0$, $\beta = 0$, $Tc = 1.2$, Wing properties of Table 5.2

Table 8.3: Yawing moment coefficient for the two example aircraft configurations in OEI conditions under zero degree angle of sideslip, modelled with the same propeller at $T_c = 1.2$

	Aircraft	IU	OU	Δ
C_n [-]	ATR 42	0.0330	0.0262	26 %
	Fokker 50	0.0340	0.0265	28 %

First it can be noted that the difference between the OU and IU rotating propeller is significant for both configurations. The increase of yawing moment increase (26 - 28 %) indicates why co-rotating propeller aircraft have a critical engine. The critical engine, whose failure would most adversely affect the performance or handling qualities of an aircraft, is therefore the OU rotating engine, leading to a significant increase of the yawing moment coefficient. To explain the difference in yawing force created, Figure 8.26 and Figure 8.27 are presented.

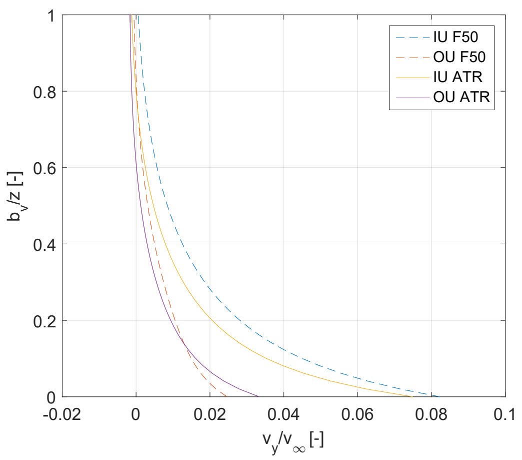

Figure 8.26: Spanwise sidewash over the vertical tail at the quarter chord position for both IU and OU condition

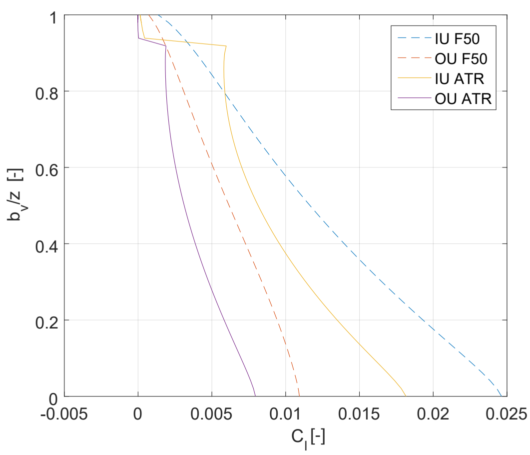

Figure 8.27: Spanwise lift coefficient created by the vertical tail for both IU and OU condition

From Figure 8.26 it can be seen that the sidewash in case of the IU rotating propeller is three times larger at the root of the vertical tail compared to the OU rotating condition. The increased sidewash coefficient creates a larger lift coefficient over the vertical tail (Figure 8.27). The difference in sidewash over the vertical tail explains the increase of yawing moment generated by the aircraft between the IU and OU rotating propeller. As expected the differences in sidewash between the Fokker 50 model and the ATR 42 are very small since the same propeller is mounted at approximately at the same position. However in the spanwise lift distribution over the vertical tail significant differences are found. First it must be said the Fokker 50 aircraft consist of a vertical tail with a bigger root and tip chord and therefore more area. The increased area causes an increase in lift coefficient. From the shape of the curves clearly the T-tail effect can be seen for the ATR 42 aircraft. The lift distribution, compared to the trend of the Fokker 50 aircraft, generates more lift at the tip section of the tail. Where the Fokker 50 tail shows a almost linear decrease towards the tip of the vertical tail. The endplate effect of the T-tail causes the decrease towards the tip to be less until the position of the vertical tail at $b_v/z = 0.95$.

It was found under a zero degree angle of sideslip that the moment created by the conventional tail is similar to that of a T-Tail configuration. The horizontal tail is emerged in the propeller wake while the horizontal tail in the T-tail configuration stays out of the wake, this having specifically effect on the longitudinal stability which is out of the scope of this research. The propeller slipstream wake under influence of the downwash of the wing is displaced downwards and more inboard due to the lower pressure near the fuselage. The propeller of the Fokker 50 is positioned slightly more inboard, which creates a smaller yawing moment however the more inboard position increases the interference effects as explained in Section 8.5.

The rear view of the OEI condition rotating OU for both aircraft is presented in Figure 8.28 and Figure 8.29. It can be seen that the vortex sheet created by the wing and the propeller stays clear of the horizontal tail for the ATR 42. It is recommended in further research to examine the effects of the wing and propeller vortex sheet on the horizontal tail to evaluate its effects.

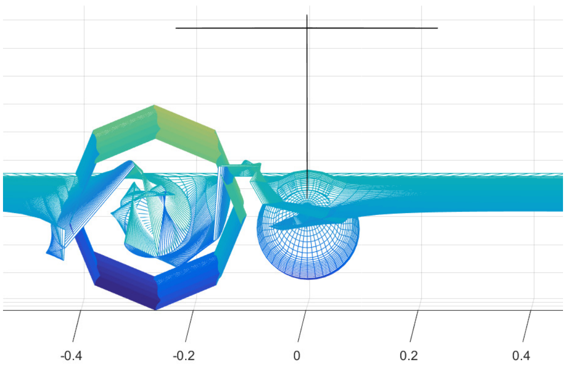

Figure 8.28: Rear-view of model, simulating ATR42 aircraft with OEI conditions, rotating outboard up

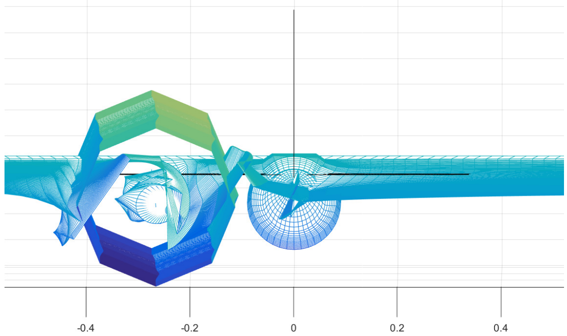

Figure 8.29: Rear-view of model, simulating Fokker 50 aircraft with OEI conditions, rotating outboard up

9
Conclusion & Recommendations

In the last chapter of this research procect the conclusions and recommendations for future research are presented.

9.1. Conclusion

To improve the vertical tail design in the conceptual design phase, the objective of this research was to analyse and identify the effects of the propeller slipstream on the aircraft directional stability derivatives for different aircraft and empennage configurations by expanding and using a potential flow model.

Since the propeller slipstream effects on the vertical tail are largely dependent on the lift distribution over the wing-fuselage combination under influence of the propeller slipstream, first an extensive verification and validation has been performed on the spanwise lift coefficient. From the validation of the spanwise lift coefficient the following conclusions can be made:

From the verification and validation of the spanwise lift coefficient of the propeller-wing-fuselage combination it was found that the accuracy of the model decreases when put under an angle of attack. The spanwise lift coefficient behind the down going blade is overestimated compared to the experimental data and the VLM method. The increase in the model is caused by the down going blade experiencing an increased angle of attack, producing an increase in the axial velocity behind the blade. However this effect is overestimated by the potential flow model. For the low thrust condition the error between the experimental data and the model is relatively small (max 10%) and the same trend can be seen in the data. From the verification and validation of the spanwise lift distribution calculated by the potential flow model it is concluded that the model shows sufficient accuracy for the prediction of the spanwise lift coefficient of the wing-fuselage-propeller combination under the influence of the propeller slipstream at low angles of attack in the conceptual design phase. Analysing previous research it was concluded that the yawing moment coefficient for a low to a high thrust coefficient for the condition without flaps shows accurate results with the windtunnel measurements of Mannée. It was found that deploying the flaps leads to a significant error up to 50% for the yawing coefficient of the complete model. Therefore, flaps are left out of scope for this research project.

From the sensitivity analysis the minimum amount of panels is determined where convergence of the results is found. Since the computational time increases significantly with the amount of panels in flow direction, the amount is kept at a minimum of 75 panels. The computational time for the model without the propeller installed is ≈25 seconds and with one propeller installed ≈50 seconds.

From the validation of the parametric analysis of the aircraft directional stability derivatives without the propeller slipstream effects several conclusions can be drawn:

The validation of the isolated vertical tail with the CFD data showed similar trends and sideforce coefficient values, an error of 2-3% for all three different vertical tail aspect ratios, showing the potential flow model can be used to predict the lift generated by the isolated vertical tail. Next the different interference effects on the installed vertical tail have been analysed and validated. For all interference effects the potential model shows the same trends as the CFD data and the correction curves used for the DATCOM method. Only for the fuselage interference effect an under prediction was found for the whole range of aft fuselage models. The error between the model and the CFD results ranges from 7% for the 'thickest' aft fuselage section to 5.5% for the most slender aft fuselage. However the reason for this could be found in the modelling of the aft fuselage section which is not extensively described in the sources and could therefore be slightly different than the approach used in this research.

In a final step of this analysis the installed vertical tail for the two example aircraft using the semi-empirical methods are compared with the potential flow model. The side force coefficient is under estimated for both the DATCOM and the VeDSC method. Comparing to the DATCOM method, the under prediction is 9% for the ATR 42 and 11% for the Fokker 50 aircraft. Comparing to the VeDSC method the under prediction is 7% and 8% for respectively the ATR 42 and Fokker 50 aircraft. The VeDSC method, recently derived from measurements using a RANS solver, developed for turbo-prop aircraft geometries, seems to be the most reliable to compare with. The underestimation of the potential flow model can be explained by the under-prediction of the fuselage and the for the Fokker 50 aircraft additionally the under prediction of the H-tail interference effect.

It can be concluded that the potential flow model, a low fidelity analysis tool, predicts the side force coefficient of the isolated and the installed vertical tail for various aircraft configurations within reasonable error. The short computational time of the potential flow model, ≈25 seconds without modelling the propeller, allows for the usage of the model in a conceptual design tool.

Following the extensive analysis and validation of the results without the propeller slipstream, in the second part of the results the influence of the propeller slipstream on the directional stability is analysed and the following conclusions can be made:

For the isolated vertical tail only a slight increase was found in the side force coefficient created by the vertical tail under influence of the propeller slipstream (2-3%), depending on the conditions. In the one engine operative condition, already a small sideforce was created under zero degrees angle of sideslip due to the asymmetric thrust condition.

Compared to the prop-off situation the effects of installing a fuselage on the vertical tail has increased under influence of the propeller slipstream. Due to the propeller slipstream the crossflow is increased, which in turn increases the effectiveness of the vertical tail from 10% for the thickest aft-fuselage ($b_v/f_D = 1.1$) section to 5% for the most slender aft fuselage section ($b_v/f_D = 4.8$).

For the influence of the propeller slipstream on the wing interference effect an extensive analysis has been conducted. It was found that the positive sideslip angle in combination with a high wing configuration causes a strong peak in the spanwise lift coefficient distribution for an IU rotating propeller. The strong asymmetric lift distribution causes a circulation to be created around the fuselage decreasing the vertical tail effectiveness 3% to 5% depending on the wing aspect ratio. For a low wing the opposite is true, the strong circulation peak is reduced due to the low wing configuration, experiencing a lower angle of attack near the fuselage region. For this reason an increase in effectiveness is found compared to the mid wing position ranging from 5% to 8% depending again on the wing aspect ratio.

When there is no sideslip angle, the high wing configuration causes the cross flow over the fuselage and vertical tail to be significantly stronger than for a low wing configuration. For this reason the lift coefficient created by the vertical tail in the root region is three times as high for the high wing as compared to the low wing aircraft. In total increasing the yawing moment coefficient in OEI condition with an IU rotating propeller for a high wing with almost 20% compared to a low wing configuration.

For the interference effect of the horizontal tail under the influence of the propeller slipstream it was found that the end-plate effect of the horizontal tail is smaller for both the low (3% lower) and T-tail configuration (8% lower). Finally, the effects of the lateral position of the propeller were investigated and validated with windtunnel data obtained by Mannée. As the propeller is placed more outboard the moment arm of the propeller increases, increasing the yawing moment created by the propeller. However, it could also be seen that the more inboard location leads to an increase of the inference effects between the propeller, fuselage and the vertical tail. For the OU rotating propeller the yawing moment coefficient is under-predicted by the potential flow model, the error is almost constant and ranging from 7% to 5% from an inboard to more outboard location. For the IU rotating propeller the results of the potential flow model fluctuate around the experimental data with a maximum error of 5%.

When evaluating the complete aircraft configuration the side force created by the vertical tail under a sideslip angle ($C_{Y_{\beta_v}}$) increases with 5% to 7% under the influence of the propeller slipstream. When evaluating the yawing moment coefficient of the two example aircraft with zero degree angle of sideslip the influence of the rotation direction is very clear. The IU rotating propeller generates a yawing moment which is 26% to 28% larger compared to the OU rotating propeller generating the same thrust. Failure of the critical engine will cause the yawing moment to be significantly higher, mainly caused by the increased crossflow over the fuselage and vertical tail.

In conclusion, contrary to the current vertical tail design process, based on semi-empirical relations where the influence of the propeller slipstream on the directional stability is almost neglected, the potential flow model calculates the directional stability derivatives of the actual aircraft configuration for different conditions under the influence of the propeller slipstream. It was found that the effects of the propeller slipstream change significantly depending on the configuration of the aircraft, where especially the wing position in combination with the propeller position have the biggest influence. The potential flow model calculates the forces and moments of the various parts of the aircraft, with a computational time of ≈50 seconds, showing promising results and functionality to operate in a conceptual design tool. However, the analysis of aerodynamic effects of the propeller slipstream on the aircraft have only been validated for a single condition using the measurements of Mannée. Extensive validation is first needed before the model can be implemented. Furthermore it is not possible to model any viscous effects using the model, limiting its use to small angles of sideslip and angles of attack.

.

9.2. RECOMMENDATIONS

It is recommended to perform an extensive validation of the results under influence of the propeller slipstream, especially on the side force coefficient of the vertical tail ($C_{Y_{\beta_v}}$). So far, only the windtunnel data of Mannée has been used for validation of the propeller slipstream effects. Validation of the sideforce coefficient of the different configurations under the influence of the propeller slipstream will give more certainty about the accuracy of the model, predicting the directional stability derivatives under the influence of the propeller slipstream.

According to literature it is known that the flaps have a significant influence on the lift distribution and on the yawing moment in OEI conditions. Therefore, it is recommended to asses the current flap model in the potential flow model and update and validate it such that it can be used for analysis in the future. However due to the large angle of attack at which flaps are deployed (10-40 degrees)

viscous forces will start to develop, which cannot be modelled using a potential flow model.
The model, operated without the propeller, only needs a run-time of ≈25 and with a propeller ≈50 seconds, making it a feasible solution for a conceptual design tool. Additionally to the calculation of the forces and moments working on the directional stability, the forces and moments generated in x,y and z direction by the fuselage, wing and empennage are calculated. For this reason it is recommended to evaluate in further research the accuracy of the model's prediction of the longitudinal stability derivatives. The verification and validation of the longitudinal stability derivatives gives an extra validation of the forces and moments working on the aircraft, generated under a angle of attack or sideslip angle under influence of the propeller slipstream. In this way the model could be used to estimate the longitudinal and directional stability derivatives of the aircraft in the conceptual design phase. Additionally the spanwise circulation distribution and the spanwise lift and drag coefficient distribution give a great insight in the aerodynamic performance of the aircraft in the conceptual design phase. For this reason it is recommended to implement the model into the conceptual design tool (the Initiator) of the Flight Performance and Propulsion group after additional validation.

BIBLIOGRAPHY

[1] A. K. Sehra and W. Whitlow. “Propulsion and power for 21st century aviation”. In: *Progress in Aerospace Sciences* 40.4-5 (2004), pp. 199–235. ISSN: 03760421.

[2] A.S. Gohardani, G. Doulgeris, and R. Singh. “Challenges of future aircraft propulsion: A review of distributed propulsion technology and its potential application for the all electric commercial aircraft”. In: *Progress in Aerospace Sciences* 47.5 (2011), pp. 369–391. ISSN: 03760421.

[3] L.L.M. Veldhuis. “Propeller wing aerodynamic interference”. PhD thesis. 2005, p. 418. ISBN: 9090195378.

[4] J. Roskam. *Airplane Flight Dynamics and Automatic Flight Controls*. Design Analysis and Research corporation (DARcorporation), 2001, pp. 1–576. ISBN: 1884885179.

[5] R. D. Finck. *USAF (United States Air Force) Stability and Control DATCOM*. Tech. rep. McDonnell Aircraft Co., St. Louis, MO, 1978.

[6] K.E.Ward Jacobs, E.N. *Interference of wing and fuselage from tests of 209 combinations in the NACA variable desinsity wind tunnel*. Tech. rep. 540. National Advisory Commitee for Aeronautics, 1935.

[7] R.J. Bamber. *Wind tunnel investigation of effect of yaw on lateral characteristics*. Tech. rep. National Advisory Committee for Aeronautics, 1941.

[8] A. Sherman. *Interference of the wing and fuselage from tests of 28 combinations in the NACA variable-density tunnel*. Tech. rep. National Advisory Committee for Aeronautics, 1935.

[9] H. Sweberg and Harold H. *Air flow surveys in the region of the tail surfaces of a single-engine airplane equipped with dual-rotating propellers*. Tech. rep. National Advisory Committee for Aeronautics, 1943.

[10] J.D. Brewer and J. Lichtenstein. *Effect of horizontal tail on low-speed static lateral stability characteristics of a model having 45 degree sweptback wing and tail surfaces*. Tech. rep. January 1950. National Advisory Committee For Aeronautics, 1950.

[11] H. Sweberg and Dingeldein R. C. *Some effects of propeller operation on the distribution of the load on the vertical tail surface of a typical pursuit airplane*. Tech. rep. March 1944. National Advisory Commitee for Aeronautics, 1944.

[12] W. Queijo and M.J. Wolhart. *Experimental investigation of the effect of vertical-tail size and length and of the fuselage shape and length on the static lateral stability characteristics of a model with 45 degree swepback wing and tail surfaces*. Tech. rep. National Advisory Committee for Aeronautics, 1951.

[13] M.J.T. Schroijen, L.L.M. Veldhuis, and R. Slingerland. “Propeller Empennage Interaction Effects on the Vertical Tail Design of Multi-engine Aircraft”. In: *Journal of Aircraft* 47.4 (2010), pp. 1133–1140. ISSN: 0021-8669.

[14] D.P. Raymer. *Aircraft Design: A Conceptual Approach*. Fifth edition. 2012. ISBN: 978-1600869112.

[15] E. Torenbeek. *Synthesis of Subsonic Airplane Design*. Delft University Press, 1976, p. 620. ISBN: 9029825057.

[16] W.F. Durand. “Aerodynamic Theory: A General Review of Progress Under a Grant of the Guggenheim Fund for the Promotion of Aeronautics”. In: *Aerodynamic Theory*. Ed. by William Frederick Durand. 1. Springer, 1934. ISBN: 9780874216561.

[17] J.T. Conway. “Exact actuator disk solutions for non-uniform heavy loading and slipstream contraction”. In: *Journal of Fluid Mechanics* 365 (1998), pp. 235–267. ISSN: 00221120.

[18] M.K. Rwigema. “Propeller Blade Element Momentum Theory with Vortex Wake Deflection”. In: *Proceedings of the 27th Congress of the Aeronautical Sciences* (2010), pp. 1–9.

[19] R. H. Stone. “Aerodynamic Modeling of the Wing-Propeller Interaction for a Tail-Sitter Unmanned Air Vehicle”. In: *Journal of Aircraft* 45.1 (2008), pp. 198–210. ISSN: 0021-8669.

[20] H. S. Ribner. “Theory of wings in slipstreams”. In: *Institute of Aerophysics* (1959).

[21] D. Hunsaker and D. Snyder. “A Lifting-Line Approach to Estimating Propeller/Wing Interactions”. In: *24th AIAA Applied Aerodynamics Conference* June (2006).

[22] A. Nispen. “Slipstream effects on the static lateral and directional control of a multi-engined propeller aircraft with one engine inoperative”. MA thesis. Delft University of Technology, 2002.

[23] M.J. T. Schroijen. “Propeller installation effects on lateral stability and control of multi-engine propeller aircraft”. MA thesis. Delft University of Technology, 2006.

[24] J. Mannée. “LR NLL Rapport A-1508 B, Windtunnel investigation of the influence of the aircraft configuration on the yawing- and rolling moments of a twin-engined, propeller-driven aircraft with one engine inoperative”. In: *Congresso Aeronautico Europeo* (1962).

[25] E. Obert. *Aerodynamic Design of Transport Aircraft*. Delft: IOS Press under the imprint Delft University Press, 2009, p. 638. ISBN: 978-1-58603-970-7.

[26] *EASA Certification Specification CS-25*. http://www.easa.europa.eu/document-library/certification-specifications/group/cs-25-large-aeroplanes#group-table. Accessed: 14^{th} September 2016.

[27] F.W. Diederich. *Approximate aerodynamic influence coefficients for wings of arbitrary plan form in subsonic flow*. Tech. rep. July. National Advisory Commitee for Aeronautics, 1950.

[28] J.A. Mulder, W.H.J.J. van Staveren, and J.C. van der Vaart. *Flight Dynamics*. Lecture notes AE3202 TU Delft. 2013.

[29] E. Obert. *Static Directional Stability and Control of Transport Aircraft*. Tech. rep. Fokker VFW B.V., 2013.

[30] S. Katzoff. *End plate effect of a horizontal tail surface on a vertical tail surface*. Tech. rep. National Advisory Commitee for Aeronautics, 1941.

[31] H.E. Murray. *Wind-tunnel Investigation of end-plate effects of horizontal tail on a vertical tail compared with available theory*. Tech. rep. No. 1050. National Advisory Committee for Aeronautics, 1949.

[32] P. Della Vecchia. “Development of Methodologies for the Aerodynamic Design and Optimization of New Regional Turboprop Aircraft”. PhD thesis. University of Naples,Faculty of Aerospace Engineering, 2014, p. 205.

[33] F. Nicolosi, P. Della Vecchia, and D. Ciliberti. “Development of New Preliminary Design Methodologies for Regional Turboprop”. In: *29th Congress of the international council of the aeronautical sciences* (), pp. 1–11.

[34] T. Hettema. “Vertical Tail Design”. MA thesis. TU Delft, 2015.

[35] T. Theodorsen. “Theory of propellers”. In: *Journal of the Franklin Institute* 246.6 (1948), p. 528. ISSN: 00160032.

[36] J.L. Crigler. *Application of Theodorsen's Theory to Propeller Design*. Tech. rep. 924. National Advisory Committee for Aeronautics, 1948, pp. 83–99.

[37] P. van den Borne and J. van Hengst. “Investigation of propeller slipstream effects on the Fokker 50 through in-flight pressure measurements”. In: *Flight Simulation Technologies Conference and Exhibit* (1990).

[38] M.J.T. Schroijen and R. Slingerland. “Propeller slipstream effects on directional aircraft control with one engine inoperative”. In: *AIAA* January (2007), pp. 1–13.

[39] A. Roosenboom E.and Heider and A. Schröder. “Propeller Slipstream Development”. In: *25th AIAA Applied Aerodynamics Conference* June (2007), pp. 1–9. URL: `http://arc.aiaa.org/doi/abs/10.2514/6.2007-3810`.

[40] P. Rauhut and R. Slingerland. “Propeller Slipstream Effects on Lateral and Directional Static Stability and Control of a Single Engine Tractor Airplane”. In: *41st Aerospace Sciences Meeting and Exhibit* January (2003).

[41] M. Renooij and R. Slingerland. “Propeller Slipstream and Wing-Fuselage Interference Effects on Three-Axis Stability And Control”. In: *42nd AIAA Aerospace Sciences Meeting and Exhibit* January (2004).

[42] E. Houghton and P.W. Carperten. *Aerodynamics for engineering students*. Fifth. 2002, p. 614. ISBN: 07050651113.

A
APPENDIX A

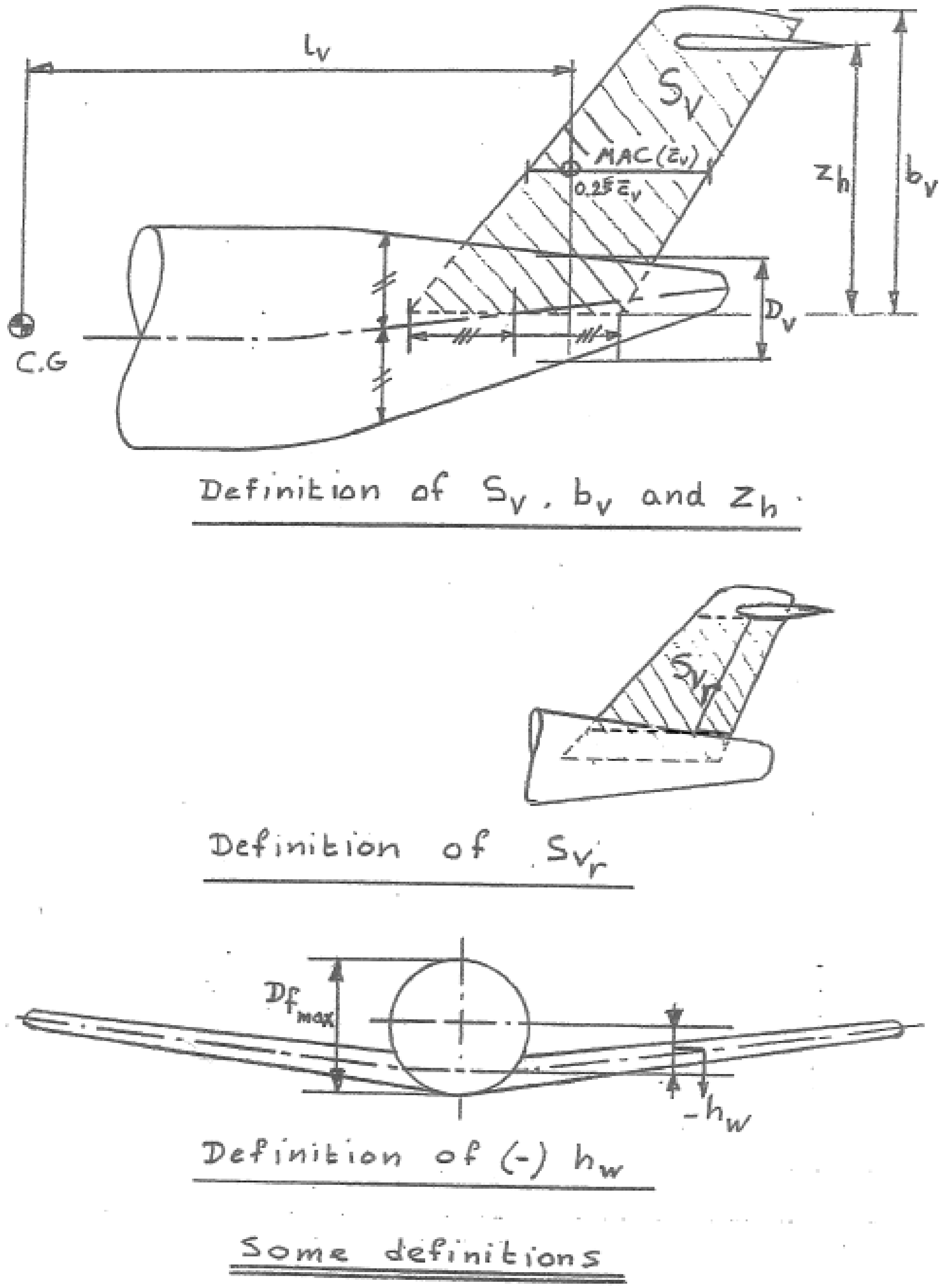
l_V
S_V
MAC (c̄_V)
0.25 c̄_V
z_h
b_V
D_V
C.G
Definition of S_V, b_V and z_h
S_Vr
Definition of S_Vr
Df_max
-h_w
Definition of (-) h_w
Some definitions

Figure A.1

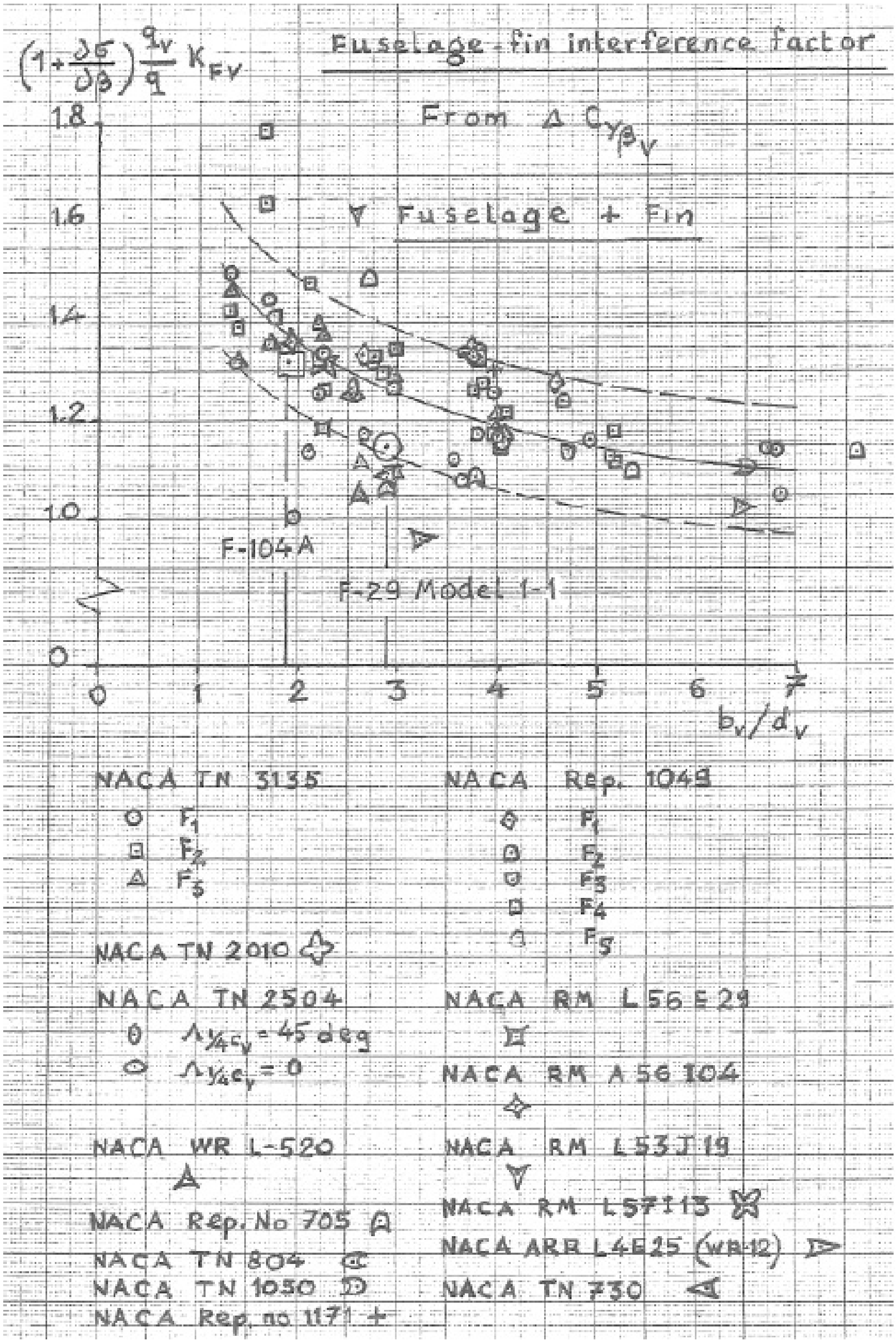

Fuselage-fin interference factor
$\left(1+\frac{\partial\sigma}{\partial\beta}\right)\frac{q_v}{q}K_{Fv}$
From $\Delta C_{Y_{\beta_v}}$
Fuselage + Fin
F-104A
F-29 Model 1-1
b_v/d_v
NACA TN 3135
F_1
F_2
F_3
NACA Rep. 1049
F_1
F_2
F_3
F_4
F_5
NACA TN 2010
NACA TN 2504
$\Lambda_{1/4 c_v} = 45$ deg
$\Lambda_{1/4 c_v} = 0$
NACA RM L56E29
NACA RM A56I04
NACA WR L-520
NACA RM L53J19
NACA RM L57I13
NACA Rep. No 705
NACA ARR L4E25 (WR 12)
NACA TN 804
NACA TN 1050
NACA TN 730
NACA Rep. no 1171

Figure A.2

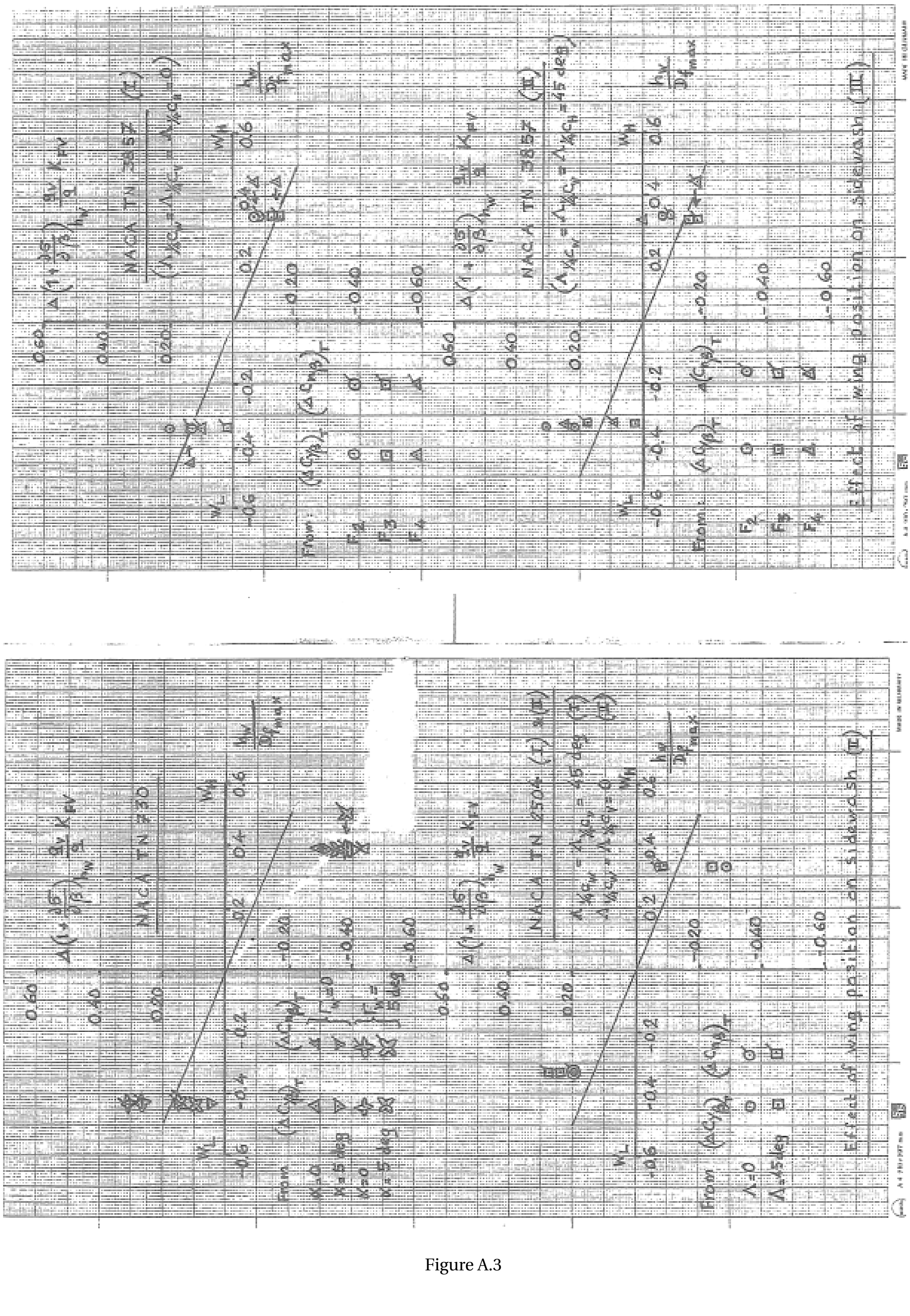
NACA TN 3857 (I)
NACA TN 3857 (II)
Effect of wing position on sidewash (III)
NACA TN 730
NACA TN 2504 (I) & (II)
Effect of wing position on sidewash (II)

Figure A.3

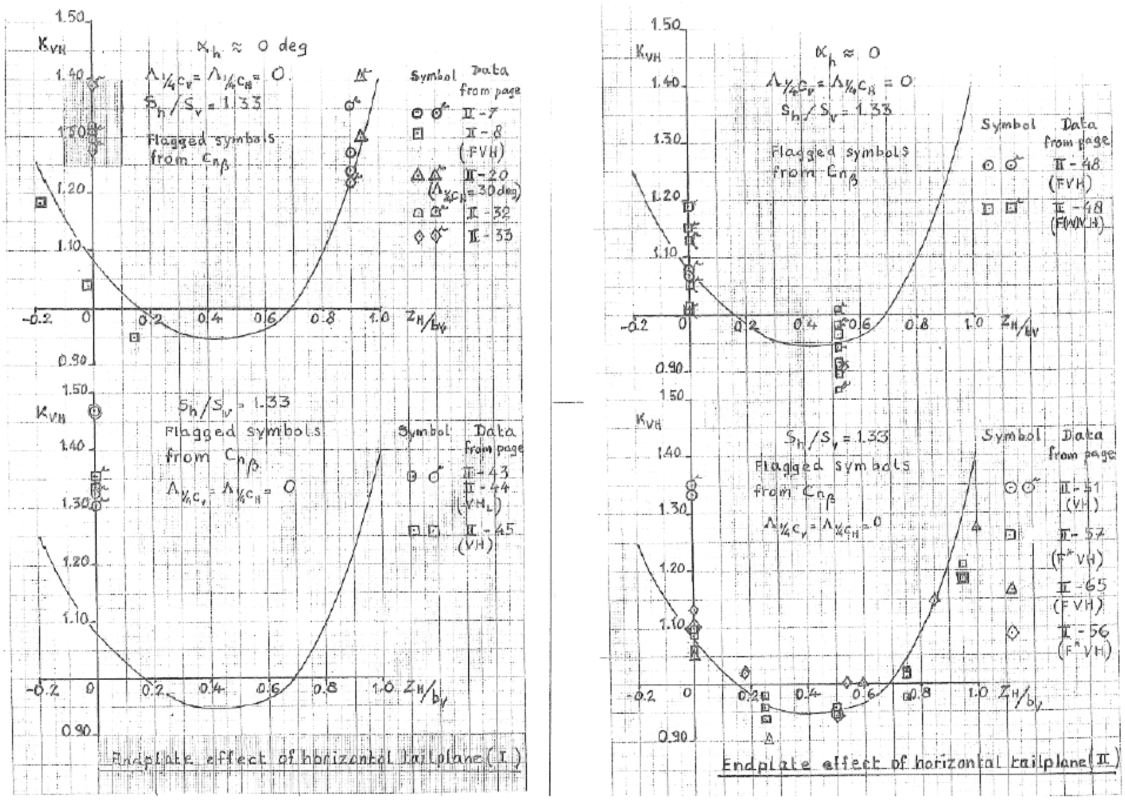
Endplate effect of horizontal tailplane (I)
Endplate effect of horizontal tailplane (II)
Flagged symbols from C_{n_β}
$S_h/S_v = 1.33$
Symbol
Data from page

Figure A.4

B

Appendix B

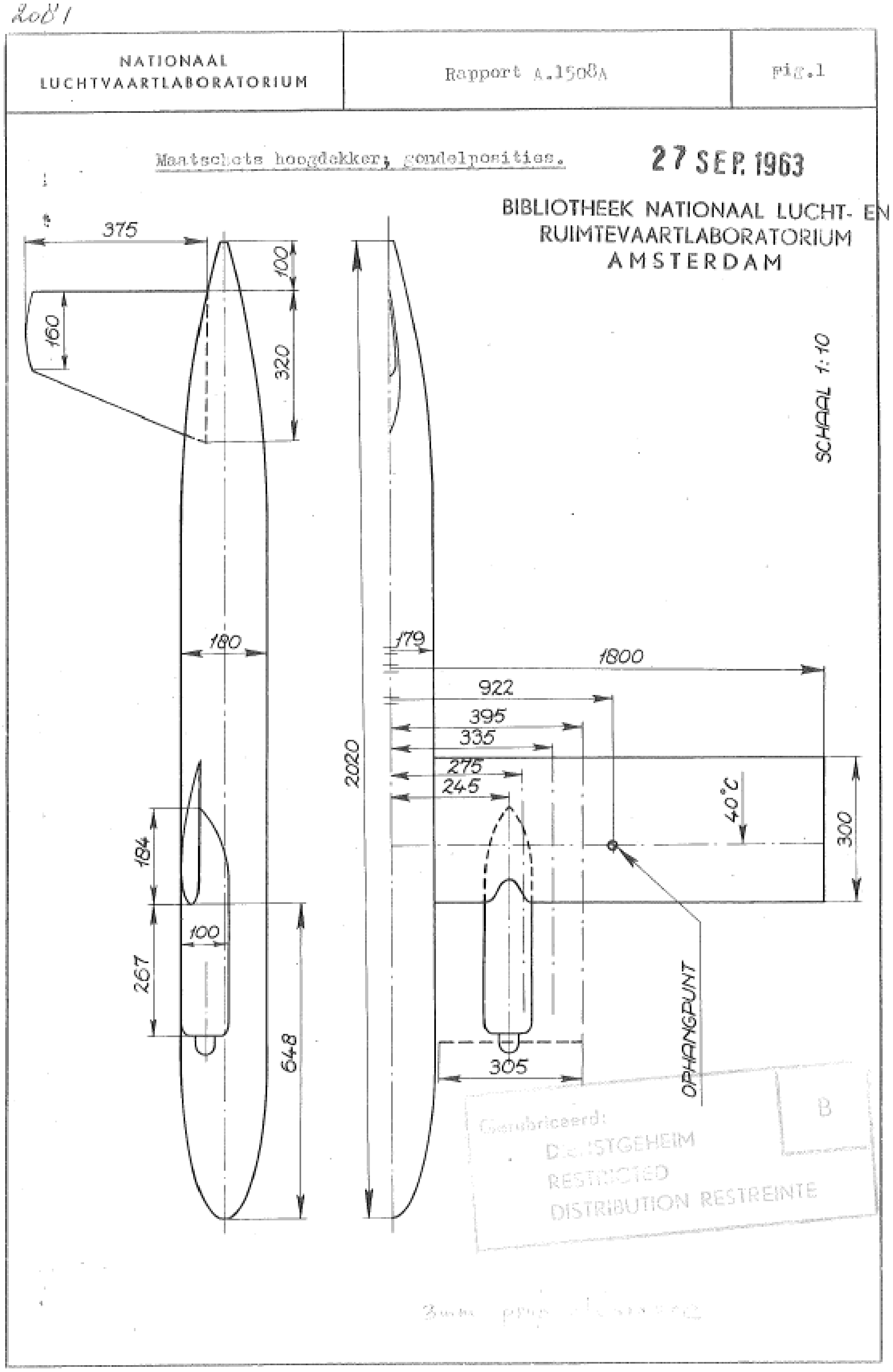
2081
NATIONAAL LUCHTVAARTLABORATORIUM
Rapport A.1508A
Fig.1
Maatschets hoogdekker; gondelposities.
27 SEP. 1963
BIBLIOTHEEK NATIONAAL LUCHT- EN RUIMTEVAARTLABORATORIUM AMSTERDAM
375
100
160
320
SCHAAL 1:10
180
179
1800
922
395
335
275
245
2020
40°C
300
184
100
267
648
305
OPHANGPUNT
Gerubriceerd:
DIENSTGEHEIM
RESTRICTED
DISTRIBUTION RESTREINTE
B

Figure B.1

NATIONAAL LUCHTVAARTLABORATORIUM	Rapport A.1508A	Fig.59

Trekkrachtijking.

Middendekker met kielvlak en klep.

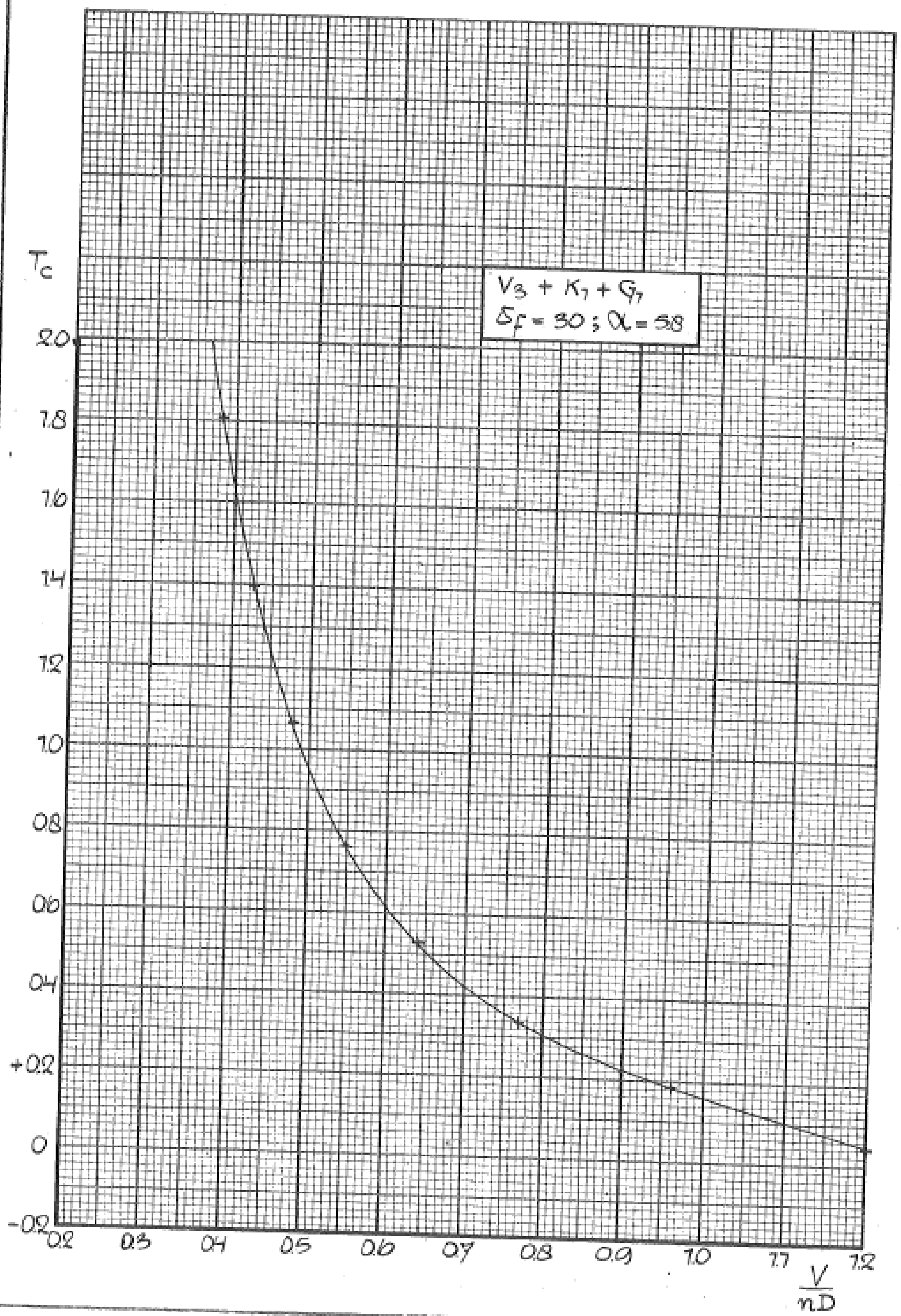

Figure B.2

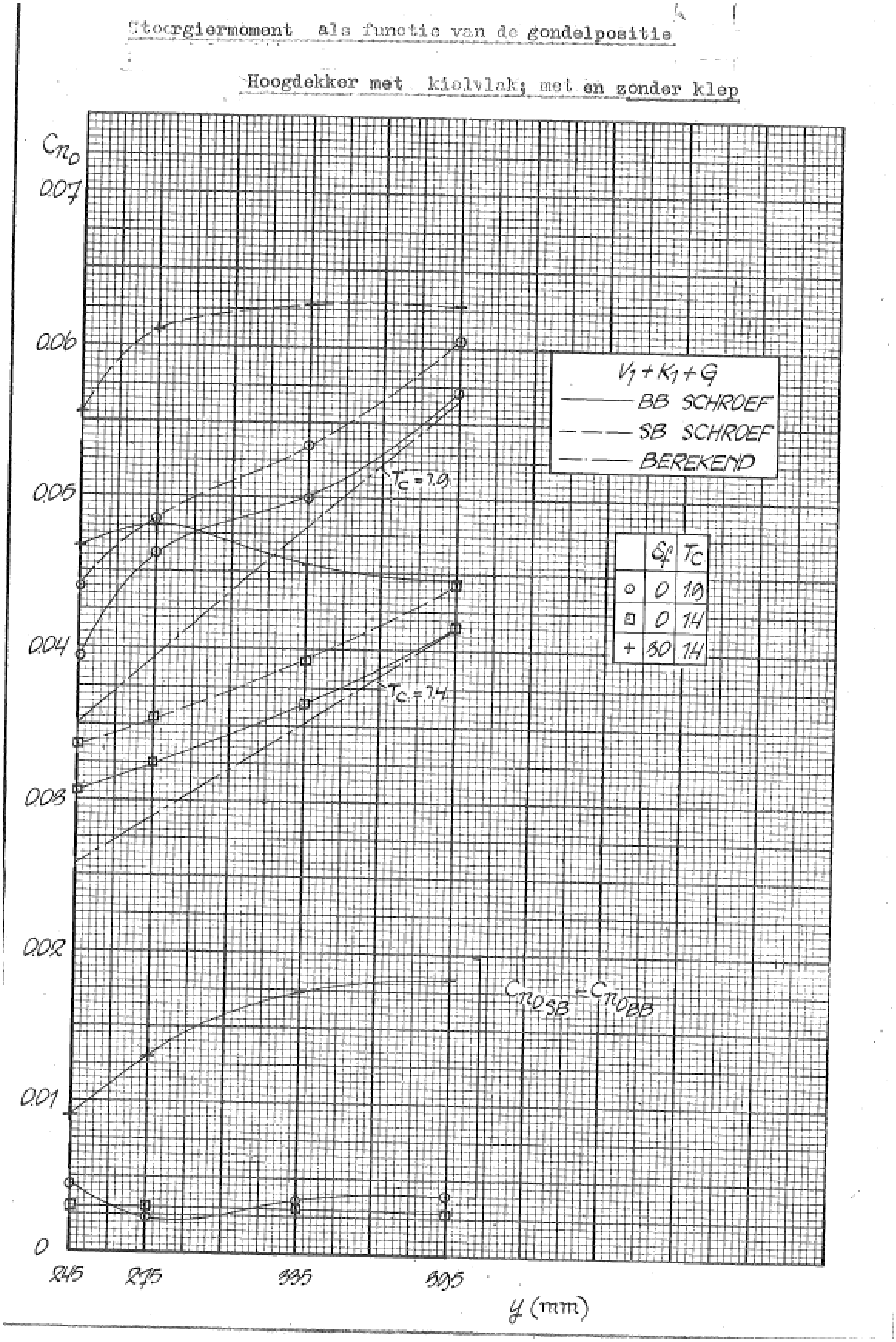
Stoorgiermoment als functie van de gondelpositie
Hoogdekker met kielvlak; met en zonder klep
C_{n_0}
0.07
0.06
0.05
0.04
0.03
0.02
0.01
0
245
275
335
395
y (mm)
$V_1 + K_1 + G$
BB SCHROEF
SB SCHROEF
BEREKEND
$T_C = 1.9$
$T_C = 1.4$
δ_f T_C
0 1.9
0 1.4
30 1.4
$C_{n_{0_{SB}}} - C_{n_{0_{BB}}}$

Figure B.3

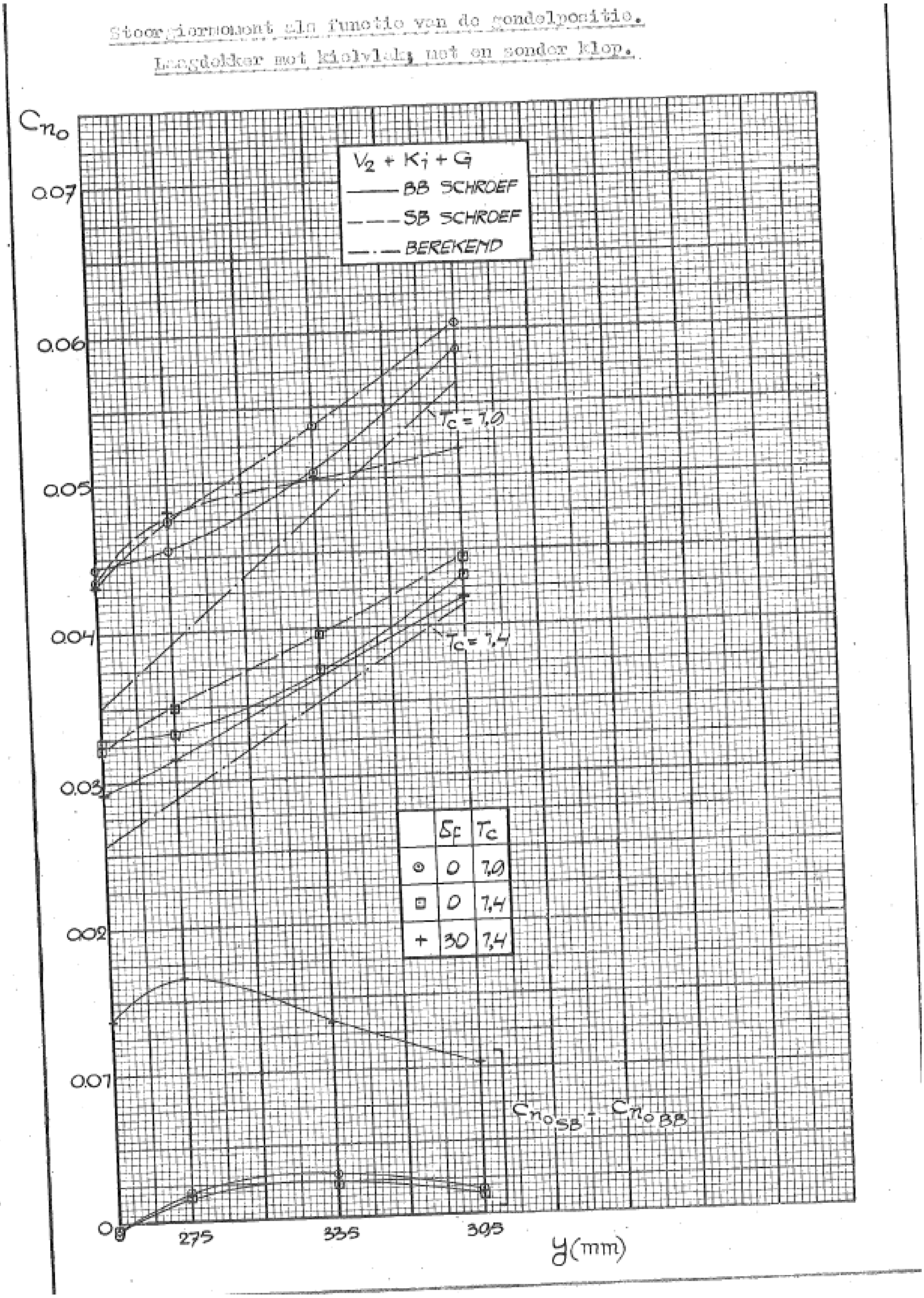
Stoorgiermoment als functie van de gondelpositie.
Langdekker met kielvlak; met en zonder klep.
Cn0
0.07
0.06
0.05
0.04
0.03
0.02
0.01
0
275
335
395
y(mm)
V2 + Ki + G
BB SCHROEF
SB SCHROEF
BEREKEND
Tc = 7,0
Tc = 7,4
δF Tc
0 7,0
0 7,4
30 7,4
Cn0SB - Cn0BB

Figure B.4